MUNI
SCI

MASARYK UNIVERSITY

FACULTY OF SCIENCE

DEPARTMENT OF CHEMISTRY

Mass Spectrometry of Chalcogenide Materials

Doctoral Dissertation

FEI HUANG

Supervisor: Prof. RNDr. Josef Havel, DrSc.

Brno 2022

Bibliographic Entry

Author:	Fei Huang Faculty of Science, Department of Chemistry Masaryk University
Title of the Dissertation:	Mass Spectrometry of Chalcogenide Materials
Degree Programme:	Chemistry
Specialisation:	Analytical Chemistry
Supervisor:	Prof. RNDr. Josef Havel, DrSc.
Academic Year:	2022
Number of Pages:	124
Keywords:	Laser ablation, laser desorption/ionization, time-of-flight mass spectrometry, chalcogenides, thin films, clusters, doping, diminishing clusters fragmentation, Raman spectroscopy

Bibliografický záznam

Autor:	Fei Huang Přírodovědecká fakulta, Ústav chemie Masarykova univerzita
Název disertační práce:	Hmotnostní spektrometrie Chalkogenid materiálů
Studijní program:	Chemie
Specializace:	Analytická chemie
Vedoucí:	Prof. RNDr. Josef Havel, DrSc.
Akademický rok:	2022
Počet stran:	124
Klíčová slova:	Laserová ablace, laserová desorpce/ionizace, hmotnostní spektrometrie s dobou letu, chalkogenidy, tenké filmy, klastry, doping, potlačení fragmentace klastrů, Ramanova spektroskopie

Declaration

I hereby declare on my honour that I worked on this Dissertation independently and that I used only the literature listed in References.

Brno, 2022 Fei Huang

© Fei Huang, Masaryk University, 2022

Acknowledgements

I have made efforts in this Ph.D. study despite unsatisfactory results. However, even such a small success would not be possible without the generous support and assistance of many individuals, for whom I would like to extend my sincere thanks, even though I am well aware that my words will not be enough.

First and foremost, it has been a great honor to undergo the training at Prof. RNDr. Josef Havel, DrSc., my Ph.D. thesis supervisor, for his guidance, professional advice, and constant supervision. I am highly indebted to his keen interest in my work and for providing the necessary encouragement whenever my projects met obstacles. His constant supervision to share his vast professional analytical chemistry knowledge made me know how the projects as well as helped me to complete my Ph.D. study on time.

Special appreciation to Prof. Ing. Petr Němec, Ph.D. and Prof. Ing. Tomáš Wágner, Ph.D. and their groups. My thanks are also due to Dr. Lubomír Prokeš, Ph.D. for his help with the measurements, kind support, and encouraging criticism.

Secondly, I would like to give my great thanks to the professors and staff members of the Department of Analytical Chemistry, Masaryk University for their encouragement and friendship during my study in Brno: prof. RNDr. Viktor Kanický, DrSc., prof. Mgr. Jan Preisler, Ph.D., prof. RNDr. Přemysl Lubal, Ph.D., prof. RNDr. Jiří Pinkas, Ph.D., doc. Mgr. Petr Táborský, Ph.D., doc. Mgr. Karel Novotný, Ph.D., doc. RNDr. Jiří Urban, Ph.D., doc. Mgr. Tomáš Vaculovič, Ph.D., RNDr. Marta Farková, CSc., Mgr. Aleš Hrdlička, Ph.D., Mgr. Lucie Šimoníková, and so on.

Last but not least, I would like to acknowledge and give my warmest thanks to my colleagues for their fruitful discussions that were not only about chemistry but also for generating a motivating and enjoyable atmosphere throughout my study: Govinda, Lukáš, Dominik, Esther, Luboš, Peter, Lenka, Houška, Staniela, Filip, Marek, Antonín, Marina, Andreas, Tomáš, Mišo, Yana, and others.

Thank you!

Abstract

The goal of the research in this thesis was to investigate the structures of selected chalcogenide materials using laser desorption ionization/laser ablation (LDI/LA) or surface-assisted laser desorption ionization (SALDI) with time-of-flight/quadrupole ion trap time-of-flight mass spectrometry (TOF/QIT TOF MS), as well as other analytical techniques that will be discussed in detail in the following sections. The dissertation is divided into four sections, each of which focuses on different chalcogenide materials.

The chemistry of chalcogenides is complex and still not completely understood. Characterizing of chalcogenide glasses by mass spectrometry is difficult. As matrix-assisted laser desorption ionization (MALDI) can not be used for the ionization, we have to apply laser desorption ionization or laser ablation of the materials, which causes mostly strong fragmentation. Thus, the possibilities of TOF mass spectrometry for the characterization of chalcogenide glasses and their structure elucidation were studied and evaluated in four cases.

(1) First, the formation of binary antimony selenides was studied via laser ablation synthesis (LAS) from various mixtures of antimony and selenium. Up to 24 new Sb_mSe_n clusters were identified. In addition, some special approaches were applied to the measurements.

(2) Second, the results of the first work were then used to help the analysis of mass spectra concerning Sb_2Se_3 polycrystalline materials. Here, 6 high mass clusters $Sb_4Se_4^+$, $Sb_5Se_{3\text{-}6}^+$, and $Sb_7Se_4^+$ were observed for the first time by adding paraffin (parafilm dissolved in xylene) to the sample. This procedure suppresses the fragmentation of chalcogenide glasses during the Laser Desorption Ionization process.

(3) Third, two very different techniques, non-destructive Raman spectroscopy and destructive LDI TOF MS, to follow the structure of chalcogenide glasses doped with the silver, were applied. Given that the chalcogenide glasses are often made from Sb, S, Se, and Ge. The properties of materials can be changed via doping with other elements. Silver doping of the ternary Ge-Sb-S was studied, and the results of MS were compared with Raman spectroscopy. It was found that while Raman spectroscopy detects the basic structural units, MS shows their fragments.

(4) At last, we studied the quaternary Ge-Sb-Se-Te system. Here, the Se is partially replaced by Te. It demonstrated that the replacement of Se with Te caused the

production of a higher number of clusters which probably indicates some increased fragility of the Te doped thin films. In addition, the same effect was observed. i.e., a higher number of clusters are produced after the addition of Te to the Ge-Sb-Se mixtures of elements.

In contrast to Raman spectroscopy, which is not fragmenting the structures, LDI or LA techniques with TOF MS can not only be used to examine the formation of structural entities (clusters) but also it is simultaneously used as a kind of synthesizer (if a mixture of elements is used as a sample). Often, new clusters are synthesized in comparison to those formed via laser fragmentation of known structures. It was demonstrated that LDI TOF MS is a powerful and useful tool to elucidate the composition of clusters formed from chalcogenide glasses via LDI and determine their stoichiometries. Even if LDI TOF MS causes chalcogenides structure to fragment into smaller clusters, this information is important. The fragmentation of chalcogenides can be suppressed by mixing the samples with paraffin.

Abstrakt

Cílem této vědecké práce je studie vybraných chalkogenidových materiálů pomocí laserové desorpční ionizace/laserové ablace (LDI/LA) nebo povrchem asistované laserové desorpční ionizace (SALDI) s time-of-flight/quadrupólovou iontovou pastí time-of-flight hmotnostní spektrometrií (TOF/QIT TOF MS) a dalšími analytickými technikami, které budou podrobně diskutovány v následujících částech. Disertační práce je rozdělena do čtyř částí, z nichž každá je zaměřena na odlišné chalkogenidové materiály.

Chemie chalkogenidů je často složitá a není dobře pochopena. Analýza chalkogenidových skel pomocí hmotnostní spektrometrie není jednoduchá. Problém je v tom, že k ionizaci nemůžeme použít matrici asistovanou laserovou desorpční ionizaci (MALDI), musíme aplikovat pouze laserovou desorpční ionizaci nebo laserovou ablaci materiálů, které způsobují silnou fragmentaci. V tomto výzkumu jsou tedy pro čtyři vybrané případy studovány a hodnoceny možnosti TOF hmotnostní spektrometrie pro charakterizaci chalkogenidových skel a objasnění jejich struktury.

(1) Nejprve byla studována tvorba binárních selenidů antimonu pomocí laserové ablační syntézy (LAS) z různých směsí antimonu a selenu a bylo identifikováno 24 nových klastrů Sb_mSe_n. Kromě toho byly k měření aplikovány některé speciální přístupy.

(2) V druhé části, výsledky první práce byly použity při analýze polykrystalických materiálů Sb_2Se_3 a bylo zde poprvé pozorováno 6 klastrů $Sb_4Se_4^+$, $Sb_5Se_{3-6}^+$ a $Sb_7Se_4^+$ s vysokou molekulovou hmotností přidáním některých speciálních rozpouštědel (parafín: parafilm rozpuštěný v xylenu) k potlačení fragmentace chalkogenidových skel během procesu laserové desorpční ionizace.

(3) Ve třetí části byly použity dvě velmi odlišné techniky, tj. nedestruktivní Ramanova spektrometrie a destruktivní LDI TOF MS pro sledování struktury chalkogenidových skel. Vzhledem k tomu, že chalkogenidová skla jsou často vyráběna z Sb, S, Se a Ge, a vlastnosti materiálů lze měnit dopováním jinými prvky tak bylo studováno dopování ternárního Ge-Sb-S systému stříbem a výsledky MS byly porovnány s Ramanovou spektroskopií. Bylo zjištěno, že zatímco Ramanova spektroskopie detekuje základní strukturní jednotky, MS ukazuje převážně jejich fragmenty.

(4) Nakonec jsme podobně jako v (3) studovali kvartérní systém Ge-Sb-Se-Te. Zde je Se částečně nahrazeno Te. Ukázalo se, že náhrada Se za Te způsobuje vyšší počet vytvořených klastrů, což pravděpodobně ukazuje na určitou křehkost tenkých vrstev dopovaných Te. Také zde byl pozorován stejný efekt, že po přidání Te do směsí prvků Ge-Sb-Se vzniká vyšší počet klastrů.

Závěrem lze konstatovat, že na rozdíl od Ramanovy spektroskopie, která nefragmentuje struktury, lze techniky LDI nebo LA s TOF MS nejen použít ke zkoumání tvorby strukturních entit (klastrů), ale zároveň je lze použít jako syntetizátor. Často jsou syntetizovány nové klastry ve srovnání s těmi, které byly vytvořeny laserovou fragmentací známých struktur. Bylo prokázáno, že LDI TOF MS je všestranný a užitečný nástroj pro objasnění složení klastrů vytvořených z chalkogenidových skel prostřednictvím klastrů produkujících LDI a stanovení jejich stechiometrie. I když LDI TOF MS způsobuje fragmentaci struktur chalkogenidů do menších klastrů, tato informace je důležitá. Fragmentaci chalkogenidů lze potlačit smícháním vzorků s parafinem.

Contents

1. Introduction 11

1.1. Mass Spectrometry 13

1.2. Chalcogenides 16

1.3. Clusters 18

2. Aims of the Dissertation 19

3. Results and Discussion 20

3.1. Laser Ablation Generation of Antimony Selenide Clusters. Laser Desorption Ionization (LDI) Quadrupole Ion Trap Time of Flight Mass Spectrometry 21

3.2. Comparison of clusters produced from Sb_2Se_3 homemade polycrystalline material, thin films, and commercial polycrystalline bulk using laser desorption ionization with time-of-flight quadrupole ion trap mass spectrometry 26

3.3. Laser Desorption Ionization Time-of-Flight Mass Spectrometry of Silver-Doped $(GeS_2)_{50}(Sb_2S_3)_{50}$ Chalcogenide Glasses 31

3.4. Ge-Sb-Se-Te Thin Films: Clusters Formation by Laser Ablation and Comparison with Clusters from Mixtures of Elements 36

4. Conclusions 40

5. References 41

6. How the aims of the Dissertation were fulfilled 49

7. List of Abbreviations 51

8. List of Appendices 52

Appendix 1A 53

Appendix 1B 59

Appendix 2A 66

Appendix 2B 73

Appendix 3A 80

Appendix 3B 88

Appendix 4A 94

Appendix 4B 104

9. List of Posters 111

Appendix 5 112

Appendix 6 115

Appendix 7 118

10. List of oral presentations 121

11. Participation in projects 122

12. Collaborations 123

13. Curriculum vitae 124

1. Introduction

Analytical chemistry is a science that studies chemical information, such as the composition, content, structure, and form of substances. It is an important branch of the four fundamental disciplines of chemistry. Analytical chemistry is committed to improving the sensitivity, selectivity, speed, and economy of detection methods. Analytical chemistry can be divided into classical and instrumental methods, as well as quantitative and qualitative analysis methods. The classification of analytical chemistry is shown in Figure 1.

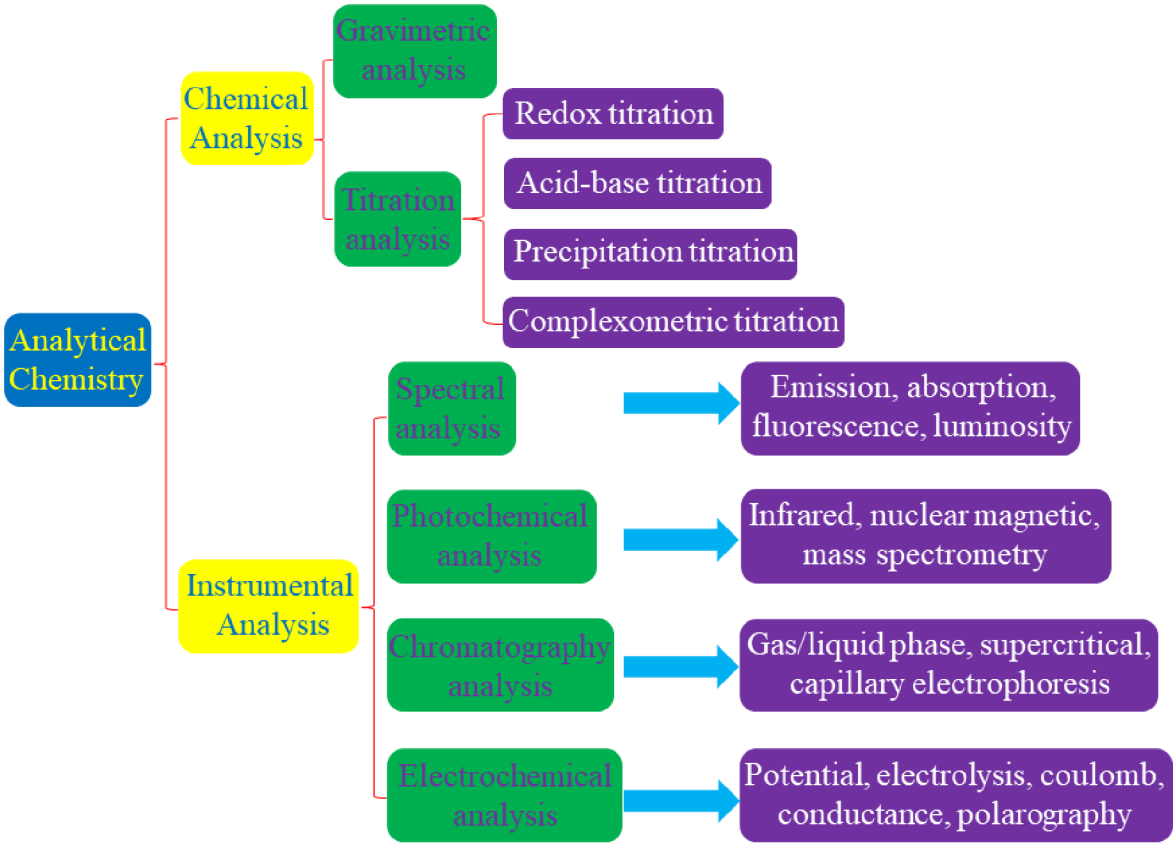

Figure 1. Classification of analytical chemistry.

Today's analytical chemistry has been effectively integrated into other disciplines, such as the intersection with biology, materials science, medicine, and others.[1] With the help of various analytical instruments, other disciplines have made considerable progress. Meantime, the innovation of analytical chemistry is promoted by the development of other disciplines. For example, chalcogenide materials have made significant progress in the past few decades which has benefitted from using many characterization methods. On the one

hand, it can be seen from the results of the characterization whether the performance of the prepared chalcogenide glass meets the expected value. On the other hand, because of the defects of the materials reflected in the characterization results, the manufacturing process of chalcogenide glass can be reversely improved to achieve the desired effect. One of the most important parts of analytical chemistry is mass spectrometry. With the application of mass spectrometry, we can obtain more detailed information about chalcogenide materials. In addition to positively charged ions, negative and neutral ones can also be present in plasma plume. Generated clusters are considered as fragments of the partial structure of the studied materials.

1.1. Mass Spectrometry

When Wilhelm Wien used electric and magnetic fields to deflect the positive ion beam in 1898, he discovered that when the electric charge is the same, ions with smaller masses deflect more and ions with larger masses deflect less. In 1913, Joseph John Thomson and Francis William Aston used a magnetic deflector to confirm that there are two isotopes of neon. Francis William Aston later made a mass spectrometer capable of resolving one hundredth of a mass unit in 1919 to determine the relative abundance of isotopes and identify many isotopes. All such discoveries are fundamental for the mass spectrometry we are using today.

In Thomson and Aston's time, mass spectrometry employed an electric or magnetic field to separate ions (charged atoms, molecular ions, isotope ions, fragment ions, rearrangement ions, multi-charged ions, metastable ions, and so on) according to their mass-to-charge ratios.

The principle of mass spectrometry is to ionize each component in the sample to generate charged ions with different mass-to-charge (*m/z*) ratios, thus forming an ion beam through the action of an accelerating electric field, which enters the mass analyser. In the electric field, the ion beam exhibits a large deflection of slow ions and a small deflection of fast ions. At the same time, mass separation can also occur in the magnetic field, so that ions with the same *m/z* ratio but different speeds are focused on the same point, and ions with different mass-to-charge ratios are focused on different points. Focus them separately to get a mass spectrum to determine their mass. Besides sampling system, vacuum system, and recording system, the mass spectrometer consists of three components: ion source (generate gaseous ions from the substance under study, the power of mass spectrometry is its ability to remove or add an electron on a molecule), a mass analyser (the heart of mass spectrometry: decompose ions into characteristic mass components according to their mass-to-charge ratio), and a detector (detect ions and record the relative abundance of each resolved ion species). A basic scheme of the mass spectrometer is shown in Figure 2.

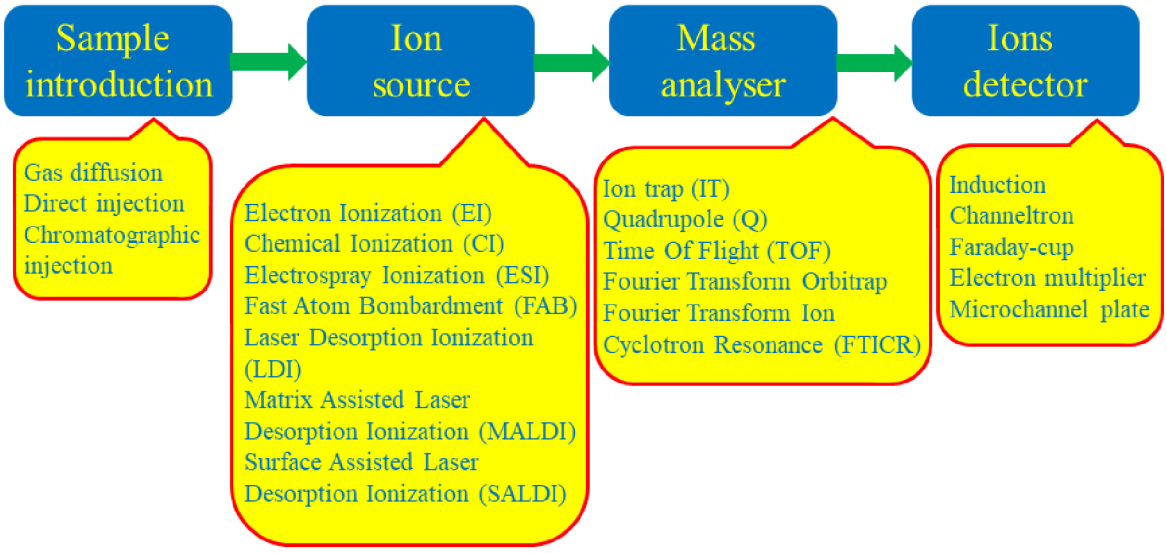

Figure 2. General scheme of a mass spectrometer.

For heat-sensitive compounds, when extremely rapid heating is performed, thermal decomposition can be avoided. MALDI uses this principle,[2] that is, in a tiny area and in a very short time interval (on the order of ns), the laser provides high-intensity pulsed energy to the analyte on the target so that it can complete desorption and ionization in an instant and does not lead to thermal decomposition. However, for the analysis of inorganic substances and low molecular weight biomolecules, the application of laser desorption ionization is more suitable. The time-of-flight mass analyser is an ion drift tube. The ions produced by the ion source are collected first. All ion velocities in the collector become zero. It is accelerated by a pulsed electric field and enters the field-less drift tube, and flies toward the ion detector at a constant speed. The higher the ion mass, the longer time it takes to reach the detector. On the contrary, the smaller the ion mass, the shorter time it takes. Based on this principle, ions of different masses can be separated according to their *m/z* value. The schematic diagram of LDI/LA is shown in Figure 3.

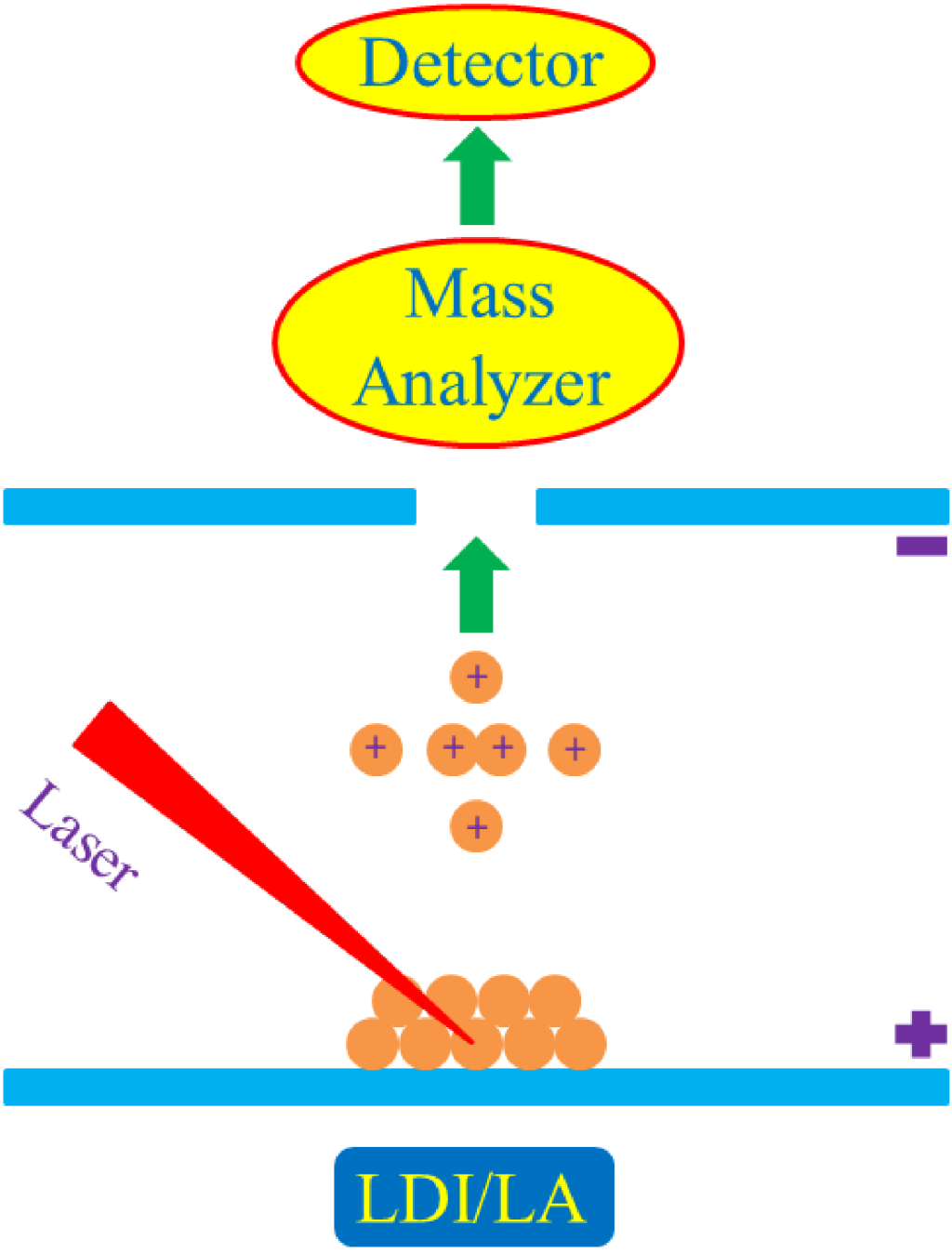

Figure 3. Scheme of the working process of LDI/LA.

1.2. Chalcogenides

Chalcogenide glasses are amorphous materials based on chalcogen elements (sulfur, selenium, or tellurium) in combination with suitable elements from the 14th or 15th group of the periodical system (germanium, arsenic, antimony, etc.). They are high–tech materials with strategic importance for phase change memory devices,[3] optical fibers,[4] and solar cells.[5, 6] An example of the periodic table highlighting chalcogen elements is illustrated in Figure 4. Chalcogenide glasses show a high refractive index, faster optical response time, increased structural stability, wide infrared transparent window, ultra-wide infrared transmission range, better structural stability, extremely high optical nonlinearity, high infrared transmittance, and other excellent performance, so it shows the great potential application in the field of modern integrated optoelectronic devices such as nonlinear integrated optical devices, infrared sensing, electro-photographic, high-density optical storage, holographic storage, bio photonics, etc.[7, 8] Summary of the applications of the chalcogenide glasses is shown in Figure 5.

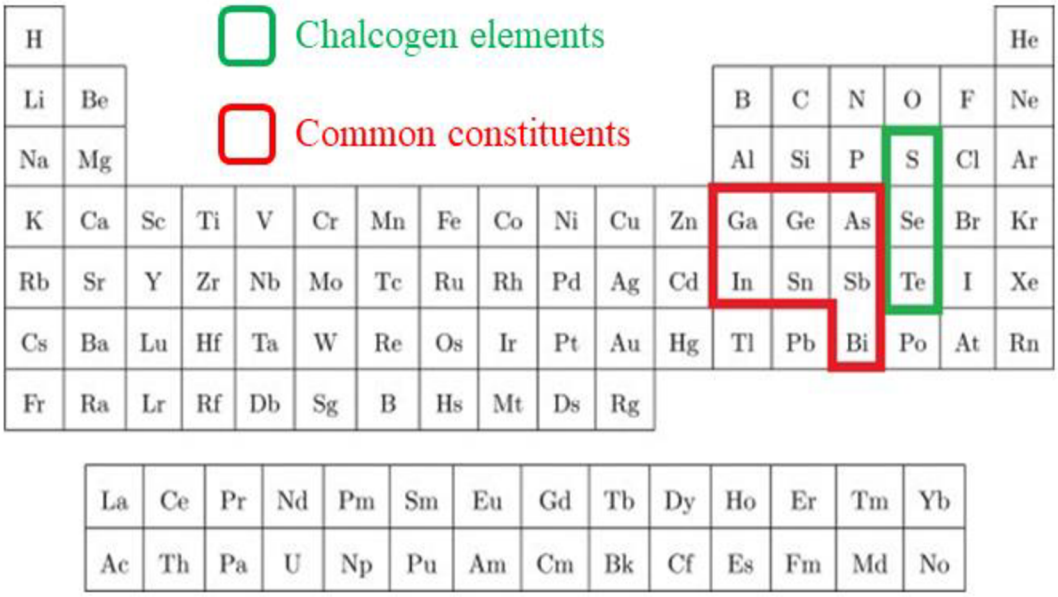

Figure 4. The most frequent elements of chalcogenide materials.

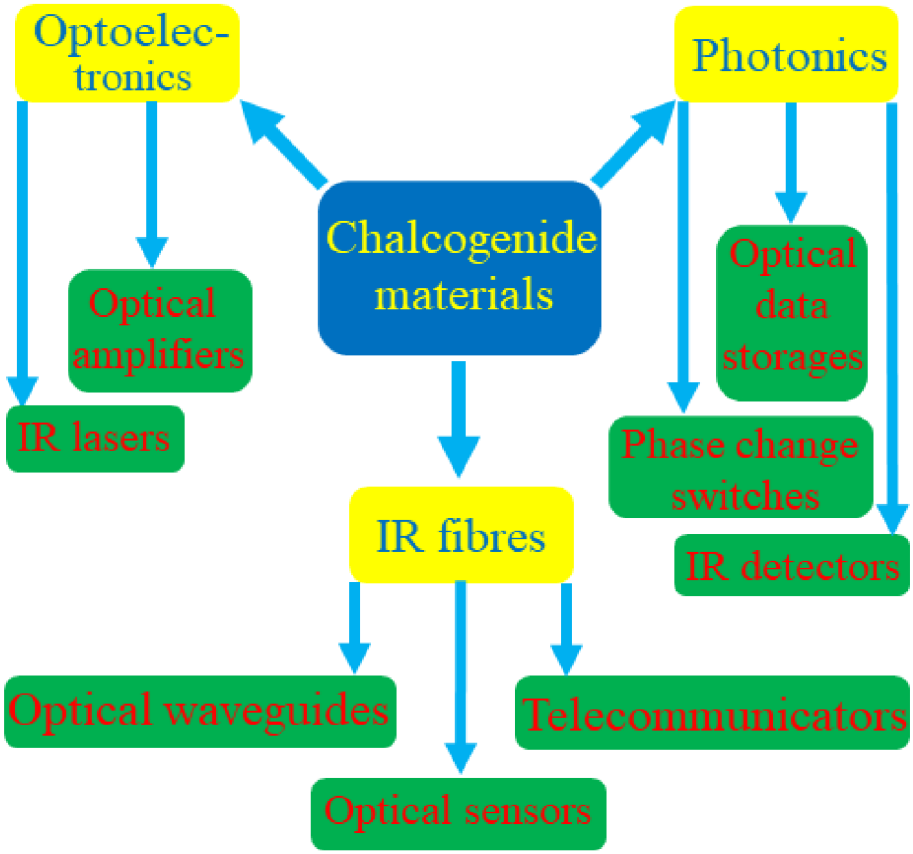

Figure 5. Applications of chalcogenide materials.

A successful example of the application of chalcogenide glass is $Ge_2Sb_2Te_5$ material. Due to the large difference of the atomic level/free electron density, the non-volatility/high stability, and the optical properties in amorphous/crystalline states, Ge-Sb-Te (GST) glass has been successfully developed as phase-change memory,[9-11] electronic nonvolatile memory devices,[12] rewritable optical recording media,[13, 14] and optical limiters.[15] $Ge_2Sb_2Te_5$ material can be produced by sputtering,[16] Pulsed Laser Deposition (PLD),[17-19] evaporation,[20, 21] Chemical Vapor Deposition (CVD),[22, 23] or Atomic Layer Deposition (ALD).[24, 25] The $Ge_2Sb_2Te_5$ bulk material has been studied by laser desorption ionization (LDI). The formation of clusters in binary Ge-Te, Sb-Te, and ternary $Ge_2Sb_2Te_5$ materials was also investigated.[26] Recently, a detailed review of Ge-Sb-Te phase-change non-volatile memories has been published.[27]

1.3. Clusters

The term ‘‘cluster’’ refers to several meanings. In chemistry, the term has been defined as ‘‘*A finite group of metal atoms which are held together mainly, or at least to a significant extent, by bonds directly between the metal atoms, even though some non-metal atoms may also be intimately associated with the cluster*’’ by Frank Albert Cotton in 1964.[28] Now the concept of clusters has evolved into that the clusters are relatively stable microscopic or sub-microscopic aggregates composed of several or even thousands of atoms, molecules, or ions through physical or chemical binding forces. Their physical and chemical properties vary with the number of atoms contained.[29]

A typical example of a cluster is carbon clusters. In 1984, Rohlfing and co-authors[30] used laser evaporation to evaporate graphite and used time-of-flight mass spectrometry to detect a series of peaks of carbon clusters. In 1985, Smalley and co-workers,[31] through the optimization of the clustering process, made the content of cage-like fullerenes composed of five- and six-membered rings such as C_{60} and C_{70} occupy absolute advantage. To date, fullerene can be obtained in large quantities through industrial methods, and it has been found a wide range of applications in chemistry, materials, astronomy, and physics. In 1996, the discoverers of fullerenes were awarded the Nobel Prize in Chemistry. In addition, most importantly, actual cluster products can be obtained by methods such as laser evaporation,[31, 32] glow discharge,[33] arc discharge,[34, 35] microwave plasma method,[36] and flame combustion method.[37-39]

2. Aims of the Dissertation

Amorphous materials, such as chalcogenide glasses, have no regular structure. Therefore, technique like X-ray cannot be used to provide information on the structure of chalcogenide glasses. Mass spectrometry, particularly LA/LDI or MALDI TOF MS, is a vital method with a wide range of applications. It is used to characterize and/or analyse a huge variety of materials. The issue is that we can't use MALDI as ionization technique for the characterization of chalcogenide materials. Instead, we must employ LA or LDI of the materials, both of which cause significant fragmentation.

Aims of Dissertation are focused on mass spectrometry of various types of chalcogenide materials, as shown below.

A) First work

- To study the formation of clusters from various mixtures of antimony and selenium via laser ablation synthesis.
- To evaluate what is going on when some special approaches were applied to the mixture of antimony and selenium in the ratio of 1:1.

B) Second work

- To compare the differences when the Sb_2Se_3 material exhibits in the form of thin films, homemade polycrystalline material, and commercial polycrystalline bulk.
- To study the effect of materials, i.e., graphene, graphene oxide, and C60, for SALDI.

C) Third work

- To evaluate the possibility of mass spectrometry and Raman spectroscopy for the characterization of silver doped chalcogenide glasses.
- To evaluate the possibility of the combination of such very different techniques (non-destructive Raman spectroscopy and destructive Mass spectrometry) help in the characterization of silver doped chalcogenide glasses.

D) Fourth work

- To evaluate the role of the tellurium when it is introduced into Ge-Sb-Se thin films.
- To study the thin films' stability when increasing the tellurium content.

3. Results and Discussion

The Dissertation is focused on LA/LDI/SALDI TOF MS of chalcogenide materials in four different cases, studying 4 different systems and/or materials: i) Generation of clusters from the mixtures of antimony and selenium and suspended in some special solvents ii) Mass spectrometry of Sb_2Se_3 in the form of homemade polycrystalline, thin films, and commercial polycrystalline bulk; iii) Study of silver doping in Ge-Sb-S glasses $(GeS_2)_{50}(Sb_2S_3)_{50}$, 5% Ag doped $(GeS_2)_{50}(Sb_2S_3)_{50}$, and 15% Ag doped $(GeS_2)_{50}(Sb_2S_3)_{50}$; iv) Examination of changes of the tellurium doping Ge-Sb-Se thin films with various Te/Se ratios. As a result, the generation of numerous clusters from these materials is studied and their structure elucidation is discussed.

Other analytical techniques such as energy-dispersive X-ray spectroscopy (EDX), scanning electron microscopy (SEM), Raman spectroscopy, and others have been utilized where necessary.

3.1. Laser Ablation Generation of Antimony Selenide Clusters. Laser Desorption Ionization (LDI) Quadrupole Ion Trap Time of Flight Mass Spectrometry

Antimony forms only a few selenides, for example Sb_2Se_3. Recently, $Ba_2Sb_2Se_5$ and $Ba_6Sb_7Se_{16}$[40] were synthesized via high-temperature solid-state reactions and their structures were determined by single-crystal X-ray diffraction. Even huge [$Sb_{12}Se_{20}^{4-}$] anion was prepared and characterized.[41] Antimony selenide can be made in the form of nano-fibers[42] and is part of Ge-As(Te)-Sb-Se chalcogenide glasses,[43-45] for example. Another example is "classical" GeSbTe (germanium-antimony-tellurium or GST) glass used in rewritable optical discs and phase-change memories. The structures of some selenium and antimony clusters have been determined.[46-49]

In this work, binary system Sb-Se generating new Sb_mSe_n clusters via laser ablation synthesis using antimony-selenium powdered mixtures of elements in various ratios was studied. Mass spectra were recorded using a mass spectrometer of Axima Resonance (Kratos, Manchester, GB) afforded with a quadrupole ion trap and TOF detection. Stoichiometry of Sb_mSe_n clusters was determined by using computer modeling of isotopic envelopes. It demonstrated that a series of Sb_mSe_n clusters ($SbSe_{1-7}$, Sb_2Se, Sb_3Se, *etc.*) were formed. The knowledge gained can contribute to elucidating structural items of Sb_mSe_n materials. The possible structures of Sb_mSe_n clusters were discussed and related to the proposal of manufacturing new chalcogenide glasses phase-change materials.

As illustrated in Figure 6, a sequence of $Sb_mSe_n^+$ clusters, including $SbSe_{1-8}^+$, $Sb_2Se_{1-6}^+$, $Sb_3Se_{1-5}^+$, $Sb_4Se_{1-3}^+$, and $Sb_5Se_{1,2}^+$ was formed in addition to Se_n^+ (n = 4–9) clusters when the amount of selenium was in equal or high excess over antimony. An example of a good agreement between theoretical models and practical results corresponding to overlapping peaks of Se_8^+, $Sb_2Se_5^+$, and $Sb_4Se_2^+$ is shown in Figure 7.

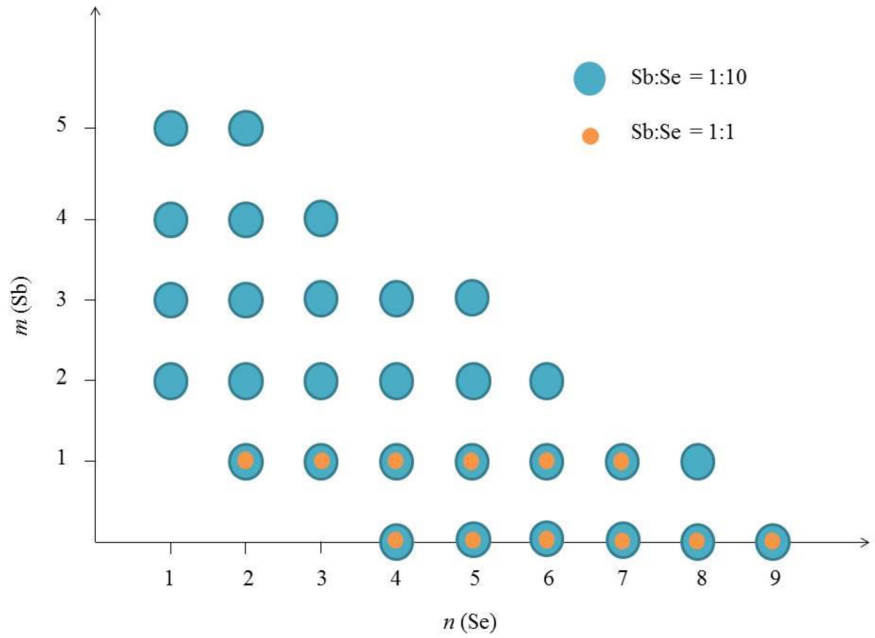

Figure 6. Overview of stoichiometry of Sb_mSe_n clusters generated from Sb:Se = 1:1 and Sb:Se = 1:10.

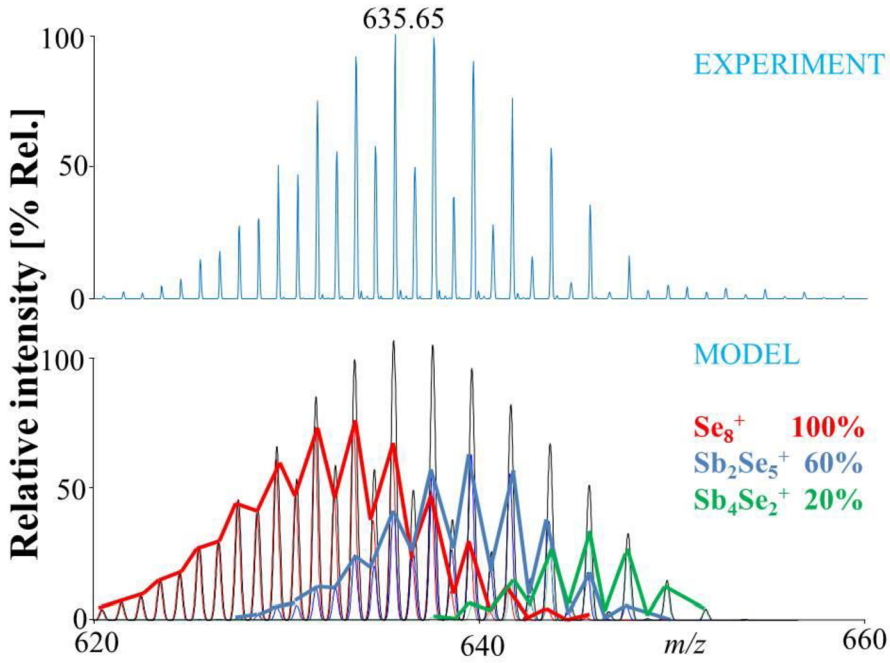

Figure 7. Comparison of experimental and theoretical isotopic patterns for Se_8^+, $Sb_2Se_5^+$, and $Sb_4Se_2^+$.

As our ultimate goal was to produce high-performance phase change memory, we believe that the structure of the material is in some way related to the performance of the phase change memory material. To some extent, the obtained clusters can reflect the structural composition of the chalcogenide glass as shown in Figure 8. This might inspire the preparation of the materials with new properties. It was shown that inorganic materials suspended in parafilm yield more complex clusters in course of laser ablation. Because parafilm consists of paraffins, it is most probable that laser-induced vaporization is not accompanied by any matrix effect like in MALDI. Therefore, we have examined how synthesis goes on when the sample was dispersed in liquid glycerin, ionic liquids, or parafilm as shown in Figure 9.

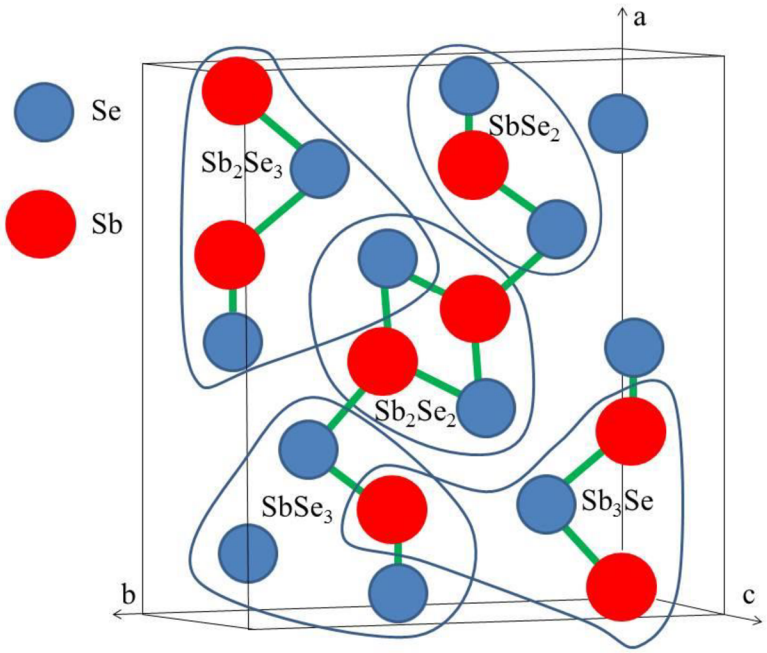

Figure 8. Example of possible formation of some clusters from a 3D structure of antimony selenide.

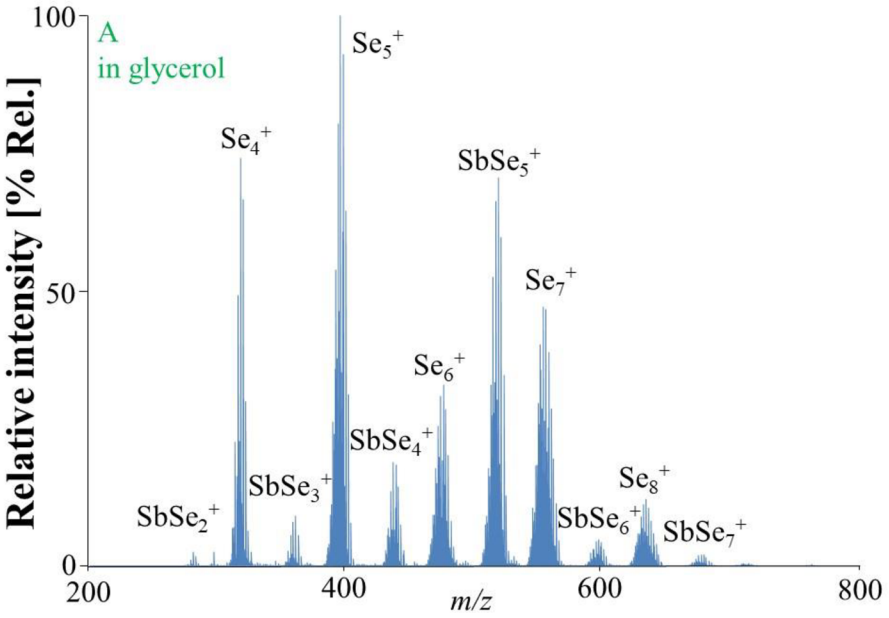
A
in glycerol
Relative intensity [% Rel.]
100
50
0
200
400
600
800
m/z
Se5+
Se4+
SbSe5+
Se7+
Se6+
SbSe4+
SbSe3+
Se8+
SbSe2+
SbSe6+
SbSe7+

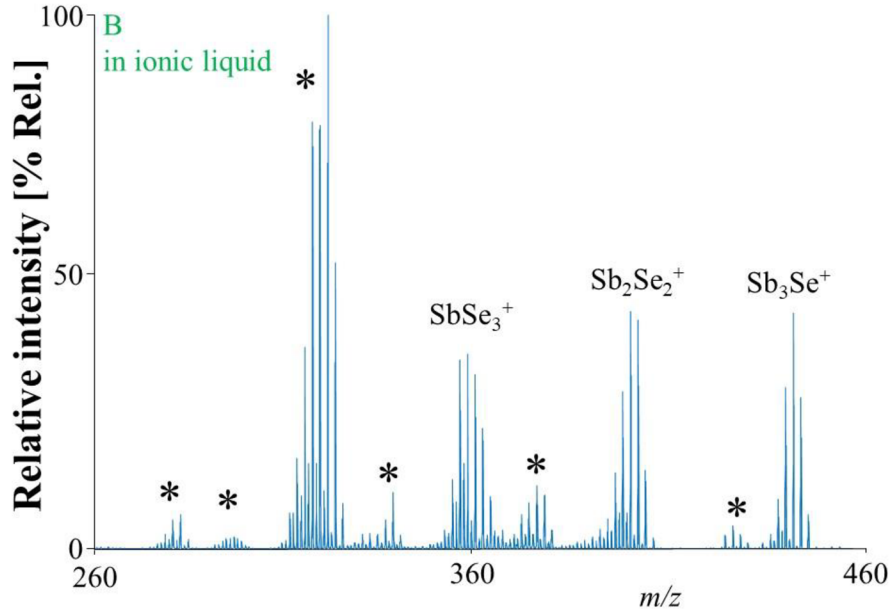
B
in ionic liquid
Relative intensity [% Rel.]
100
50
0
260
360
460
m/z
*
SbSe3+
Sb2Se2+
Sb3Se+

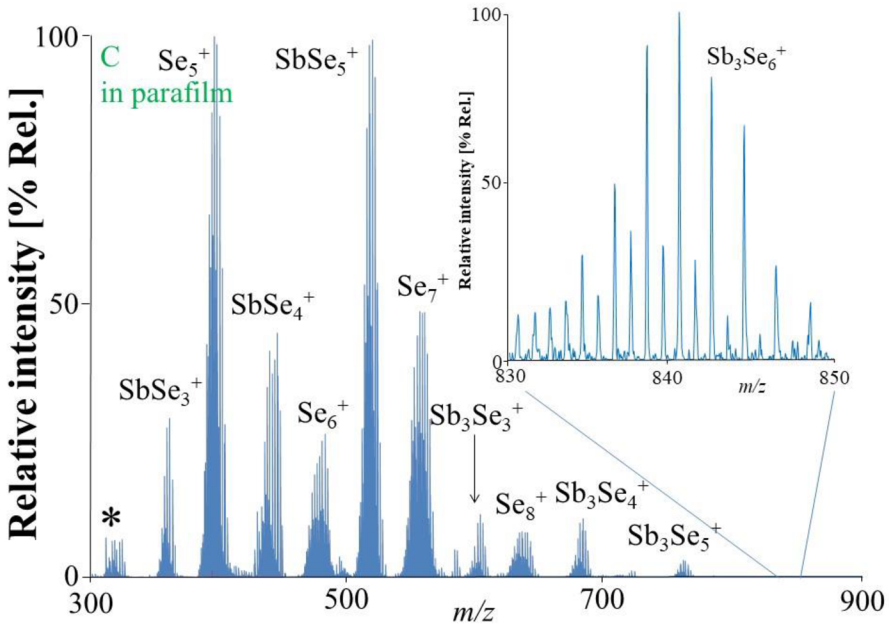

Figure 9. (A) Mass spectra recorded from LDI of Sb:Se mixture in the glycerol with the ratio of elements equal to 1:1. Conditions: positive ion mode, laser energy 130 a.u. (B) Mass spectra recorded from LDI of Sb:Se mixture in the ionic liquid with the ratio of elements equal to 1:1. Conditions: positive ion mode, laser energy 130 a.u. (C) Mass spectra recorded from LDI of Sb:Se mixture in the parafilm with the ratio of elements equal to 1:1. Conditions: positive ion mode, laser energy 160 a.u.; an asterisk (*) means that isotopic pattern is too complex or the spectra intensity is too low to identify clusters.

Concluding, this work describes the application of laser ablation mass spectrometry for binary elemental mixtures. The generation of several new charged clusters has been noted. This work stressed out the possibility of MS instrumentation which can assist as “a synthesizer”, while the process of “synthesis” can be followed by analyzing the formed products by mass spectrometric analysis. The 24 new antimony selenide clusters generated from antimony-selenium powdered mixtures in various ratios demonstrated a powerful methodology of laser ablation generation with quadrupole ion trap time-of-flight mass spectrometry. The results may open the way to preparing high-performance phase change materials with new properties.

3.2. Comparison of clusters produced from Sb_2Se_3 homemade polycrystalline material, thin films, and commercial polycrystalline bulk using laser desorption ionization with time-of-flight quadrupole ion trap mass spectrometry

Sb_mSe_n system is an important member of chalcogenide glasses. Some glasses, for example, Sb_2Se_3, were synthesized via melt-quenched.[50] Their structures were determined by high-temperature Raman spectroscopy and anomalous wide angle X-ray scattering.[51] The Sb_2Se_3, a mineral antimonselite, was discovered in China.[52] To date, Sb_mSe_n glasses are widely used in phase-change memories,[53-55] fabrication of solar cells,[56, 57] and lithium/sodium batteries.[58, 59] In the previous work, we studied the case of clusters produced by mixtures of different ratios of Sb and Se. Some special methods were used to study their effect on these clusters produced by the mixtures. In addition, we also compared the different clusters generated between commercial Sb_2Se_3 compound and mixtures. Finally, we identified 24 new Sb_mSe_n clusters.

In this work, we were dealing with the study of Sb_mSe_n clusters generation from different Sb-Se materials and with the stoichiometry determination of Sb_mSe_n clusters. We do laser ablation synthesis (LAS) of clusters by using the laser in a mass spectrometer. In addition, the deposition of the thin layer of Sb-Se was done by co-sputtering to produce Sb-Se thin layer. This work aimed to study the formation of clusters from the mixtures of elements (Sb+Se), Sb-Se thin layers, and Sb-Se crystalline material (commercial and home-made).

The Sb_2Se_3 glasses in the form of bulk, nanolayer (film), and Sb_2Se_3 crystal were studied via laser desorption ionization (LDI) Time of Flight Mass Spectrometry with Quadrupole Ion Trap Mass Spectrometry (QIT-MS) and stoichiometry of $Sb_mSe_n^{+/-}$ clusters formed was determined.

Some materials that operate as surface-assisted LDI (SALDI) matrices (graphene [G], graphene oxide [GO], and fullerene [C_{60}]) were employed to examine the influence of various surfaces on cluster formation (Figure 10). The use of these SALDI materials, especially GO, can significantly increase the mass spectra intensity.

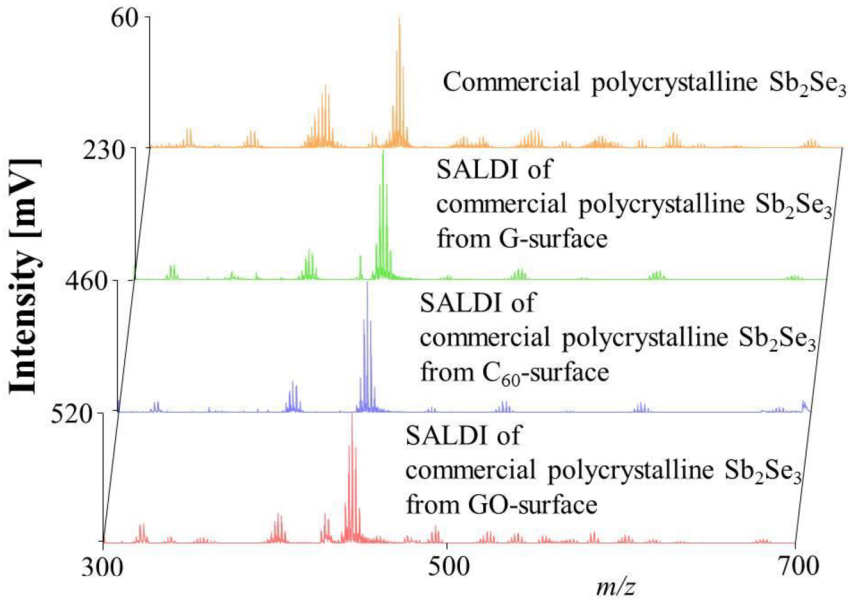

Figure 10. Mass spectra from LDI of commercial polycrystalline Sb_2Se_3 on the surface of GO, C_{60}, and G and on a common metal target in the 300–700 m/z range. Conditions: positive ion mode; 120 a.u. laser energy

To evaluate the stability of the thin film, glass, and Sb_2Se_3 crystal, mass spectra of three materials were measured at the same laser energy (120 a.u.), as shown in Figure 11. At this laser energy, the order of intensity of thin-film, glass, and crystal Sb_2Se_3 decreases, which indicates that the stability of these three materials increases. Both in mass spectra of the glass and Sb_2Se_3 crystal, the most intensive signal is Sb_3Se^+ cluster. Whereas in mass spectra of the thin film, it is Sb_2Se^+ cluster. The highest intensity cluster was observed in mass spectrum of the thin film at laser energy 140–180 a.u. become Sb_3Se^+. In addition, the Sb_2Se_3 crystal produced more clusters. Simply, it was found that Sb_2Se_3 glass is quite stable in comparison to film or crystal, and its mass spectra showed a minimum number of the clusters formed.

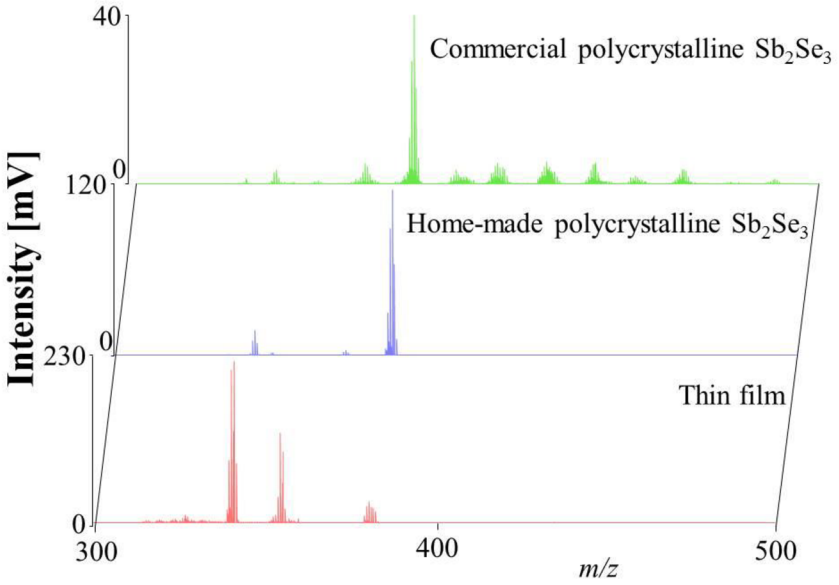

Figure 11. Mass spectra from LDI of commercial and homemade Sb_2Se_3 polycrystalline material as well as amorphous Sb_2Se_3 thin film in the 300–500 *m/z* range. Conditions: positive ion mode; 120 a.u. laser energy

From the Figure 12 we can find that clusters Sb_mSe_n (1,2), (2,1), (2,2), (2,3), (3,0), (3,1), (3,2), (4,0) are common to all precursors. Cluster (1,2) was also observed from the mixture of elements. It indicated that six clusters (1,2), (2,1), (2,2), (2,3), (3,1), (3,2) are common to LAS and LDI. Thus, most probably they are the basic structural units of all materials.

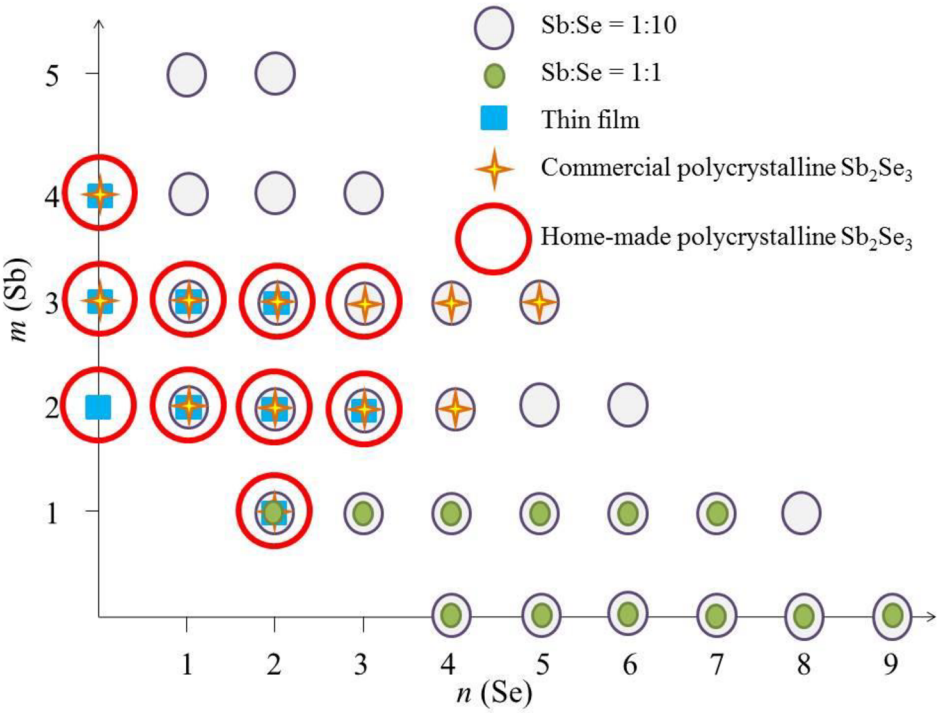

Figure 12. Overview of clusters observed by using paraffin and Sb_mSe_n cluster stoichiometry generated from commercial/homemade Sb_2Se_3 polycrystalline material, amorphous Sb_2Se_3 thin film, and mixtures of antimony with selenium (Sb/Se = 1:1 or 1:10). ★ New clusters by using paraffin; ○ Sb/Se = 1:10; ● Sb/Se = 1:1; ■ thin film; ✦ commercial polycrystalline Sb_2Se_3; ○ home-made polycrystalline Sb_2Se_3

In addition, the effect of paraffin was performed. We found that fragmentation of studied materials can be suppressed by using paraffin, as shown in Figure 13. The role of paraffin is not clear. Perhaps because particles of the material were covered with a paraffin layer which absorbed part of the energy. Therefore, the fragmentation was diminished. It was found that some of the high mass clusters are the summation of observed two lower massive ones (for example $SbSe^+ + Sb_2Se^+$ clusters give $Sb_3Se_2^+$; $SbSe^+ + Sb_2Se_2^+$ clusters give $Sb_3Se_3^+$). However, such a bimolecular reaction is of lower probability. With the use of paraffin, we observed some higher mass clusters. It means that we obtained a relatively more complete part of the unit cell. Briefly, parafilm worked as a protective agent to diminish the fragmentation of the materials, and 6 novel clusters were observed for the first time with the help of using parafilm.

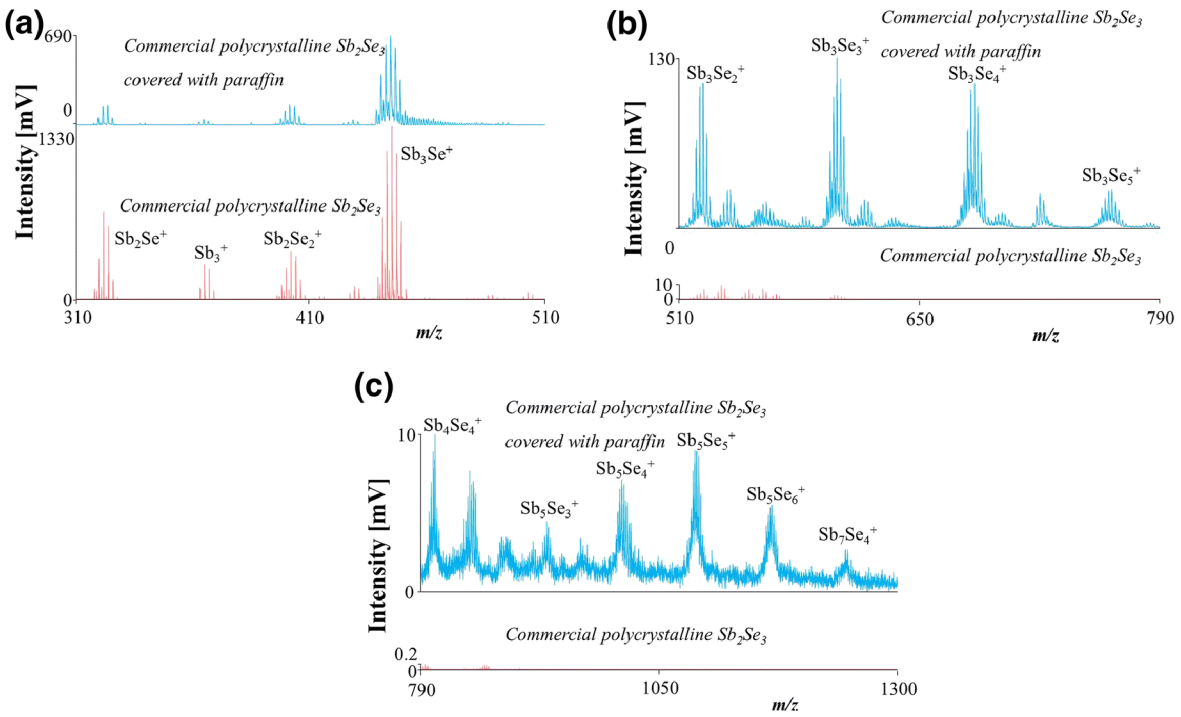

Figure 13. Mass spectra from LDI of commercial polycrystalline Sb2Se3, and the same sample covered with paraffin, (a) in the 310–510 m/z range, (b) in the 510–790 m/z range, and (c) in the 790–1300 m/z range. Conditions: positive ion mode; 160 a.u. laser energy.

Concluding, we have proposed a new methodology of MS structure analysis based on the comparison of clusters obtained via fragmentation of various materials and laser ablation synthesis (LAS). We characterized the structures of the materials using mass spectra obtained from i) laser-induced fragmentation of materials and ii) LAS of the mixture of Sb and Se in different ratios. The clusters produced from different precursors were compared. The obtained results provide a fresh perspective on the application of mass spectrometry and promote the understanding of the structure of the studied materials deeply.

3.3. Laser Desorption Ionization Time-of-Flight Mass Spectrometry of Silver-Doped $(GeS_2)_{50}(Sb_2S_3)_{50}$ Chalcogenide Glasses

The Ge-Sb-S system is a key component of the chalcogenide glasses family. Optical,[60] structural,[61] and mechanical[62] characteristics of Ge-Sb-S glasses have already been investigated. Ag-doped materials have already been found in extensive applications in various fields.[63-67] The optical transmittance, reflectivity, optical gap, and other properties of Ge-Sb-S materials alter with the addition of Ag. Compared to silver-free chalcogenide glasses,[68] the susceptibility to alkaline etching is lower, the index of refraction is higher, and the absorption is red-shifted. Based on these advantages of Ag-doped Ge-Sb-S glasses, besides being utilized in RAM memory, they are also widely used in many other fields, including holographic devices,[69] solid electrolytes,[70] and electrochemical sensors.[71] Inorganic hydrides are a diverse group of chemicals that have been widely studied.[72] The effect of hydrogen on chalcogenide glass fibers optical and emission properties has been investigated.[73, 74] The hydrogenated chalcogenide glasses, on the other hand, were purposefully created and exhibited some distinctive features.[75, 76] As a result, chalcogenide glasses containing hydrogen atoms are potential candidates for increasing performance and even displaying some latent functions. The effects of Ag-doping on the structure and several physical properties[77], and thermokinetic behavior[78] have recently been studied.

In this work, the characterization of $(GeS_2)_{50}(Sb_2S_3)_{50}$ chalcogenide glasses doped with silver by LDI-MALDI-TOF MS and Raman spectroscopy is presented. These glasses were prepared by adding different amounts of silver (5% and 15%, respectively). The obtained mass and Raman spectra were compared with those of silver-free chalcogenide glasses. These studies were well performed with MS spectra in negative and positive modes and Raman spectra. The results were described and discussed in detail. Moreover, the effect of the laser energy in the MS spectra of 5% Ag doped $(GeS_2)_{50}(Sb_2S_3)_{50}$ chalcogenide glass in negative ion mode was also discussed, which allows the determination of the composition of clusters generated by LDI. The present study aimed to elucidate the chemistry of these materials via studying the clusters generated by laser desorption ionization of $(GeS_2)_{50}(Sb_2S_3)_{50}$, 5% Ag doped $(GeS_2)_{50}(Sb_2S_3)_{50}$, and 15% Ag doped $(GeS_2)_{50}(Sb_2S_3)_{50}$, along with the evaluate if such combination of very different techniques might help in characterization of silver doped chalcogenides glasses studied.

This study compared the clusters formed from $(GeS_2)_{50}(Sb_2S_3)_{50}$, and two different Ag doped chalcogenide glasses (5% Ag doped $(GeS_2)_{50}(Sb_2S_3)_{50}$ and 15% Ag doped $(GeS_2)_{50}(Sb_2S_3)_{50}$) using laser desorption ionization (LDI) time of flight coupled with quadrupole ion trap mass spectrometry. The stoichiometry of these generated clusters was also investigated. The experimental results showed that, in addition to SbS_c^+ (c = 1, 2), $Sb_2S_c^+$ (c = 1–3), $Sb_3S_c^+$ (c = 1–5), $Sb_4S_c^+$ (c = 3, 4), $Sb_5S_2^+$, and Sb_c^+ (c = 3, 5) clusters, many Ag contained clusters, Ag_a^+ (a = 1, 2), $AgGeS^+$, $AgSb_b^+$ (b = 1, 2, 4), $AgSbS^+$, $AgSb_2S_c^+$ (c = 1–5), $AgSb_3S_3^+$, $AgSb_4S_4^+$, $Ag_2Sb_3S_c^+$ (c = 4, 5), $Ag_4Sb_2S_3^+$, and $Ag_5SbS_3^+$ were generated. Without the addition of silver, no Ge-containing clusters were detected as shown in Figure 14. However, when doping with silver, only one Ge-containing cluster was observed.

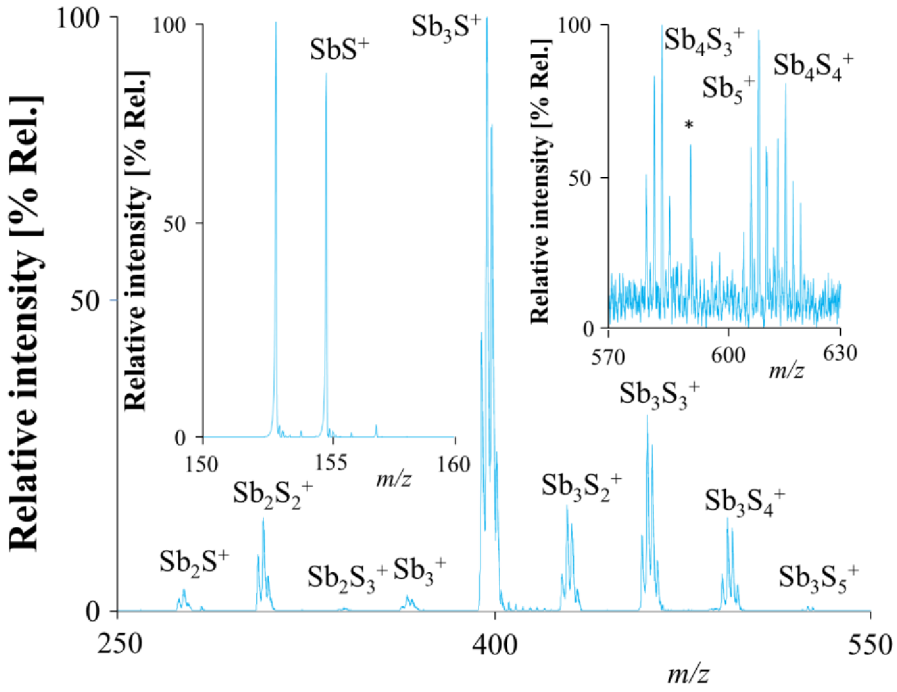

Figure 14. Mass spectra of $(GeS_2)_{50}(Sb_2S_3)_{50}$ glass. Insets show the mass spectra in 150-160 and 570-630 *m/z* ranges. Conditions: positive ion mode; laser energy 170 a.u. * means the isotopic pattern is too complex or the spectra intensity is too low to identify clusters.

The novelty and motivation of this work were based on the use of two different techniques, non-destructive Raman spectrometry (as shown in Figure 15) and destructive LDI TOF MS, to determine the structure of silver doped Ge-Sb-S glasses. In spite of the fact that the level of hydrogen in glasses studied is very low (not detectable by Raman spectroscopy), we have shown by MS how hydrogen contaminant is reacting with glass components, preferably with sulfur, silver, and antimony. The formation of mixed hydrides was also discovered as shown in Figure 16. The formation of hydrides in glasses detected by MS was probably reported in this work for the first time.

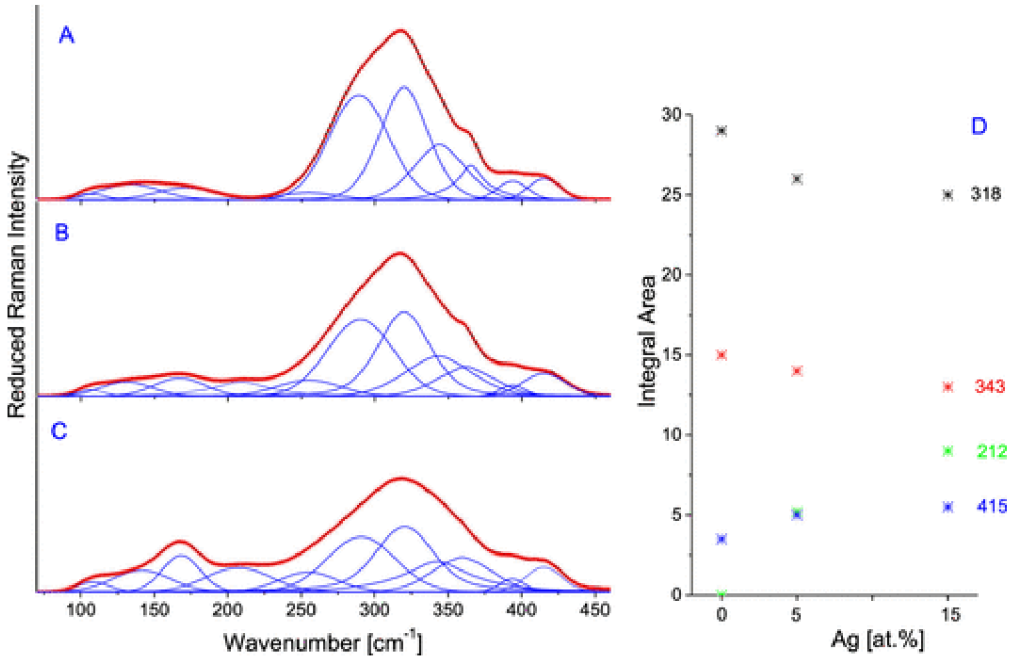

Figure 15. Raman spectra of (A) $(GeS_2)_{50}(Sb_2S_3)_{50}$, (B) 5% Ag-doped glass, and (C) 15% Ag-doped glass and (D) comparison of the integral intensities of the Raman bands at 212, 318, 343, and 415 cm^{-1}.

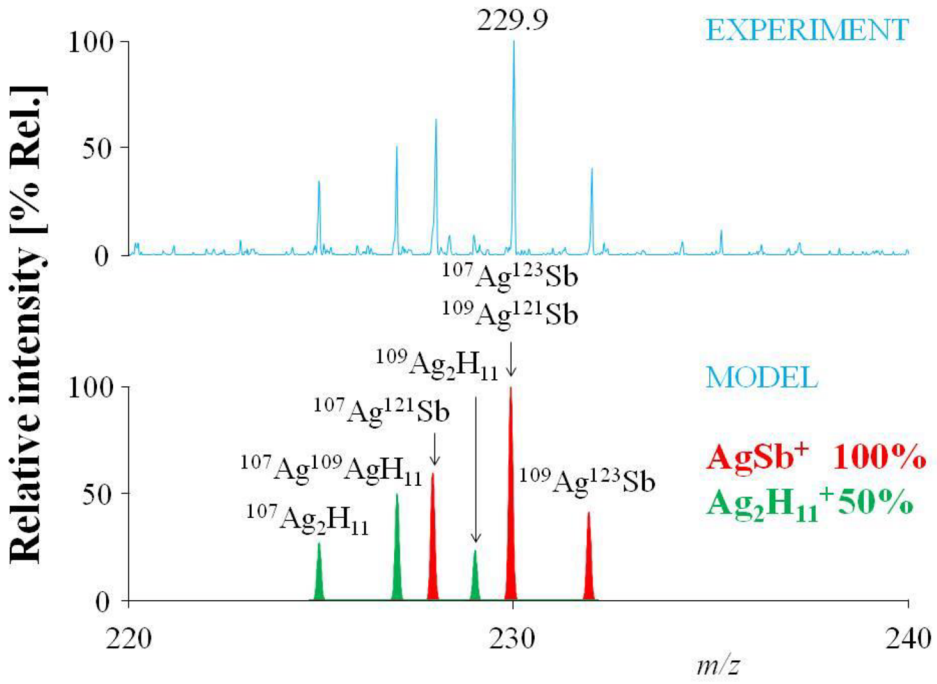

Figure 16. Comparison of experimental and theoretical isotopic patterns for overlap of $AgSb^+$ and $Ag_2H_{11}^+$ clusters. Conditions: positive ion mode; laser energy 170 a.u.

Finally, we compared the results of Raman with Mass Spectra in this work. As shown in Table 1, some structural units detected by Raman were not observed by MS and vice versa. Few units were detected in both techniques (for example, Sb-Sb). The ions detected by MS are mostly fragments of these structural units or they can be products of reactions in plasma plume (which are difficult to identify and/or eliminate).

Table 1 Comparison of the results of Raman spectroscopy with Mass Spectrometry

Structural units detected by Raman Spectroscopy	Band position cm^{-1}	**Fragments* detected by Mass Spectrometry**
Ge-Ge	250	No fragments detected
corner–shared GeS_4 tetrahedral	343 and 390	
edge-shared GeS_4 tetrahedral	360	
S_3Ge-GeS_3 ethane-like structure	250	
S_3Ge-S-GeS_3	415	
Sb-Sb	170	Sb^+ Sb-Sb^+ Sb_3^+ Sb_5^+
SbS_3 pyramids	290 and 318	SbS^+ SbS_2^+ Sb_2S^+ $Sb_2S_2^+$ $Sb_2S_3^+$
S_2Sb-SbS_2 bi-pyramidal	170	Sb_3S^+ $Sb_3S_2^+$ $Sb_3S_3^+$ $Sb_3S_4^+$ $Sb_3S_5^+$ $Sb_4S_3^+$ $Sb_4S_4^+$ $Sb_5S_2^+$
Ag-S	212	Ag^+ Ag_2^+
Ag_2GeS_3 amorphous phase	Not detected	$AgGeS^+$
Ag-S-Sb structural units	Not detected	$AgSb^+$ $AgSb_2^+$ $AgSb_4^+$ $AgSbS^+$ $AgSb_2S^+$ $AgSb_2S_2^+$ $AgSb_2S_3^+$ $AgSb_2S_4^+$ $AgSb_2S_5^+$ $AgSb_3S_3^+$ $AgSb_4S_4^+$ $Ag_2Sb_3S_4^+$ $Ag_2Sb_3S_5^+$ $Ag_4Sb_2S_3^+$ $Ag_5SbS_3^+$

*Fragments might be also including reaction products formed in the plasma plume

Concluding, LDI can efficiently generate clusters from the Ge-Sb-S and its Ag-doped chalcogenide glasses using Time-Of-Flight (TOF) mass spectrometry (MS). LDI TOF MS can also be used to determine the composition of clusters. The methodology has already been shown to be a powerful method for studying the formation of various clusters from inorganic compounds. We showed that the Ge-containing cluster was not observed when LDI of non-doped $(GeS_2)_{50}(Sb_2S_3)_{50}$ glass was carried out. In the case of $(GeS_2)_{50}(Sb_2S_3)_{50}$ glass doped with silver, only one Ge-containing cluster was generated. Despite the studied materials made from 5N purity of elements (Ag, Ge, Sb, and S), seven hydrogenated clusters, $SbS_3H_8^+$, $Sb_4S_2H^+$, $Ag_2H_{11}^+$, $Ag_2Sb_3H_4^+$, $Ag_3Sb_2H_4^+$, $Ag_4Sb_2H_2^+$, and $Ag_4S_3H_8^+$, were detected. A comparison of Raman spectroscopy analysis and MS results help to understand the structure of the silver-doped Ge-Sb-S chalcogenide glasses. These results enable us to understand the structural motifs of the Ag-doped Ge-Sb-S chalcogenide glasses. Moreover, the findings obtained can contribute to proposing new and more efficient phase-change memory materials.

3.4. Ge-Sb-Se-Te Thin Films: Clusters Formation by Laser Ablation and Comparison with Clusters from Mixtures of Elements

Chalcogenides, containing Ge, S, Se, or Sb as their main components, are widely applied in many applications[79-82] because of the distinct advantages of high (non)linear refractive index, broad transmission window in IR spectral region, and photosensitivity to light exposure.[7, 45, 83-85]

Ternary Ge-Sb-Se glasses are important members of the chalcogenide range of glasses and their properties such as optical, physicochemical, and elastic-plastic have been intensively studied.[86-93] However, the short-wavelength weak absorption tail of the Ge-Sb-Se glasses is excessively high, which strongly enhances attenuation loss in the fibers. Since the weak absorption tail usually comes from structural defects in the glass network,[94] this tail is difficult to be removed once the composition or glass structure is determined. Even the introduction of a low percentage of Te into these glasses alters the glassy structure and leads to the fact that doped glasses present photosensitivity, high refractive index values, and transparency in the infrared spectral region.[95, 96] Furthermore, the properties of Ge-Sb-Se-Te glasses, such as structure,[97] crystallization kinetics,[98, 99] glass-forming ability,[100] and amorphous-crystallization transformation,[95] have been studied. The results showed that such quaternary system glasses are potential candidates for the application of integrated optics.

The Ge-Sb-Se bulk glasses have been studied by laser desorption ionization.[43] However, the role and chemistry changes are not sufficiently explained when doping of Te to Ge-Sb-Se material. This work aimed to evaluate the changes in glass chemistry when Se is partially replaced with Te by studying clusters formed by using laser ablation of Te doping Ge-Sb-Se thin films with varying ratios of Te to Se. A summary of thin-film deposition parameters with their chemical composition of the produced thin films is listed in Table 2.

This study compared the stoichiometry of clusters generated via laser ablation quadrupole ion trap time of flight mass spectrometry of Te doped Ge-Sb-Se thin films with those of non-Te doped Ge-Sb-Se thin films and elemental mixtures. By comparing the clusters obtained from Ge-Sb-Se-Te and Ge-Sb-Se thin films, it was found that 16 clusters were observed from Te doping Ge-Sb-Se thin films which are fewer than those from Ge-Sb-Se of 26 clusters (9 clusters $Sb_{1,3}^+$, $SbSe^+$, $Sb_2Se_{1,2}^+$, and $Sb_3Se_{1-4}^+$ are

common to each other). It shows that the introduction of Te to Ge-Sb-Se thin films can stabilize the system. The details of clusters are shown in Table 3. The clusters produced by Te-doped thin films exhibited the same behavior (Figure 17). The stability of the thin film increases with the mass fractions of Te increasing. The missing (Se_2^+, $Ge_{1-4}Sb^+$, and $GeSe_{1-2}^+$) and new (Ge^+ and $Sb_{1-3}Te^+$) clusters indicated that Ge and Se were partially replaced by Te. In addition, when comparing the clusters generated from Ge-Sb-Se-Te thin films with those from the mixtures of the elements (an example of the mass spectra of germanium-antimony mixtures with different molar ratios is shown in Figure 18) of Ge-Sb-Se-Te, only 2 clusters Sb_3^+ and $SbSe^+$ are the same.

Table 2. The summary of deposition parameters of Ge-Sb-Se-Te thin films. Chemical composition (±1 at. %) was determined by EDS

Film Nr.	Sputtering target	Power (W)	Ar pressure (Pa)	Composition (at. %)
1	$Ge_{19.4}Sb_{16.7}Se_{58.9}Te_5$	10	0.5	$Ge_{22.0}Sb_{16.9}Se_{54.6}Te_{6.5}$
2		10	1	$Ge_{19.5}Sb_{16.6}Se_{56.5}Te_{7.4}$
3		15	0.5	$Ge_{20.7}Sb_{17.3}Se_{55.0}Te_{6.9}$
4		15	1	$Ge_{19.3}Sb_{17.0}Se_{56.4}Te_{7.4}$
5	$Ge_{19.4}Sb_{16.7}Se_{53.9}Te_{10}$	10	0.5	$Ge_{21.7}Sb_{17.9}Se_{49.8}Te_{10.7}$
6		10	1	$Ge_{19.3}Sb_{17.4}Se_{51.2}Te_{12.1}$
7		15	0.5	$Ge_{20.5}Sb_{18.1}Se_{50.1}Te_{11.3}$
8		15	1	$Ge_{20.0}Sb_{17.7}Se_{50.9}Te_{11.4}$
9	$Ge_{19.4}Sb_{16.7}Se_{48.9}Te_{15}$	10	0.5	$Ge_{21.3}Sb_{18.1}Se_{45.6}Te_{15.0}$
10		10	1	$Ge_{19.9}Sb_{17.6}Se_{46.4}Te_{16.2}$
11		15	0.5	$Ge_{19.4}Sb_{19.1}Se_{45.0}Te_{16.6}$
12		15	1	$Ge_{19.1}Sb_{17.9}Se_{46.0}Te_{16.9}$
13	$Ge_{19.4}Sb_{16.7}Se_{43.9}Te_{20}$	10	0.5	$Ge_{19.1}Sb_{17.4}Se_{42.1}Te_{21.4}$
14		10	1	$Ge_{17.8}Sb_{19.8}Se_{39.8}Te_{22.7}$
15		15	0.5	$Ge_{18.7}Sb_{20.2}Se_{39.3}Te_{21.7}$
16		15	1	$Ge_{17.7}Sb_{19.7}Se_{40.0}Te_{22.6}$

Table 3. Clusters generated from Ge-Sb-Se bulk glasses, Ge-Sb-Te thin layers/bulk glasses, and Ge-Sb-Se-Te thin films

System	Clusters					References
Ge-Sb-Se	Se_2^+					[27]
	Sb^+	Sb_3^+				
	$GeSb_3^+$	$Ge_2Sb_3^+$	$Ge_3Sb_3^+$	$Ge_4Sb_3^+$		
	$GeSe^+$	$GeSe_2^+$				
	$SbSe^+$	$SbSe_2^+$				
	Sb_2Se^+	$Sb_2Se_2^+$	$Sb_2Se_3^+$	$Sb_2Se_4^+$		
	Sb_3Se^+	$Sb_3Se_2^+$	$Sb_3Se_3^+$	$Sb_3Se_4^+$	$Sb_3Se_5^+$	
	$GeSbSe_2^+$	$GeSb_4Se^+$	$GeSb_5Se^+$			
	$Ge_9Sb_2Se_5^+$	$Ge_9Sb_2Se_6^+$	$Ge_9Sb_2Se_7^+$			
Ge-Sb-Te	Ge^+	Ge_2^+				[32]
	Te_2^+	Te_3^+				
	$GeTe^+$	$GeTe_2^+$				
	$SbTe_2^+$					
	Sb_2Te^+	$Sb_2Te_3^+$				
	Sb_3Te^+					
	$GeSbTe_2^+$	$GeSbTe_3^+$				
Ge-Sb-Se-Te	Ge^+					This work
	Sb^+	Sb_3^+				
	$SbSe^+$					
	Sb_2Se^+	$Sb_2Se_2^+$				
	Sb_3Se^+	$Sb_3Se_2^+$	$Sb_3Se_3^+$	$Sb_3Se_4^+$		
	$TeSb^+$	$TeSb_2^+$	$TeSb_3^+$			
	Sb_3SeTe^+					
	$Ge_4SbSe_4^+$					
	$GeSb_2SeTe_2^+$					

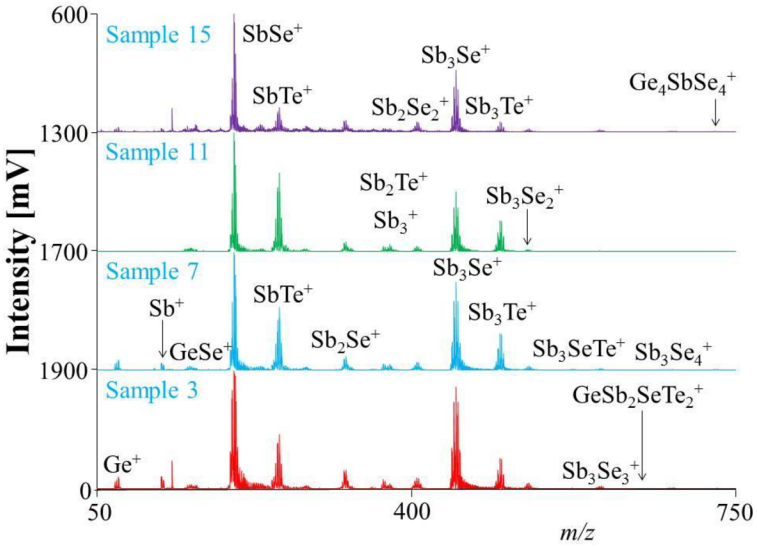

Figure 17. LA TOFMS data of Ge-Sb-Se-Te thin films in the 50-750 *m/z* range. Conditions: positive ion mode; laser energy 150 a.u.

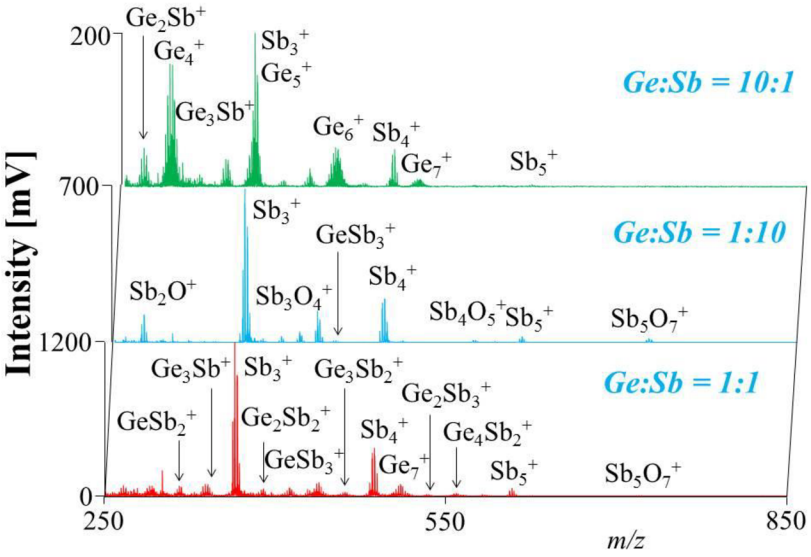

Figure 18. Mass spectra from LAS of germanium-antimony mixtures with different molar ratios in the 250-650 *m/z* range. Conditions: positive ion mode; laser energy 120 a.u.

In conclusion, this work brings new and important information about structural units, clusters, and their stoichiometry, which exist in thin films deposited by magnetron sputtering using laser ablation quadrupole ion trap time of flight mass spectrometry. Studied chalcogenide material belongs to so-called phase-change materials, which were investigated for their real and potential applications in electronics and optoelectronics. It demonstrated that the replacement of selenium with tellurium caused fewer clusters to form, which indicates more excellent stability of the Te doped thin films. Furthermore, we found that the stability of thin film improves as the amount of tellurium in the thin film rises. Apart from this, nine clusters ($Sb_{1,3}^+$, $SbSe^+$, $Sb_2Se_{1,2}^+$, and $Sb_3Se_{1\text{-}4}^+$) are the same as those generated from the non-Te doped thin films. The structure of Te doped Ge-Sb-Se thin films was discussed. When comparing species formed from Te-doped thin films to those obtained from non-Te doped thin films, we found that i) Ge containing species $Ge_{1\text{-}4}Sb^+$ and $GeSe_{1\text{-}2}^+$ as well as Se_2^+ cluster were missing; ii) $Sb_{1\text{-}3}Te^+$ and Ge^+ clusters are new; iii) $Sb_{1,3}^+$ and most Sb-Se clusters are the same. These findings indicate that Ge and Se were partially replaced by Te or the bonds -Se-Se-, -Ge-Sb-, -Ge-Se- were combined with others. The results obtained are a new contribution to mass spectrometry and are helpful to understand better the structure of the Te doped Ge-Sb-Se thin films.

4. Conclusions

The results obtained indicate that LA/LDI TOF mass spectrometry is a powerful approach for characterizing diverse chalcogenide materials such as Sb_2Se_3 glasses/thin films, silver doped/non-doped $(GeS_2)_{50}(Sb_2S_3)_{50}$ glasses, and Germanium-antimony-selenium-tellurium thin films. The use of "protective agents" like paraffin not only helps to reduce the fragmentation of the materials studied (formation of higher mass clusters) but also increases the intensity of mass spectra in the high mass range. Mass spectrometry was also shown to be a viable approach for elucidating the basic structural components of diverse materials by evaluating the stoichiometry of clusters. Understanding the stoichiometry of clusters may aid in understanding the processes taking place in the plasma plume.

In general, the findings could aid in the development of innovative materials with unique features.

5. References

1. Danzer, K.: Analytical Chemistry: theoretical and metrological fundamentals. Springer Science & Business Media, (2007)

2. Houck, M.M., Siegel, J.A.: Illicit drugs. Fundamentals of forensic science, pp 315-352 (2015)

3. Jiang, F., Okuda, M.: The effect of doping on the erasure speed and stability of reversible phase-change optical recording films. *Jpn. J. Appl. Phys*. 30, 97 (1991)

4. Gannon, J.R.: In Materials for mid-infrared waveguides, Infrared Fibers, International Society for Optics and Photonics, pp 62-68 (1981)

5. Carlson, D.E., Wronski, C.R.: Amorphous silicon solar cell. *Appl. Phys. Lett*. 28, 671-673 (1976)

6. Kushwaha, N., Kushwaha, V., Shukla, R., Kumar, A.: Effect of lead additive on photoconductive properties of Se-Te chalcogenide films. *J. Non-Crystal. Solids*. 351, 3414-3420 (2005)

7. Zakery, A., Elliott, S.: Optical properties and applications of chalcogenide glasses: a review. *J. Non-Crystal. Solids*. 330, 1-12 (2003)

8. Adam, J.-L., Zhang, X.: Chalcogenide glasses: preparation, properties, and applications. Woodhead publishing, (2014)

9. Wuttig, M., Yamada, N.: Phase-change materials for rewriteable data storage. *Nat. Mater*. 6, 824-832 (2007)

10. Kolobov, A.V., Fons, P., Frenkel, A.I., Ankudinov, A.L., Tominaga, J., Uruga, T.: Understanding the phase-change mechanism of rewritable optical media. *Nat. Mater*. 3, 703-708 (2004)

11. Qureshi, M.K., Srinivasan, V., Rivers, J.A.: In Scalable high performance main memory system using phase-change memory technology, Proceedings of the 36th annual international symposium on Computer architecture, pp 24-33 (2009)

12. Nakayama, K., Kojima, K., Hayakawa, F., Imai, Y., Kitagawa, A., Suzuki, M.: Submicron nonvolatile memory cell based on reversible phase transition in chalcogenide glasses. *Jpn. J. Appl. Phys*. 39, 6157 (2000)

13. Ohta, T.: Phase-change optical memory promotes the DVD optical disk. J. Optoelectron. *Adv. Mater*. 3, 609-626 (2001)

14. Kuwahara, M., Takehara, S., Kashihara, Y., Watabe, K., Nakano, T., Tanaka, M., Nakamura, N., Ohsawa, H., Satoh, H.: Experimental study of high-density rewritable optical disk using a blue-laser diode. *Jpn. J. Appl. Phys*. 42, 1068 (2003)

15. Sarangan, A., Duran, J., Vasilyev, V., Limberopoulos, N., Vitebskiy, I., Anisimov, I.: Broadband reflective optical limiter using GST phase change material. *IEEE Photonics J*. 10, 1-9 (2018)

16. Bakan, G.: Electrothermal characterization of phase-change films and devices. *Anadolu University Journal of Science and Technology A-Applied Sciences and Engineering*, 18, 1057-1065 (2017)

17. Němec, P., Nazabal, V., Moréac, A., Gutwirth, J., Beneš, L., Frumar, M.: Amorphous and crystallized Ge–Sb–Te thin films deposited by pulsed laser: Local structure using Raman scattering spectroscopy. *Mater. Chem. Phys*. 136, 935-941 (2012)

18. Němec, P., Moréac, A., Nazabal, V., Pavlišta, M., Přikryl, J., Frumar, M.: Ge–Sb–Te thin films deposited by pulsed laser: An ellipsometry and Raman scattering spectroscopy study. *J. Appl. Phys*. 106, 103509 (2009)

19. Yoon, H., Jo, W., Lee, E., Lee, J., Kim, M., Lee, K., Khang, Y.: Generation of phase-change Ge–Sb–Te nanoparticles by pulsed laser ablation. *J. Non-Crystal. Solids*. 351, 3430-3434 (2005)

20. Orava, J., Wágner, T., Šik, J., Přikryl, J., Frumar, M., Beneš, L.: Optical properties and phase change transition in $Ge_2Sb_2Te_5$ flash evaporated thin films studied by temperature dependent spectroscopic ellipsometry. *J. Appl. Phys*. 104, 043523 (2008)

21. Wágner, T., Orava, J., Přikryl, J., Kohoutek, T., Bartos, M., Frumar, M.: Medium-term thermal stability of amorphous $Ge_2Sb_2Te_5$ flash-evaporated thin films with regards to change in structure and optical properties. *Thin solid films*, 517, 4694-4697 (2009)

22. Kim, R.-Y., Kim, H.-G., Yoon, S.-G.: Structural properties of $Ge_2Sb_2Te_5$ thin films by metal organic chemical vapor deposition for phase change memory applications. *Appl. Phys. Lett*. 89, 102107 (2006)

23. Choi, B.J., Choi, S., Shin, Y.C., Hwang, C.S., Lee, J.W., Jeong, J., Kim, Y.J., Hwang, S.-Y., Hong, S.K.: Cyclic PECVD of $Ge_2Sb_2Te_5$ films using metallorganic sources. *J. Electrochem. Soc*. 154, H318 (2007)

24. Choi, B.J., Choi, S., Shin, Y.C., Kim, K.M., Hwang, C.S., Kim, Y.J., Son, Y.J., Hong, S.K.: Combined atomic layer and chemical vapor deposition, and selective growth of $Ge_2Sb_2Te_5$ films on TiN/W contact plug. *Chem. Mater*. 19, 4387-4389 (2007)

25. Lee, J., Choi, S., Lee, C., Kang, Y., Kim, D.: GeSbTe deposition for the PRAM application. *Appl. Surf. Sci*. 253, 3969-3976 (2007)

26. Houška, J., Peña-Méndez, E.M., Kolář, J., Přikryl, J., Pavlišta, M., Frumar, M., Wágner, T., Havel, J.: Laser desorption time-of-flight mass spectrometry of atomic switch memory $Ge_2Sb_2Te_5$ bulk materials and its thin films. *Rapid Commun. Mass Spectrom*. 28, 699-704 (2014)

27. Guo, P., Sarangan, A.M., Agha, I.: A review of germanium-antimony-telluride phase change materials for non-volatile memories and optical modulators. *Appl. Sci*. 9, 530 (2019)

28. Cotton, F.A.: Metal atom clusters in oxide systems. Inorg. Chem. 3, 1217-1220 (1964)

29. Luo, Z., Khanna, S.N.: An Overview of Metal Clusters and Their Reactivity. In: Metal Clusters and Their Reactivity. Springer, Singapore, pp 1-9 (2020)

30. Rohlfing, E. A., Cox, D. M., Kaldor, A.: Production and characterization of supersonic carbon cluster beams. *J. Chem. Phys*. 81, 3322-3330 (1984)

31. Kroto, H.W., Heath, J.R., O'Brien, S.C., Curl, R.F., Smalley, R.E.: C_{60}: buckminsterfullerene. *Nature* 318, 162-163 (1985)

32. Xie, S.-Y., Huang, R.-B., Ding, J., Yu, L.-J., Wang, Y.-H., Zheng, L.-S.: Formation of buckminsterfullerene and its perchlorinated fragments by laser ablation of perchloroacenaphthylene. *J. Phys. Chem. A* 104, 7161-7164 (2000)

33. Krätschmer, W., Lamb, L.D., Fostiropoulos, K., Huffman, D.R.: Solid C_{60}: a new form of carbon. *Nature* 347, 354-358 (1990)

34. Xie, S.-Y., Huang, R.-B., Chen, L.-H., Huang, W.-J., Zheng, L.-S.: Glow discharge synthesis and molecular structures of perchlorofluoranthene and other perchlorinated fragments of buckminsterfullerene. *Chem. Commun*. 2045-2046 (1998)

35. Xie, S.-Y., Huang, R.-B., Deng, S.-L., Yu, L.-J., Zheng, L.-S.: Synthesis, separation, and characterization of fullerenes and their chlorinated fragments in the glow discharge reaction of chloroform. *J. Phys. Chem. B* 105, 1734-1738 (2001)

36. Xie, S.-Y., Deng, S.-L., Huang, R.-B., Yu, L.-J., Zheng, L.-S.: Five isomers of C_{60} generated in microwave plasma of chloroform. *Chem. Phys. Lett*. 343, 458-464 (2001)

37. Howard, J.B, McKinnon, J.T., Makarovsky, Y., Lafleur, A.L., Johnson, M.E.: Fullerenes C_{60} and C_{70} in flames. *Nature* 352, 139-141 (1991)

38. Gao, Z.-Y., Jiang, W.-S., Sun, D., Xie, S.-Y., Huang, R.-B., Zheng, L.-S.: Synthesis of C_{3v}-$^{\#1911}$C64H4 using a low-pressure benzene/oxygen diffusion flame: Another pathway toward non-IPR fullerenes. *Combust. Flame*. 157, 966-969 (2010)

39. Weng, Q.-H., He, Q., Liu, T., Huang, H.-Y., Chen, J.-H., Gao, Z.-Y., Xie, S.-Y., Lu, X., Huang, R.-B., Zheng, L.-S.: Simple combustion production and characterization of octahydro [60] fullerene with a non-IPR C_{60} cage. *J. Am. Chem. Soc*. 132, 15093-15095 (2010)

40. Wang, J., Lee, K., Kovnir, K.: Synthesis, crystal structure, and thermoelectric properties of two new barium antimony selenides: $Ba_2Sb_2Se_5$ and $Ba_6Sb_7Se_{16}$. *J. Mater. Chem. C*. 3, 9811-9818 (2015)

41. Martin, T.M., Wood, P.T., Kolis, J.W.: Synthesis and structure of an $[Sb_{12}Se_{20}]^{4-}$ salt: The largest molecular zintl ion. *Inorg. Chem*. 33, 1587-1588 (1994)

42. Yang, R. B., Bachmann, J., Pippel, E., Berger, A., Woltersdorf, J., Gösele, U., Nielsch, K.: Pulsed Vapor-Liquid-Solid Growth of Antimony Selenide and Antimony Sulfide Nanowires. *Adv. Mater*. 21, 3170-3174 (2009)

43. Šútorová, K., Prokeš, L., Nazabal, V., Bouška, M., Havel, J., Němec, P.: Laser desorption ionisation time-of-flight mass spectrometry of chalcogenide glasses from $(GeSe_2)_{100-x}(Sb_2Se_3)_x$ system. *J. Am. Ceram. Soc*. 98, 4107-4110 (2015)

44. Šútorová, K.; Hawlová, P.; Prokeš, L.; Němec, P.; Boidin, R.; Havel, J., Laser desorption ionization time-of-flight mass spectrometry of Ge-As-Te chalcogenides. *Rapid Commun. Mass Spectrom*. 29, 408-414 (2015)

45. Olivier, M., Tchahame, J.C., Němec, P., Chauvet, M., Besse, V., Cassagne, C., Boudebs, G., Renversez, G., Boidin, R., Baudet, E., Nazabal, V.: Structure, nonlinear properties, and photosensitivity of $(GeSe_2)_{100-x}(Sb_2Se_3)_x$ glasses. *Opt. Mater. Express*. 4, 525-540 (2014)

46. Tideswell, N.W., Kruse, F.H., McCullough, J.D.: The crystal structure of antimony selenide, Sb_2Se_3. *Acta Cryst*. 10, 99-102 (1957)

47. Voutsas, G.P., Papazoglou, A.G., Rentzeperis, P.J., Siapkas, D.: The crystal structure of antimony selenide, Sb_2Se_3. *Z. Kristallogr. Cryst. Mater*. 171, 261-268 (1985)

48. Vadapoo, R., Krishnan, S., Yilmaz, H., Marin, C.: Electronic structure of antimony selenide (Sb_2Se_3) from GW calculations. *Phys. Status Solidi B*. 3, 700-705 (2011)

49. Deringer, V.L., Stoffel, R.P., Wuttig, M., Dronskowski, R.: Vibrational properties and bonding nature of Sb_2Se_3 and their implications for chalcogenide materials. *Chem. Sci*. 6, 5255-5262 (2015)

50. Chen, S., Qiao, X., Zheng, Z., Cathelinaud, M., Ma, H., Fan, X., Zhang, X.: Enhanced electrical conductivity and photoconductive properties of Sn-doped Sb_2Se_3 crystals. *J. Mater. Chem. C*. 6, 6465-6470 (2018)

51. Parize, R., Cossuet, T., Chaix-Pluchery, O., Rousse, H., Appert, E., Consonni, V.: In situ analysis of the crystallization process of Sb_2S_3 thin films by Raman scattering and X-ray diffraction. *Mater. Des*. 121, 1-10 (2017)

52. Min, M., Zhai, J., Wang, X., Shen, B., Wen, G., Fan, T.: Refinement of the crystal structure for a new mineral-antimonselite. *Chin. Sci. Bull*. 43, 413-416 (1998)

53. Malligavathy, M., Ananth Kumar, R.T., Das, C., Asokan, S., Pathinettam Padiyan, D.: Growth and characteristics of amorphous Sb_2Se_3 thin films of various thicknesses for memory switching applications. *J. Non-Crystal. Solids*. 429, 93-97 (2015)

54. Shylashree, N., Uma, B.V., Dhanush, S., Sagar, A., Nisarga, A., Aashith, K., Sangeetha, B.G.: Preparation and characterization of Sb_2Se_3 devices for memory applications. *AIP Conference Proceedings*. 1966, 020032 (2018)

55. Zhang, X., Korolkov, I., Fan, B., Cathelinaud, M., Ma, H., Adam, J.-L., Merdrignac, O., Calvez, L., Lhermite, H., Le Brizoual, L., Pasquinelli, M., Simon, J.-J.: Chalcogenide glass-ceramic with self-organized heterojunctions: application to photovoltaic solar cells. *EPJ Photovoltaics*. 9, 3 (2018)

56. Choi, Y., Mandal, T., Yang, W., Lee, Y., Im, S.H., Noh, J., Seok, S.: Sb_2Se_3-sensitized inorganic–organic heterojunction solar cells fabricated using a single-source precursor. *Angew. Chem*. 53, 1329-1333 (2014)

57. Zeng, K., Xue, D.-J., Tang, J.: Antimony selenide thin-film solar cells. *Semicond. Sci. Technol*. 31, 063001 (2016)

58. Xue, M.-Z., Fu, Z.-W.: Pulsed laser deposited Sb_2Se_3 anode for lithiumion batteries. *J. Alloys Compd*. 458, 351-356 (2008)

59. Ge, P., Cao, X., Hou, H., Li, S., Ji, X.: Rodlike Sb_2Se_3 wrapped with carbon: the exploring of electrochemical properties in sodium-ion batteries. *ACS Appl. Mater. Interfaces*. 9, 34979-34989 (2017)

60. Choi, J.W., Han, Z., Sohn, B.U., Chen, G.F.R., Smith, C., Kimerling, L.C., Richardson, K.A., Agarwal, A.M., Tan, D.T.H.: Nonlinear characterization of GeSbS chalcogenide glass waveguides. *Sci. Rep*. 6, 39234 (2016)

61. Lin, C., Li, Z., Ying, L., Xu, Y., Zhang, P., Dai, S., Xu, T., Nie, Q.: Network structure in GeS_2-Sb_2S_3 chalcogenide glasses: Raman spectroscopy and phase transformation study. *J. Phys. Chem. C* 116, 5862-5867 (2012)

62. Petit, L., Carlie, N., Adamietz, F., Couzi, M., Rodriguez, V., Richardson, K.C.: Correlation between physical, optical and structural properties of sulfide glasses in the system Ge-Sb-S. *Mater. Chem. Phys*. 97, 64-70 (2006)

63. Chao, H.E., Yun, Y.U., Xingfang, H.U., Larbot, A.: Effect of silver doping on the phase transformation and grain growth of sol-gel titania powder. *J. Eur. Ceram. Soc*. 23, 1457-1464 (2003)

64. Ecclestone, L.J., Reaney, I.M., Lee, W.E.: Correlation of microstructures with electrical performance of Ag-based metal electrode−PZT electroceramic interfaces. *J. Eur. Ceram. Soc*. 25, 1647-1655 (2005)

65. Xu, J., Liu, B., Song, Z., Feng, S., Chen, B.: Crystallization and C-RAM application of Ag-doped Sb_2Te_3 material. *Mat. Sci. Eng. B* 127, 228-232 (2006)

66. Esteban-Tejeda, L., Cabal, B., Malpartida, F., López-Píriz, R., Torrecillas, R., Saiz, E., Tomsia, A.P., Moya, J.S.: Soda-lime glass-coating containing silver nanoparticleson Ti−6Al−4V alloy. *J. Eur. Ceram. Soc*. 32, 2723-2729 (2012)

67. Reddy, M.V., Pathak, M.: Sol-gel combustion synthesis of Ag doped $CaSiO_3$: in vitro bioactivity, antibacterial activity and cytocompatibility studies for biomedical applications. *Mater. Technol*. 33, 38-47 (2018)

68. Frumar, M., Wágner, T.: Ag doped chalcogenide glasses and their´ applications. *Curr. Opin. Solid State Mater. Sci*. 7, 117-126 (2003)

69. Mitkova, M.: Applications of Non-Crystalline Materials-C. Real time optical recording on thin films of amorphous semiconductors. In Insulating and Semiconducting Glasses, 1st ed.; Boolchand, P., Ed.; World Scientific Publishing Co. Pte. Ltd: Cincinnati, pp 813-843 (2000)

70. Rau, C., Armand, P., Pradel, A., Varsamis, C.P.E., Kamitsos, E.I., Granier, D., Ibanez, A., Philippot, E.: Mixed cation effect in chalcogenide glasses $Rb_2S−Ag_2S−GeS_2$. *Phys. Rev. B: Condens. Matter Mater. Phys*. 63, 184201-184204 (2001)

71. Schubert, J., Schöning, M.J., Mourzina, Y.G., Legin, A.V., Vlasov, Y.G., Zander, W., Lüth, H.: Multicomponent thin films for electrochemical sensor applications prepared by pulsed laser deposition. *Sens. Actuators, B* 76, 327-330 (2001)

72. Shaw, B.L.: Inorganic Hydrides, 1st ed.; Shaw, B.L., Ed.; Elsevier Ltd: Leeds, pp 1-152 (1967)

73. Devyatykh, G.G., Churbanov, M. F., Scripachev, I.V., Dianov, E.M., Plotnichenko, V.G.: The Role Of Impurities In The Optical Losses Of Chalcogenide Glass Fibers. *Infrared Fiber Optics*; 1048, 80-84 (1989)

74. Churbanov, M.F., Velmuzhova, A.P., Sukhanov, M.V., Snopatin, G.E., Skripachev, I.V., Plotnichenko, V.G.: Arsenic-sulfide glasses with low content of hydrogen impurity for fiber optics. *Opt. Mater*. 77, 87-92 (2018)

75. Dezhong, M., Masafumi, S., Katsuya, S., Yuki, I., Hiroyuki, S., Toyoto, S., Shigeyuki, T., Shin-ichi, O.: Superconductivity of the hydrogen-rich metal hydride Li_5MoH_{11} under high pressure. *Phys. Rev. B* 99, 024508 (2019)

76. Fritzsche, H., Šmíd, V., Ugur, H., Gaczi. P.: Plasma-deposited hydrogenated chalcogenide glasses. *J. Phys. Colloques*. 42, 699-702 (1981)

77. Fraenkl, M., Frumarová, B., Podzemna, V., Slang, S., Benes, L., Vlcek, M., Wágner, T.: How silver influences the structure and physical properties of chalcogenide glass $(GeS_2)_{50}(Sb_2S_3)_{50}$. *J. Non-Cryst. Solids*. 499, 412-419 (2018)

78. Svoboda, R., Fraenkl, M., Frumarová, B., Wágner, T., Málek, J.: Thermokinetic behaviour of Ag-doped $(GeS_2)_{50}(Sb_2S_3)_{50}$ glasses. *J. Non-Cryst. Solids*. 449, 12-19 (2016)

79. Savage, J.A.: Infrared Optical Materials and their Anti-Reflection Coatings, Bristol, Adam Hilger, (1985)

80. Andriesh, A.M.: Properties of chalcogenide glasses for optical waveguides. *J. Non-Cryst. Solids*. 77, 1219-1228 (1985)

81. Kanamori, T., Terunuma, Y., Takahashi, S., Miyashita, T.: Chalcogenide glass fibers for mid-infrared transmission. *J. Light. Technol*. 2, 607-613 (1984)

82. Devyatykh, G.G.: Research in KRS-5 and chalcogenide glass fibers. *SPIE Proc*. 484, 105-111 (1984)

83. Lucas, P., Yang, Z., Fah, M.K., Luo, T., Jiang, S., Boussard-Pledel, C., Anne, M-L., Bureau, B.: Telluride glasses for far infrared photonic applications. *Opt. Mater. Express*. 3, 1049-1058 (2013)

84. Shimakawa, K., Kolobov, A., Elliott, S.: Photoinduced effects and metastability in amorphous semiconductors and insulators. *Adv. Phys*. 44, 475-588 (1995)

85. Calvez, L., Yang, Z., Lucas, P.: Light-induced matrix softening of Ge-As-Se network glasses. *Phys. Rev. Lett*. 101, 177402 (2008)

86. Svoboda, R., Brandová, D., Málek, J.: Crystallization behavior of $GeSb_2Se_4$ chalcogenide glass. *J. Non-Cryst. Solids*. 388, 46-54 (2014)

87. Varshneya, AK., Mauro, D.J.: Microhardness, indentation toughness, elasticity, plasticity, and brittleness of Ge–Sb–Se chalcogenide glasses. *J. Non-Cryst. Solids*. 353, 1291-1297 (2007)

88. Sharma, P., Rangra, V., Sharma, P., Katyal, S.: Far-infrared study of amorphous $Ge_{0.17}Se_{0.83-x}Sb_x$ chalcogenide glasses. *J. Alloys Compd*. 480, 934-937 (2009)

89. Giridhar, A., Narasimham, P., Mahadevan, S.: Density and microhardness of Ge-Sb-Se glasses. *J. Non-Cryst. Solids*. 43, 29-35 (1981)

90. Vazquez, J., Barreda, D.G-G., Lopez-Alemany, P., Villares, P., Jiménez-Garay, R.: Levels of thermal stability in some glassy alloys of the Ge–Sb–Se system by differential scanning calorimetry. *J. Alloys Compd*. 390, 94-99 (2005)

91. Olivier, M., Němec, P., Boudebs, G., Boidin, R., Focsa, C., Nazabal, V.: Photosensitivity of pulsed laser deposited Ge-Sb-Se thin films. *Opt. Mater. Express*. 5, 781-793 (2015)

92. Němec, P., Olivier, M., Baudet, E., Kalendova, A., Benda, P., Nazabal, V.: Optical properties of $(GeSe_2)_{100-x}(Sb_2Se_3)_x$ glasses in near-and middle-infrared spectral regions. *Mater. Res. Bull*. 51, 176-179 (2014)

93. Halenkovič, T., Gutwirth, J., Kuriakose, T., Bouška, M., Chauvet, M., Renversez, G., Němec, P., Nazabal, V.: Linear and nonlinear optical properties of co-sputtered Ge-Sb-Se amorphous thin films. *Opt. Lett*. 45, 1523-1526 (2020)

94. Wood, D., Tauc, J.: Weak absorption tails in amorphous semiconductors. *Phys. Rev. B*. 5, 3144 (1972)

95. Svoboda, R., Málek, J.: Amorphous-to-crystalline transition in Te-doped $Ge_2Sb_2Se_5$ glass. *J. Therm. Anal. Calorim*. 117, 1073-1083 (2014)

96. Yin, N., Xu, J., Chang, F., Jian, Z., Gao, C.: Effect of Te proportion on the properties of $Ge_{25}Sb_{10}Se_{65-x}Te_x$ chalcogenide glasses. *Infrared Phys. Technol*. 96, 361-365 (2019)

97. Fabian, M., Svab, E., Pamukchieva, V., Szekeres, A., Todorova, K., Vogel, S., Ruett, U.: Reverse Monte Carlo modeling of the neutron and X-ray diffraction data for new chalcogenide Ge–Sb–S (Se)–Te glasses. *J. Phys. Chem. Solids*. 74, 1355-1362 (2013)

98. Svoboda, R., Bezdička, P., Gutwirth, J., Málek, J.: Crystallization processes in $Ge_2Sb_2Se_4Te$ glass. *Mater. Res. Bull*. 61, 207-214 (2015)

99. Svoboda, R., Málek, J.: Thermal behavior of Se-rich $GeSb_2Se_{(4-y)}Te_y$ (glassy) system. *J. Alloys Compd*. 670, 222-228 (2016)

100. Bordas, S., Casas-Vazquez, J., Clavaguera, N., Clavagura-Mora, M.: Glass-forming ability in the Ge-Sb-Te-Se quaternary system. *Thermochim. Acta*. 28, 387-393 (1979)

6. How the aims of the Dissertation were fulfilled

The main goal of this Dissertation was to study chalcogenide materials using MS.

A) In the first task,

In addition to a series of Sb_m^+, Se_n^+, and $Sb_mSe_n^+$ clusters, several oxidized clusters and partially hydroxylated clusters are also generated. When some special approaches were applied to measure, the intensity of the mass spectra is different or the clusters detected is not the same compared to those mass spectra measured from normal samples.

B) In the second task,

The clusters observed are not the same when the Sb_2Se_3 material exhibits in different forms. When comparing the stability of the studied materials, it was found that commercial polycrystalline bulk was the most stable one, followed by a homemade, and finally thin film. The use of GO, G, and C_{60} increased the intensity of mass spectra up to 10 times which indeed act as a SALDI.

C) In the third task,

A lot of $Ag_aGe_bSb_cS_d$ clusters were obtained by the MS. Despite that all glass components are made by five-ninth purity elements, MS has shown the ability to detect trace impurity such as oxidized or hydrogenated clusters. Structural units of the studied material were observed by Raman spectroscopy. Some structure units were not observed by MS but detected by Raman spectroscopy, and vice versa. This phenomenon is indicating that the structure units such as GeS_4 tetrahedral and SbS_3 pyramid are too stable to be decomposed by MS.

D) In the fourth task,

Fewer clusters were observed from the tellurium doped Ge-Sb-Se thin films when compared to non-doped one. This indicates that tellurium act as a role of stabilization of Ge-Sb-Se thin films. Furthermore, it was found that when tellurium is introduced into thin films and its content increases, the thin film's stability improves. This is inferred from the fact that when the amount of tellurium in studied thin films increases, the intensity of the spectra decreases.

Concluding, the dissertation's objectives were achieved, and the aims were fulfilled.

7. List of Abbreviations

C_{60}	Fullerene
EDS	Energy dispersive x-ray spectroscopy
G	Graphene
GO	Graphene oxide
LA	Laser ablation
LAS	Laser ablation synthesis
LDI	Laser desorption ionization
MALDI	Matrix-assisted laser desorption ionization
MS	Mass spectrometry
QIT TOF MS	Quadrupole ion trap time-of-flight mass spectrometry
SALDI	Surface-assisted laser desorption ionization
SEM	Scanning electron microscopy
TOF MS	Time-of-flight mass spectrometry
XRD	X-ray diffraction

8. List of Appendices

Appendix 1A	Huang, F., Prokeš, L. & Havel, J. *J. Am. Soc. Mass Spectrom*. 2019, **30**, 634–638.
Appendix 1B	Huang, F., Prokeš, L. & Havel, J. *J. Am. Soc. Mass Spectrom*. 2019, **30**, 634–638. Supporting information
Appendix 2A	Huang F., Prokeš, L., Němec P., Nazabal V. & Havel, J. *J. Am. Soc. Mass Spectrom.* 2019, **30**, 12, 2756–2761.
Appendix 2B	Huang F., Prokeš, L., Němec P., Nazabal V. & Havel, J. *J. Am. Soc. Mass Spectrom.* 2019, **30**, 12, 2756–2761. Supporting information
Appendix 3A	Huang, F., Wágner, T., Frumarová, B., Fraenkl, M., Koštál, P. & Havel, J. *ACS Omega* 2020, **5**, 45, 28965–28971.
Appendix 3B	Huang, F., Wágner, T., Frumarová, B., Fraenkl, M., Koštál, P. & Havel, J. *ACS Omega* 2020, **5**, 45, 28965–28971. Supporting information
Appendix 4A	Huang F., Halenkovič, T., Baillieul, M., Nazabal V., Němec, P. & Havel, J. *J. Am. Ceram. Soc.*2022,**105**,1992–2000.
Appendix 4B	Huang F., Halenkovič, T., Baillieul, M., Nazabal V., Němec, P. & Havel, J. *J. Am. Ceram. Soc.*2022,**105**,1992–2000. Supporting information

Appendix 1A

Fei HUANG, Lubomír PROKEŠ, and Josef HAVEL: Laser Ablation Generation of Antimony Selenide Clusters: Laser Desorption Ionization (LDI) Quadrupole Ion Trap Time of Flight Mass Spectrometry. *J. Am. Soc. Mass Spectrom.* **30**, 634-638 (2019).
IF: 3.109, Quartile: Q1

(https://link.springer.com/article/10.1007/s13361-018-2119-3)

© American Society for Mass Spectrometry, 2019

J. Am. Soc. Mass Spectrom. (2019) 30:634–638
DOI: 10.1007/s13361-018-2119-3

RESEARCH ARTICLE

Laser Ablation Generation of Antimony Selenide Clusters: Laser Desorption Ionization (LDI) Quadrupole Ion Trap Time of Flight Mass Spectrometry

Fei Huang,[1] Lubomír Prokeš,[1,2,3] Josef Havel[1]

[1]Department of Chemistry, Faculty of Science, Masaryk University, Kamenice 5/A14, 62500, Brno, Czech Republic
[2]Department of Physical Electronics, Faculty of Science, Masaryk University, Kotlářská 2, 61137, Brno, Czech Republic
[3]CEPLANT, R&D Centre for Low-Cost Plasma and Nanotechnology Surface Modification, Masaryk University, Kotlářská 2, 61137, Brno, Czech Republic

Downloaded via MASARYK UNIV on October 1, 2021 at 09:22:20 (UTC).
See https://pubs.acs.org/sharingguidelines for options on how to legitimately share published articles.

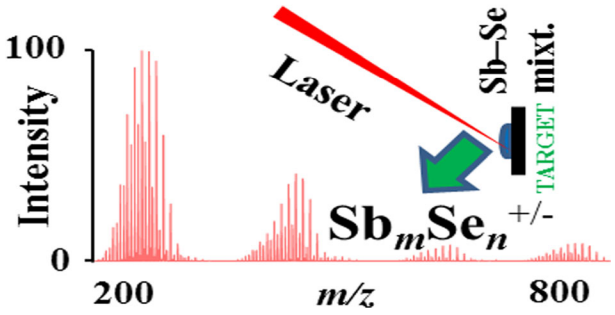

Abstract. The binary system Sb-Se was studied via laser ablation using antimony-selenium mixtures made from powdered elements in various ratios generating new Sb_mSe_n clusters. The results show that in addition to Sb_m^+ ($m = 1–8$) and Se_n^+ ($n = 2–9$) clusters, a series of $Sb_mSe_n^+$ clusters such as $SbSe_{1–8}^+$, $Sb_2Se_{1–6}^+$, $Sb_3Se_{1–5}^+$, $Sb_4Se_{1–3}^+$, and $Sb_5Se_{1,2}^+$ is generated. In addition, some low intensity oxidized clusters like $Se_6O_2^+$, $Se_7O_2^+$, and $SbSe_{2-6}O_5^+$ and partially hydroxylated clusters ($SbSeO_2H_7^+$, $SbSe_5O_4H^+$) are also formed. In total, 24 new antimony selenide clusters were generated. The knowledge gained can contribute to the elucidation of the structure of Sb_mSe_n glasses.

Keywords: Antimony selenides, Laser ablation, Clusters, Laser desorption ionization, Quadrupole ion trap mass spectrometry, Chalcogenide glasses

Received: 15 August 2018/Revised: 5 December 2018/Accepted: 10 December 2018/Published Online: 15 January 2019

Introduction

Antimony forms several selenides. The structure of Sb_2Se_3 has been determined [1–4]. Recently, polycyclic polycations $[Sb_{10}Se_{10}]^{2+}$, $[Sb_7Se_8Br_2]^{3+}$ and $[Sb_{13}Se_{16}Br_2]^{5+}$ [5, 6], $Ba_2Sb_2Se_5$, and $Ba_6Sb_7Se_{16}$ compounds [7] and a huge $Sb_{12}Se_{20}^{4-}$ zintl anion [8] have been prepared and characterized. Antimony-selenium glasses are important members of the chalcogenide range of glasses, especially Ge-As(Te)-Sb-Se. Ge-Sb-Se moldable compounds are used in infrared optics [9–11].

In this work, the binary system Sb-Se was studied via laser ablation generating Sb_mSe_n clusters, in both positive and negative ion modes, using antimony-selenium powdered mixtures in various ratios as precursors. Laser ablation generation with quadrupole ion trap time-of-flight mass spectrometry (QIT-TOFMS) has already been shown to be an important and powerful methodology for studying the formation of clusters [12]; while the composition of Sb_mSe_n clusters was determined via computer simulation of the isotopic envelopes.

Experimental

Chemicals

1-Butyl-3-methylimidazolium chloride, antimony, and selenium powders were purchased from Sigma-Aldrich (St. Louis, Mo., USA). Glycerol and xylene were purchased from Lach-Ner (Neratovice, Czech Republic). *Parafilm* was purchased from Bemis NA (Neenah, Wis., USA). Acetonitrile and hydrochloric acid were purchased from Sigma-Aldrich (Steinheim, Germany). Red phosphorus was obtained from Riedel de Haën (Hannover, Germany) and was purified via sublimation in a nitrogen atmosphere. Water was double distilled using a quartz

Electronic supplementary material The online version of this article (https://doi.org/10.1007/s13361-018-2119-3) contains supplementary material, which is available to authorized users.

Correspondence to: Josef Havel; *e-mail:* havel@chemi.muni.cz

apparatus from Heraeus Quarzschmelze (Hanau, Germany). All other reagents were of analytical grade purity.

Mass Spectrometry

Mass spectra were recorded in both positive and negative ion modes using the mass spectrometer AXIMA Resonance from Kratos Analytical Ltd. (Manchester, UK) coupled with a quadrupole ion trap and time-of-flight detection. The instrument was equipped with a nitrogen laser (337 nm). The laser repetition rate was set to 5 Hz with a pulse time width of 3 ns.

Software and Computation

Stoichiometry of Sb_mSe_n clusters was determined via computer modeling of the isotopic envelopes using Launchpad software (Kompact version 2.9.3, 2011) from Kratos Analytical Ltd. (Manchester, UK).

Sample Preparation for Mass Spectrometry

The surface of solid antimony in pellets was cleaned by applying 0.1 M hydrochloric acid for 5 min. The pellets were then washed with double-distilled water and acetonitrile. Solid antimony was then powdered in an agate mortar. Finally, antimony, selenium, and antimony-selenium mixtures were suspended in acetonitrile (1 mg/ml). From these suspensions, 10 µL was deposited on a target and dried.

For laser ablation in glycerol a 10-µL sample of the Sb-Se suspension in acetonitrile was deposited on a target and dried as mentioned above. After adding 10-µL glycerol, the sample for laser ablation in glycerol was obtained.

For laser ablation generation in mixture of paraffines, 1 cm^2 of parafilm was dissolved in 1 ml of xylene, and then the powdered mixture of antimony-selenium (1 mg) was suspended in this solution. Then, about 1 µL of the suspension was deposited on a target. After drying, the mass spectra were generated.

For laser ablation generation in ionic liquid, the powdered Sb-Se mixture was mixed with an ionic liquid (1-butyl-3-methyl imidazolium chloride), dissolved in acetonitrile, and ~ 1 µL of the suspension was deposited onto a target and dried.

Results

Antimony, selenium, and antimony-selenium clusters generated via laser ablation were studied. A reflectron mode was employed to record the mass spectra in both positive and negative ion modes. It was shown that many more clusters were generated in positive ion mode and the clusters produced in negative ion mode were of low intensity. The results will therefore be presented mainly for the positive ion mode. The majority of the clusters were formed in the *m/z* range of 200–800.

Antimony and Selenium

The overview of clusters generated from antimony and selenium is given in Table 1. Apart from Sb_m^+ ($m = 1$–6) and Se_n^+ ($n = 2$–9) clusters, several oxygen containing clusters were also detected.

Antimony Selenium Mixture (Molar Ratio Sb:Se = 1:1)

Examples of selected mass spectra are given in Figure 1, where identified clusters are also provided. For the ratio Sb:Se = 1:1, some Se_n^+ clusters ($n = 4$–9) and several $SbSe_n^+$ ($n = 3$–7) were detected. In addition, two oxidized clusters of $Se_6O_2^+$ and $Se_7O_2^+$ were identified. A comparison of experimental and theoretical isotopic patterns for $SbSe_2^+$ is given in Fig. S1 A, and these are in good agreement.

Antimony Selenium Mixture (Molar Ratio Sb:Se = 10:1)

Here, the mass spectra recorded from the ratio Sb:Se = 10:1 are given in Figure 2a. In addition to several Se_n^+ ($n = 4$–9) and $SbSe_n^+$ ($n = 2$–7) clusters, some other clusters such as $SbSe_nO_5^+$ ($n = 2$–6) were also detected, while the latter ones were always overlapped with $SbSe_n^+$ clusters. Also, another two $SbSe_5O_4H^+$ and $Sb_5O_7^+$ clusters are shown in the inset spectrum. Comparison of experimental and theoretical isotopic patterns demonstrating the overlap of $SbSe_3^+$ and $SbSe_2O_5^+$ clusters is shown in Fig. S1 B and there is good agreement between the experimental results and the theoretical model.

Antimony Selenium Mixture (Molar Ratio Sb:Se = 1:10)

When selenium was in high excess over antimony, the mass spectra were different (Figure 2b). In this case, $SbSe_n^+$ ($n = 2$–8), $Sb_2Se_n^+$ ($n = 1$–6), $Sb_3Se_n^+$ ($n = 1$–5), $Sb_4Se_n^+$ ($n = 1$–3) and $Sb_5Se_n^+$ ($n = 1, 2$) clusters were detected. Apart from these clusters, Se_n^+ ($n = 4$–9) clusters were also observed. Comparison of theoretical isotopic patterns corresponding to overlapping peaks of Se_8^+, $Sb_2Se_5^+$, and $Sb_4Se_2^+$ with the experimental spectrum is given in Fig. S1 C. Good agreement between the theoretical models and the experimental results was observed.

The Effect of Laser Energy (Molar Ratio Sb:Se = 1:1, Negative Ion Mode)

Spectra in the negative ion mode (Fig. S2) are different when compared to the positive ion mode. The most intensive peak is Se_4^- which contrasts with positive ion mode where Se_5^+ was the most intensive peak (cf. Figure 1). The effect of laser energy shown in this figure demonstrates that the intensity of clusters increases when laser energy goes from 90 to 100 a.u., but the mass spectra intensities decrease when the laser energy is increased to 110 a.u. A similar trend was observed for the Se_4^- cluster. Except for Se_4^-, the intensity of spectra

Table 1. Overview of Sb_mO_x and Se_nO_x Formed from Antimony or Selenium and Sb_mSe_n Clusters Formed from Antimony-Selenium Mixtures (1:1, 1:10, 10:1) via Laser Ablation in Positive Ion Mode. (Comment: Oxygen Containing Clusters are Not Given for the Antimony-Selenium Mixtures)

					only antimony				
	Sb^+	Sb_2^+	Sb_3^+	Sb_4^+	Sb_5^+	Sb_6^+			
	SbO^+	Sb_2O^+	Sb_3O^+	Sb_4O^+	Sb_5O^+				
					only selenium				
		Se_2^+	Se_3^+	Se_4^+	Se_5^+	Se_6^+	Se_7^+	Se_8^+	Se_9^+
						$Se_6O_2^+$	$Se_7O_2^+$	$Se_8O_2^+$	$Se_9O_2^+$
					$Se_5O_3^+$				
m					Sb:Se = 1:1				
					,				
0				Se_4^+	Se_5^+	Se_6^+	Se_7^+	Se_8^+	Se_9^+
1		$SbSe_2^+$	$SbSe_3^+$	$SbSe_4^+$	$SbSe_5^+$	$SbSe_6^+$	$SbSe_7^+$		
					Sb:Se = 10:1				
0				Se_4^+	Se_5^+	Se_6^+	Se_7^+	Se_8^+	Se_9^+
1		$SbSe_2^+$	$SbSe_3^+$	$SbSe_4^+$	$SbSe_5^+$	$SbSe_6^+$	$SbSe_7^+$		
					Sb:Se =1:10				
0				Se_4^+	Se_5^+	Se_6^+	Se_7^+	Se_8^+	Se_9^+
1		$SbSe_2^+$	$SbSe_3^+$	$SbSe_4^+$	$SbSe_5^+$	$SbSe_6^+$	$SbSe_7^+$	$SbSe_8^+$	
2	Sb_2Se^+	$Sb_2Se_2^+$	$Sb_2Se_3^+$	$Sb_2Se_4^+$	$Sb_2Se_5^+$	$Sb_2Se_6^+$			
3	Sb_3Se^+	$Sb_3Se_2^+$	$Sb_3Se_3^+$	$Sb_3Se_4^+$	$Sb_3Se_5^+$				
4	Sb_4Se^+	$Sb_4Se_2^+$	$Sb_4Se_3^+$						
5	Sb_5Se^+	$Sb_5Se_2^+$							

grows as the laser energy increases. It is interesting to note that in both positive and negative ion modes, $SbSeO_2H_7^{+/-}$ clusters were detected (Fig. S3).

Review of Sb_mSe_n Clusters

An overview of the Sb_mSe_n clusters generated from Sb:Se = 1:1, Sb:Se = 1:10, and Sb:Se = 10:1 is given in Table 1 and Fig.

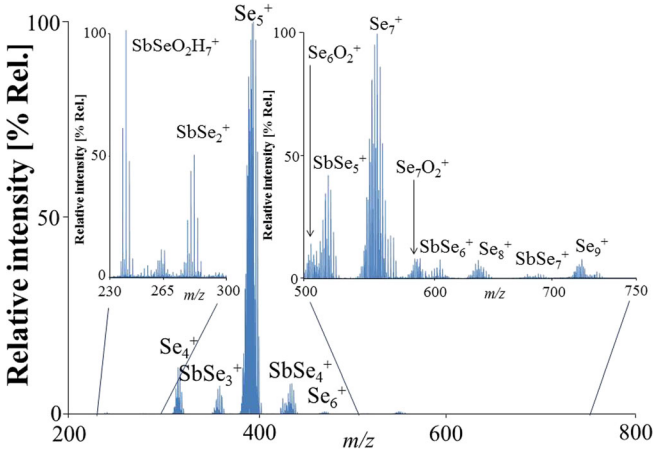

Figure 1. Mass spectra recorded from LDI of Sb:Se mixture with the ratio of elements equal to 1:1. Insets show the magnification of spectra in *m/z* ranges 230–300 and 500–750. Conditions: positive ion mode, laser energy 130 a.u

S4. Interestingly, all Sb_mSe_n clusters produced when using Sb:Se = 1:1 are also observed when Sb:Se was equal to 10:1.

Some Special Approaches to Measurement

In addition to laser ablation of the Sb-Se mixtures, some special approaches were examined.

Laser Ablation Generation in the "Hole" When the laser was fired on one point (Fig. S5) with a power from 80 a.u. to 180 a.u., there is a formation of a "*hole*" in the deposited sample material (Sb:Se = 1:1). The generation goes on in the reaction "crucible" (hole formed by the laser) and the clusters were observed at 140 a.u. (trace point). Although the intensities of clusters are low, some new Sb_2Se^+, $Sb_2Se_2^+$, Sb_3Se^+, and Sb_3^+ clusters are formed (compare to Figure 1). As the laser energy increased, the proportion of $Sb_2Se_2^+$ overlaying Se_5^+ and $Sb_2Se_2^+$ increased.

Laser Ablation Generation of Sb_mSe_n Clusters in Glycerol, Parafilm, and in Ionic Liquid When a mixture of Sb:Se = 1:1 was prepared in glycerol, laser ablation of this mixture showed the same clusters (compare with Figure 1), except for $SbSeO_2H_7^+$, $Se_6O_2^+$, and $Se_7O_2^+$ clusters (Fig. S6), but the spectra were of lower intensity.

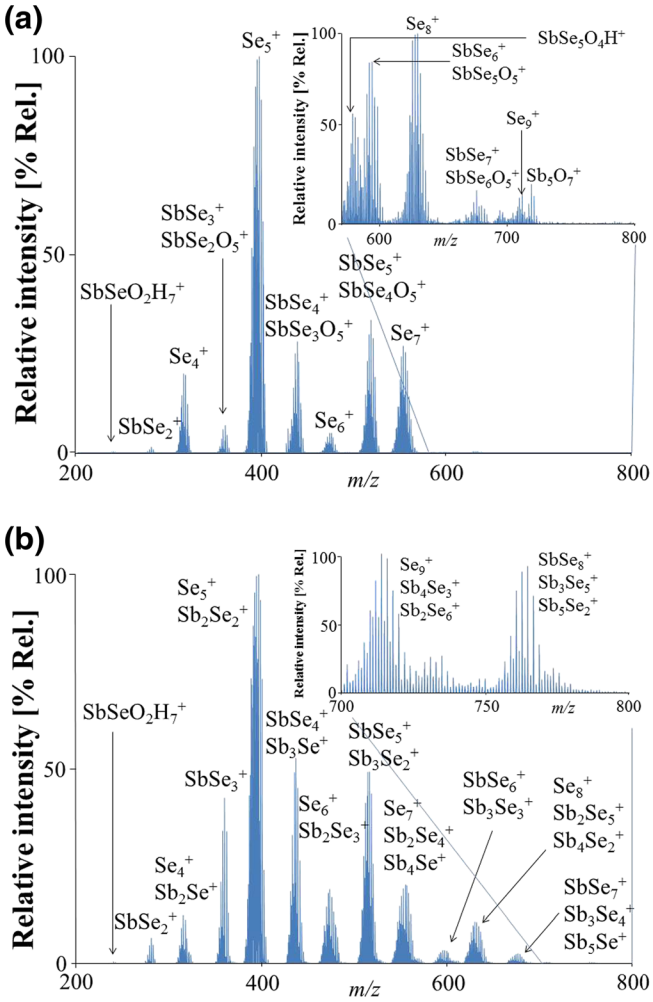

Figure 2. (**a**) Mass spectra recorded from LDI of Sb:Se mixture with the ratio of element equal to 10:1. Inset shows magnification of spectra in *m/z* range 550–800. Conditions: positive ion mode, laser energy 130 a.u. (**b**) Mass spectra recorded from LDI of Sb:Se mixture with the ratio of elements equal to 1:10. Inset shows magnification of spectra in *m/z* range 700–800. Conditions: positive ion mode, laser energy 180 a.u

When the mixture of Sb:Se = 1:1 was prepared in parafilm, the clusters produced in *m/z* range 300–600 are the same as those observed using just a 1:1 mixture (Figure 1), but they are different in *m/z* range 600–900 (Figure 3), where four clusters $Sb_3Se_n^+$ ($n = 3$–6) were generated.

When a mixture of antimony-selenium (1:1) was prepared in an ionic liquid, in comparison to Figure 1, $SbSe_3^+$ and two new clusters $Sb_2Se_2^+$ and Sb_3Se^+ were identified in the mass spectrum (Fig. S7). Some clusters were of complex overlay and were not identified.

Laser Ablation of a Commercial Sb_2Se_3 Compound

Laser desorption ionization of commercial crystalline Sb_2Se_3 shows the formation of $SbSe_2^+$, $SbSe_3^+$, $Sb_2Se_{2-4}^+$, $Sb_2Se_{3-4}^+$, and $Sb_3Se_{1-5}^+$ clusters, the same as when mixtures of Sb:Se =

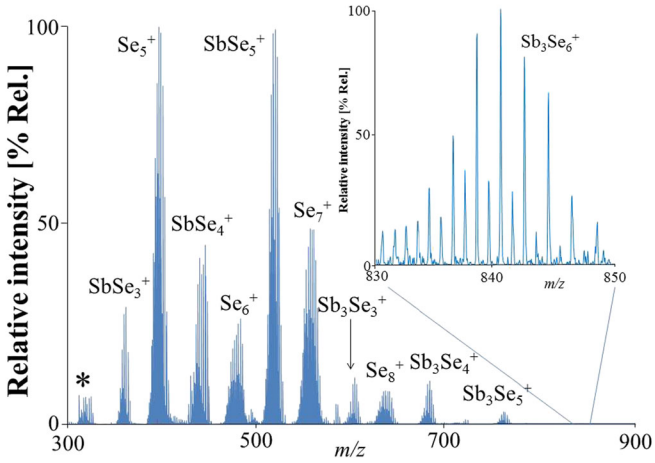

Figure 3. Mass spectra recorded from LDI of Sb:Se mixture in the parafilm with the ratio of elements equal to 1:1. Conditions: positive ion mode, laser energy 160 a.u.; asterisk (*) means that isotopic pattern is too complex or the spectra intensity is too low to identify clusters

1:10 were ablated. The only exceptions are Se_n^+ clusters. Missing Se_n^+ clusters is natural, as Se_n^+ structural fragments with Se-Se bounds are not part of Sb_2Se_3 crystal structure (Figure 4). In negative ion mode, only $SbSe_2^-$, Sb_2Se^-, $SbSe_3^-$, and $Sb_2Se_2^-$ clusters were detected.

Structure of Sb_mSe_n Clusters

Structures of some unary clusters were recently determined for selenium [12–15] and antimony [16, 17] clusters. However, structures of generated binary clusters are not known. The determination of the structures from mass spectra is not possible and quantum chemistry computation is outside the scope of this work.

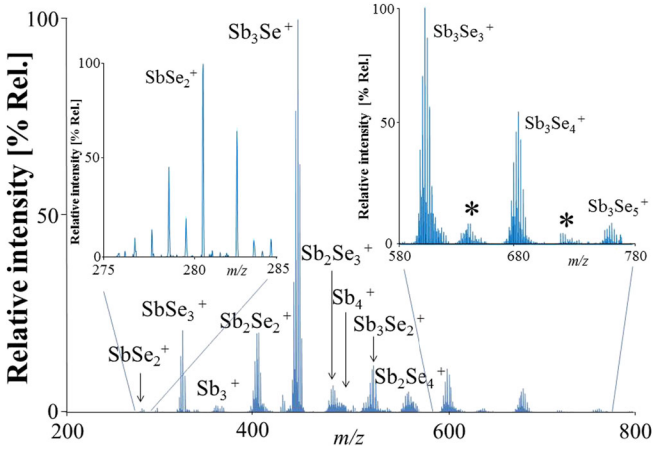

Figure 4. Mass spectra recorded from LDI of commercial Sb_2Se_3 crystals. Conditions: positive ion mode, laser energy 130 a.u.; asterisk (*) means the isotopic pattern is too complex or the spectra intensity is too low to identify clusters

Discussion

In order to understand the structures of Sb-Se chalcogenide glasses, we studied the formation of clusters generated from a mixture of Sb-Se in three different ratios and in different media. Comparing the results obtained, the clusters formed when using the ratio Sb:Se = 1:1 and 10:1 was quite similar. Contamination of $Sb_mSe_n^+$ clusters with oxidized $Sb_mSe_nO_5^+$ species was not observed for Sb:Se = 1:1 samples. This is probably because antimony is easily oxidized and thus oxidized specie was detected from samples with high excess of antimony. Therefore, when antimony was in high excess, some oxidized species like $Sb_mSe_nO_5^+$ could be produced in greater extend. The situation was different when Sb:Se = 1:10, many new $Sb_mSe_n^+$ clusters were observed which were not generated in Sb:Se = 1:1. The reason could be that selenium has a smaller atomic diameter and lower melting temperature than antimony. Therefore, when selenium is in molar excess, the selenium surrounds the antimony, and under the influence of the laser, it will melt first and combine with the antimony around it to form various clusters.

When the laser acts on one point, a "hole" will be created. Although low laser energy is not enough to form ions, chemical reactions actually took place between the elements.

Conclusions

Laser desorption ionization with quadrupole ion trap time-of-flight mass spectrometry (QIT-TOFMS) can be used as a type of efficient device to generate various Sb_mSe_n clusters. The clusters Sb_m, Se_n, and Sb_mSe_n were generated from mixtures of the elements antimony and selenium. In total, 24 new antimony selenide clusters were observed. The results obtained contribute to a deeper understanding of the preparation and structure of Sb_mSe_n materials, glasses, or various phase-change products.

Acknowledgements

This work was funded with support from the Grant Agency of the Czech Republic (Projects No. GA18-03823S). This research has been also supported by CEPLANT, the project R&D center for low-cost plasma and nanotechnology surface modification, and CZ.1.05/2.1.00/03.0086 funding by the European Regional Development Fund and the Project CZ.1.07/2.3.00/30.0058 of the Ministry of Education, Youth and Sports of the Czech Republic.

References

1. Tideswell, N.W., Kruse, F.H., McCullough, J.D.: The crystal structure of antimony selenide, Sb_2Se_3. Acta Cryst. **10**, 99–102 (1957)
2. Voutsas, G.P., Papazoglou, A.G., Rentzeperis, P.J., Siapkas, D.: The crystal structure of antimony selenide, Sb_2Se_3. Z. Kristallogr. Cryst. Mater. **171**, 261–268 (1985)
3. Vadapoo, R., Krishnan, S., Yilmaz, H., Marin, C.: Electronic structure of antimony selenide (Sb_2Se_3) from GW calculations. Phys. Status Solidi B. **3**, 700–705 (2011)
4. Deringer, V.L., Stoffel, R.P., Wuttig, M., Dronskowski, R.: Vibrational properties and bonding nature of Sb_2Se_3 and their implications for chalcogenide materials. Chem. Sci. **6**, 5255–5262 (2015)
5. Ahmed, E., Isaeva, A., Fiedler, A., Haft, M., Ruck, M.: $[Sb_{10}Se_{10}]^{2+}$, a heteronuclear polycyclic polycation from a room-temperature ionic liquid. Chem. Eur. J. **17**, 6847–6852 (2011)
6. Ahmed, E., Breternitz, J., Groh, M.F., Isaeva, A., Ruck, M.: $[Sb_7Se_8Br_2]^{3+}$ and $[Sb_{13}Se_{16}Br_2]^{5+}$- double and quadruple spiro cubanes from ionic liquids. Eur. J. Inorg. Chem. **19**, 3037–3042 (2014)
7. Wang, J., Lee, K., Kovnir, K.: Synthesis, crystal structure, and thermoelectric properties of two new barium antimony selenides: $Ba_2Sb_2Se_5$ and $Ba_6Sb_7Se_{16}$. J. Mater. Chem. C. **3**, 9811–9818 (2015)
8. Martin, T.M., Wood, P.T., Kolis, J.W.: Synthesis and structure of an $[Sb_{12}Se_{20}]^{4-}$ salt: the largest molecular zintl ion. Inorg. Chem. **33**, 1587–1588 (1994)
9. Ko, J.B., Myung, T.-S.: Structural and thermal properties of Ge-Sb-Se chalcogenide glasses for an application in infrared optical product design and manufacture. J. Ceram. Process. Res. **12**, 132–134 (2011)
10. Choi, J.H., Cha, D.-H., Kim, J.-H., Kim, H.-J.: Development of thermally stable and moldable chalcogenide glass for flexible infrared lenses. J. Mater. Res. **31**, 1674–1680 (2016)
11. Parnell, H., Butterworth, J.H., Sakr, H., Tang, Z., Furniss, D., Benson, T.M., Scotchford, C., Seddon, A.B.: Ge-Sb-Se glass fiber-optics for in-vivo mid-infrared optical biopsy. Proc. SPIE. **9703**, 970309 (2016)
12. Prokeš, L., Kubáček, P., Peña-Méndez, E.M., Amato, F., Conde, J.E., Alberti, M., Havel, J.: Laser ablation synthesis of gold selenides by using a mass spectrometer as a synthesizer: laser desorption ionization time-of-flight mass spectrometry. Chem. Eur. J. **22**, 11261–11268 (2016)
13. Hohl, D., Jones, R.O., Car, R., Parrinello, M.: The structure of selenium clusters - Se_3 to Se_8. Chem. Phys. Lett. **139**, 540–545 (1987)
14. Xu, W., Bai, W.: The selenium clusters Se_n (n = 1–5) and their anions: structures and electron affinities. J. Mol. Struc.-THEOCHEM. **854**, 89–105 (2008)
15. Alparone, A.: Density functional theory Raman spectra of cyclic selenium clusters Se_n (n = 5–12). Comput. Theor. Chem. **988**, 81–85 (2012)
16. Geusic, M.E., Freeman, R.R., Duncan, M.A.: Neutral and ionic clusters of antimony and bismuth: a comparison of magic numbers. J. Chem. Phys. **89**, 223–229 (1988)
17. Zhai, H.-J., Wang, L.-S., Kuznetsov, A.E., Boldyrev, A.I.: Probing the electronic structure and aromaticity of pentapnictogen cluster anions Pn^{5-} (P*n* = P, As, Sb, and Bi) using photoelectron spectroscopy and ab initio calculations. J. Phys. Chem. A. **106**, 5600–5606 (2002)

Appendix 1B

Fei HUANG, Lubomír PROKEŠ, and Josef HAVEL: Laser Ablation Generation of Antimony Selenide Clusters: Laser Desorption Ionization (LDI) Quadrupole Ion Trap Time of Flight Mass Spectrometry. *J. Am. Soc. Mass Spectrom.* **30**, 634-638 (2019).

Supporting information

(https://link.springer.com/article/10.1007/s13361-018-2119-3)

Laser Ablation Generation of Antimony Selenide Clusters. Laser Desorption Ionization (LDI) Quadrupole Ion Trap Time-of -Flight Mass Spectrometry

Fei Huang,[1] Lubomír Prokeš,[1,2,3] Josef Havel[1*]

[1]Department of Chemistry, Faculty of Science, Masaryk University, Kamenice 5/A14, 62500 Brno, Czech Republic

[2]Department of Physical Electronics, Faculty of Science, Masaryk University, Kotlářská 2, 61137 Brno, Czech Republic

[3]CEPLANT, R&D Centre for Low-Cost Plasma and Nanotechnology Surface Modification, Masaryk University, Kotlářská 2, 61137 Brno, Czech Republic

*Author to whom correspondence should be addressed. Email: havel@chemi.muni.cz

Phone: +420 549494114, Fax: +420 549492494

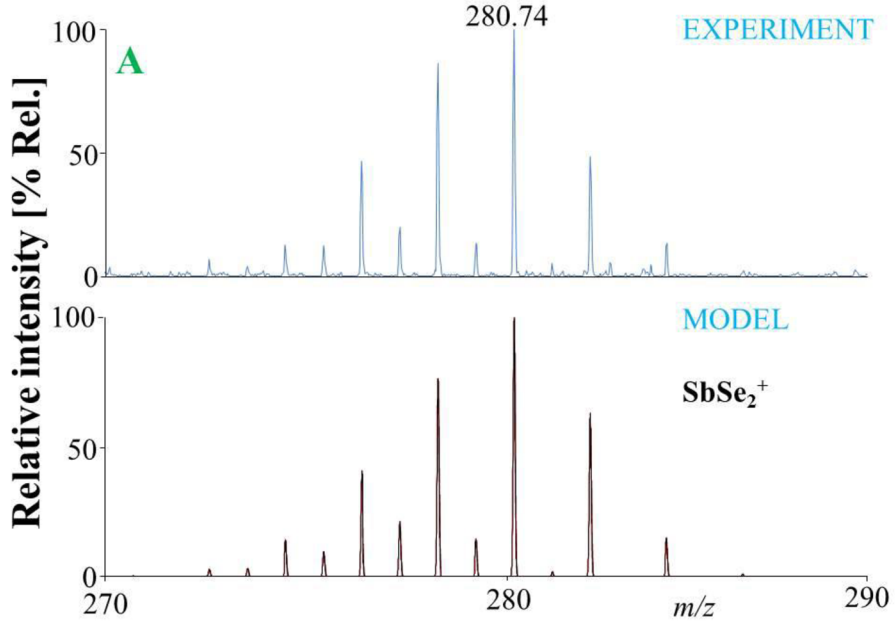

Figure S1 A. Comparison of experimental and theoretical isotopic pattern for $SbSe_2^+$. Conditions: positive ion mode, laser energy 130 a.u.

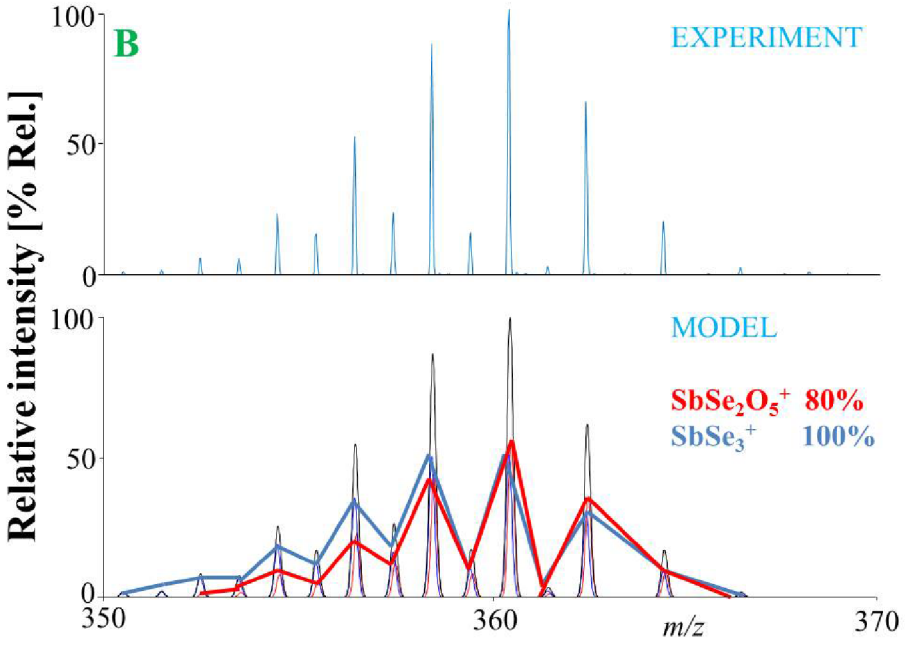

Figure S1 B. Comparison of experimental and theoretical isotopic patterns for $SbSe_2O_5^+$ and $SbSe_3^+$ clusters. Conditions: positive ion mode, laser energy 130 a.u.

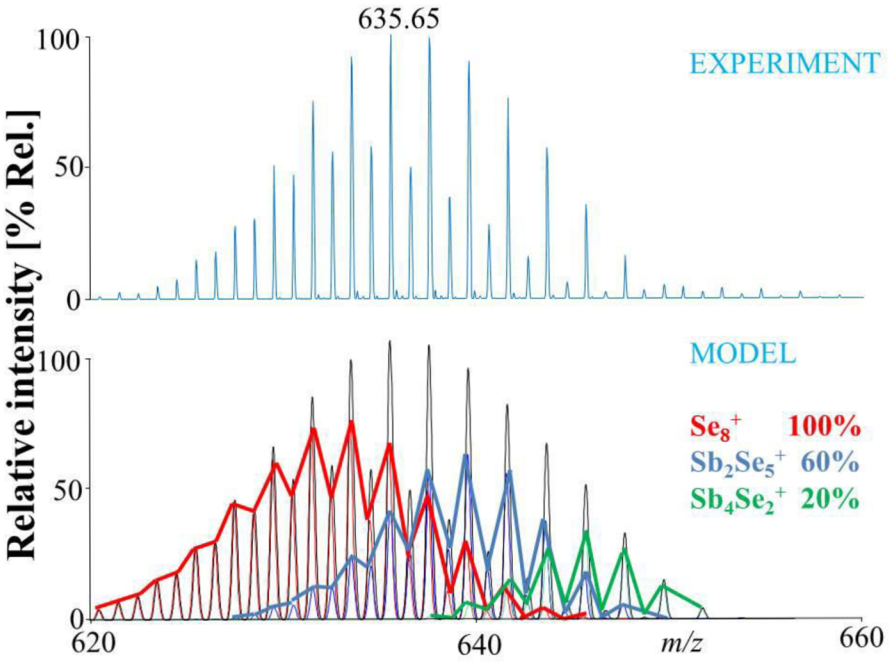

Figure S1 C. Comparison of experimental and theoretical isotopic patterns for Se_8^+, $Sb_2Se_5^+$, and $Sb_4Se_2^+$. Conditions: positive ion mode, laser energy 180 a.u.

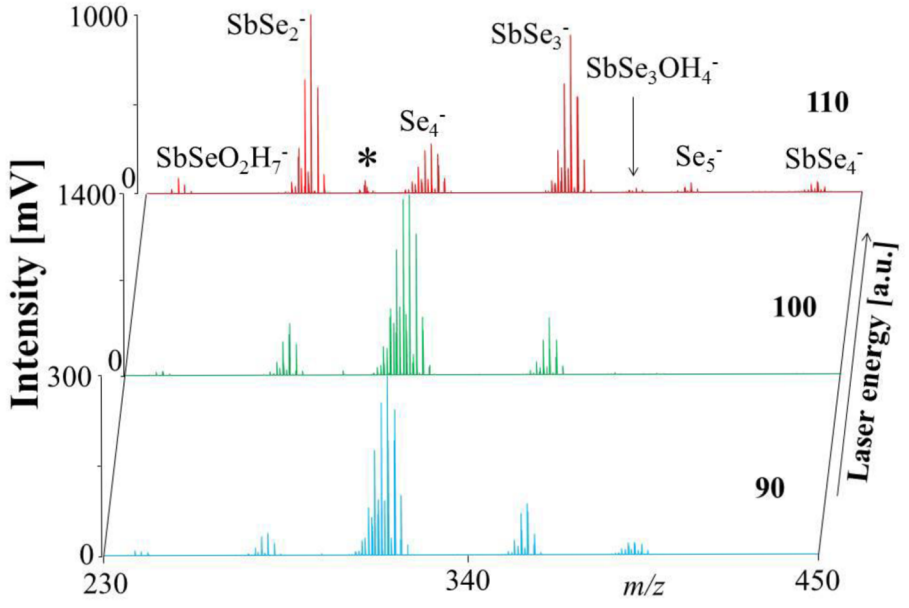

Figure S2. Mass spectra recorded from LDI of Sb:Se mixture with the ratio of elements equal to 1:1 in the *m/z* range 200-600. The effect of laser energy. Conditions: negative ion mode, laser energy 90-110 a.u.; * means the isotopic pattern is too complex or spectra of low intensity to identify clusters.

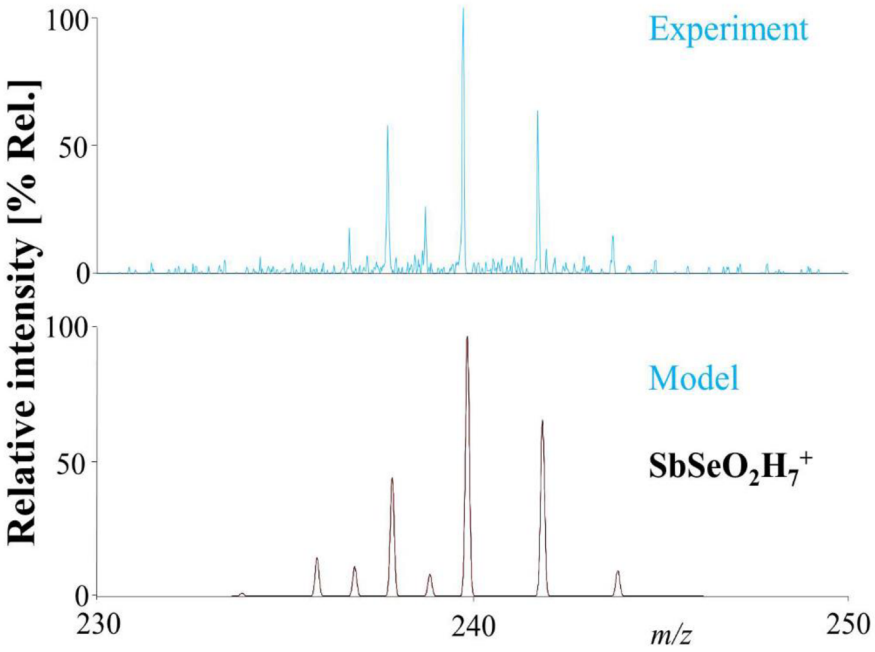

Figure S3. Comparison of experimental and theoretical isotopic pattern for $SbSeO_2H_7^+$. Conditions: positive ion mode, laser energy 130 a.u.

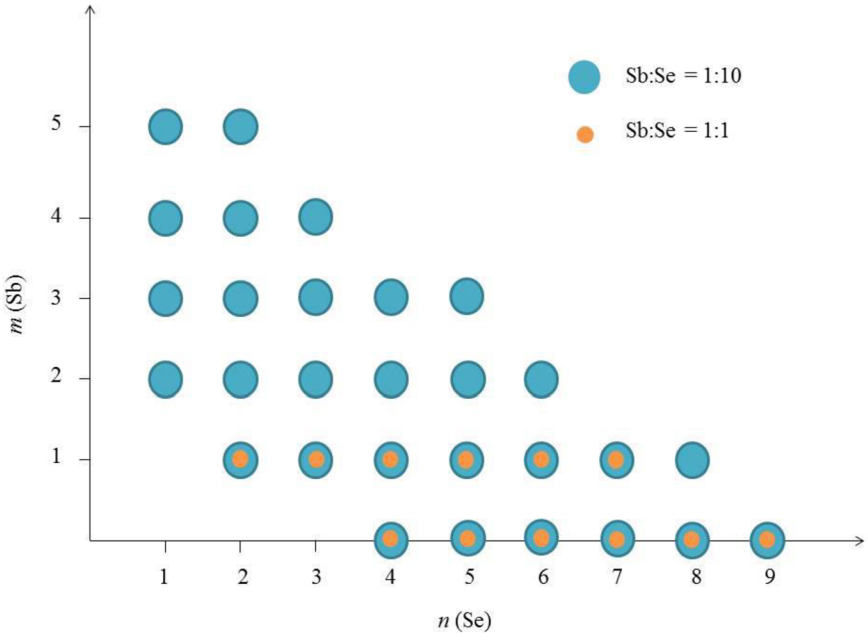

Figure S4. Overview of stoichiometry of Sb_mSe_n clusters generated from Sb:Se = 1:1 and Sb:Se = 1:10.

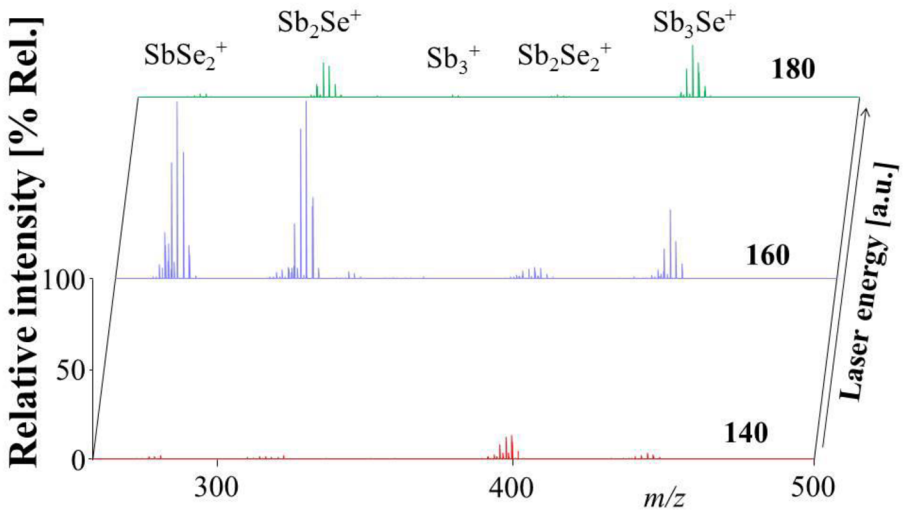

Figure S5. Mass spectra recorded from LDI of Sb:Se mixture with the ratio of elements equal to 1:1 in *m/z* range 250-500 (synthesis in the "hole"). The effect of laser energy. Conditions: laser acts on one point, positive ion mode, laser energy 140-180 a.u.

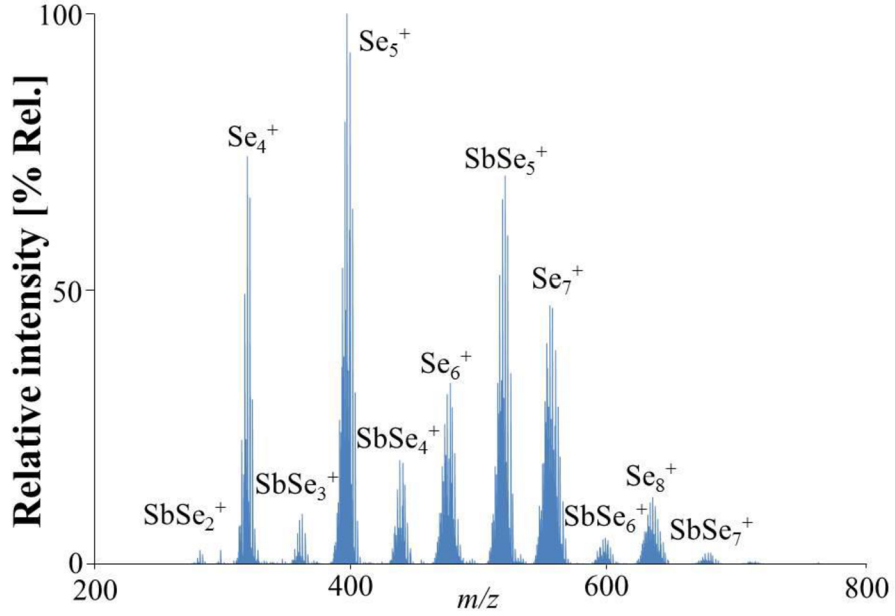

Figure S6. Mass spectra recorded from LDI of Sb:Se mixture in the glycerol with the ratio of elements equal to 1:1. Conditions: positive ion mode, laser energy 130 a.u.

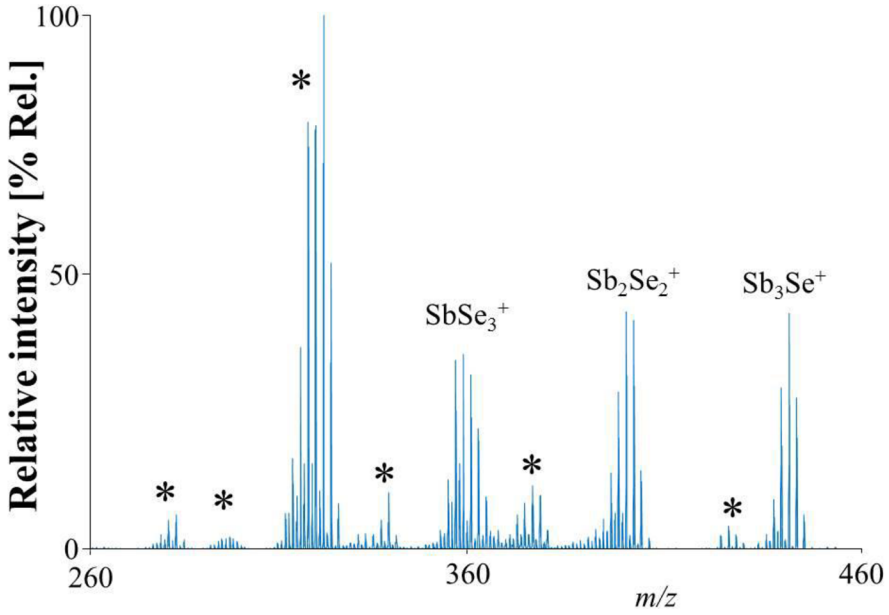

Figure S7. Mass spectra recorded from LDI of Sb:Se mixture in the ionic liquid with the ratio of elements equal to 1:1. Conditions: positive ion mode, laser energy 130 a.u.

Appendix 2A

Fei HUANG, Lubomír PROKEŠ, Petr NĚMEC, Virginie NAZABAL, and Josef HAVEL: Comparison of Clusters Produced from Sb2Se3 Homemade Polycrystalline Material, Thin Films, and Commercial Polycrystalline Bulk Using Laser Desorption Ionization with Time of Flight Quadrupole Ion Trap Mass. *J. Am. Soc. Mass Spectrom.* **30**, 2756-2761 (2019).
IF: 3.109, Quartile: Q1

(https://pubs.acs.org/doi/full/10.1007/s13361-019-02346-9)

© American Society for Mass Spectrometry, 2019

J. Am. Soc. Mass Spectrom. (2019) 30:2756–2761
DOI: 10.1007/s13361-019-02346-9

RESEARCH ARTICLE

Comparison of Clusters Produced from Sb_2Se_3 Homemade Polycrystalline Material, Thin Films, and Commercial Polycrystalline Bulk Using Laser Desorption Ionization with Time of Flight Quadrupole Ion Trap Mass Spectrometry

Fei Huang,[1] Lubomír Prokeš,[1] Petr Němec,[2] Virginie Nazabal,[2,3] Josef Havel[1]

[1]Department of Chemistry, Faculty of Science, Masaryk University, Kamenice 5/A14, 62500, Brno, Czech Republic
[2]Department of Graphic Arts and Photophysics, Faculty of Chemical Technology, University of Pardubice, Studentská 573, 53210, Pardubice, Czech Republic
[3]Institut des Sciences Chimiques de Rennes, UMR-CNRS 6226, Equipe Verres et Céramiques, Université de Rennes 1, 35042, Rennes, France

Downloaded via MASARYK UNIV on October 1, 2021 at 09:26:05 (UTC).
See https://pubs.acs.org/sharingguidelines for options on how to legitimately share published articles.

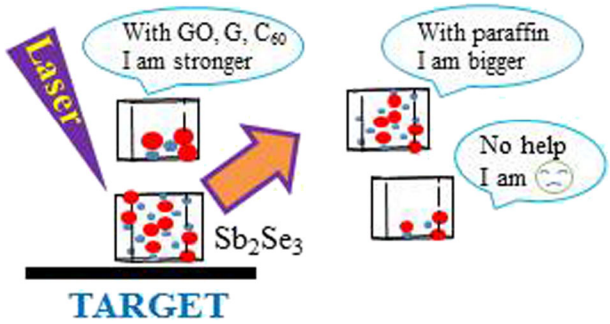

Abstract. This study compared Sb_2Se_3 material in the form of commercial polycrystalline bulk, sputtered thin film, and homemade polycrystalline material using laser desorption ionization (LDI) time of flight mass spectrometry with quadrupole ion trap mass spectrometry. It also analyzed the stoichiometry of the Sb_mSe_n clusters formed. The results showed that homemade Sb_2Se_3 bulk was more stable compared to thin film; its mass spectra showed the expected cluster formation. The use of materials for surface-assisted LDI (SALDI), i.e., graphene, graphene oxide, and C_{60}, significantly increased the mass spectra intensity. In total, 19 Sb_mSe_n clusters were observed. Six novel, high-mass clusters—$Sb_4Se_4^+$, $Sb_5Se_{3\text{-}6}^+$, and $Sb_7Se_4^+$—were observed for the first time when using paraffin as a protective agent.

Keywords: Antimony selenide, Clusters, Laser desorption ionization, Paraffin, Chalcogenides

Received: 25 July 2019/Revised: 11 September 2019/Accepted: 29 October 2019 /Published Online: 23 October 2019

Introduction

Sb_2Se_3 is known in nature as the mineral antimonselite. The crystal and electronic structure of antimony selenide as well as its vibrational properties were previously determined [1–4]. Generally, the Sb_mSe_n system is an important member of chalcogenide materials. Under typical experimental conditions of chalcogenide glass synthesis, the glass-forming region in the Sb_mSe_n system is limited to rather low antimony content (up to 30%) and smaller glass batches often face phase separation problems [5–7]. On the other hand, it is possible to fabricate amorphous, stoichiometric, and thin Sb_2Se_3 films by physical vapor deposition techniques such as radiofrequency magnetron sputtering [8] or thermal evaporation [9]. Moreover, Sb_2Se_3 forms stable glasses and amorphous thin films with other glass-forming selenides like $GeSe_2$ [10–13]. Today, Sb_mSe_n materials, especially in the form of thin films, have been widely studied as for memory switching application [14, 15], as glass-ceramic or antimony selenide thin films for solar cells [16–20], as Sb_2Se_3 anode for lithium, and sodium batteries [21, 22].

In a previous article [23], we examined the formation of clusters produced by laser ablation from mixtures of Sb and Se elements in different ratios. We observed 24 Sb_mSe_n clusters that were generated from metal surface of common target. In this study, we would like to compare the stoichiometry of clusters formed by laser desorption ionization (LDI) from Sb_2Se_3 materials in the form of commercial polycrystalline bulk, thin film, and homemade

Electronic supplementary material The online version of this article (https://doi.org/10.1007/s13361-019-02346-9) contains supplementary material, which is available to authorized users.

Correspondence to: Josef Havel; *e-mail:* havel@chemi.muni.cz

polycrystalline material to the clusters generated by laser ablation synthesis (LAS) from the mixtures of elements (antimony and selenium). Additionally, in order to evaluate the influence of various surfaces on cluster formation, some other materials that act as surface-assisted LDI (SALDI) matrices (graphene [G], graphene oxide [GO], and fullerene [C_{60}]) were used. Since paraffin (as a protective agent) was found to increase the intensity of chalcogenide high mass clusters [24], we also studied the assistance of paraffin in detail.

Experimental

Chemicals

Polycrystalline Sb_2Se_3 was purchased from Sigma-Aldrich (St. Louis, MO, USA). Homemade polycrystalline Sb_2Se_3 was synthesized using high-purity elements (Sb and Se of 99.999% purity). Acetonitrile, G, GO, and C_{60} were purchased from Sigma-Aldrich (Steinheim, Germany). Parafilm was purchased from Bemis NA (Neenah, Wis., USA). Red phosphorus was obtained from Riedel de Haën (Hannover, Germany) and was purified via sublimation in a nitrogen atmosphere. Water was double distilled using a quartz apparatus from Heraeus Quarzschmelze (Hanau, Germany). All other reagents were of analytical-grade purity. Amorphous Sb_2Se_3 thin films were fabricated by radio-frequency magnetron sputtering using an MPE600S (Plassys-Bestek, France) multichamber physical vapor deposition system. For the depositions, single crystalline silicon <100> substrates and a polycrystalline Sb_2Se_3 sputtering target (99.999%, ALB Materials, USA) were employed. The experimental details of thin film deposition are provided elsewhere [8]. No Bragg peaks were detected in the X-ray diffraction patterns of deposited thin films, which confirms their amorphous state.

Mass Spectrometry

AXIMA Resonance and AXIMA CFR mass spectrometers, both from Kratos Analytical Ltd. (Manchester, UK), coupled with a quadrupole ion trap and time-of-flight detection, were used to record mass spectra in both positive and negative ion modes. Both instruments were equipped with a nitrogen laser (337 nm), and the laser repetition rate was set to 5 Hz with a pulse time width of 3 ns.

Software and Computation

Launchpad software (Kompact version 2.9.3, 2011) from Kratos Analytical Ltd. (Manchester, UK) was used to determine Sb_mSe_n cluster stoichiometry via comparison of isotopic envelopes.

Sample Preparation for Mass Spectrometry

1. Commercial Sb_2Se_3 polycrystalline bulk, homemade polycrystalline material and amorphous Sb_2Se_3 thin film

An agate mortar was used to pulverize the polycrystalline Sb_2Se_3; the powder was then suspended in acetonitrile (1 mg/ml). From the prepared suspensions, 10 μL was deposited on a MALDI target and dried in open air. The amorphous Sb_2Se_3 thin film was fixed on the target with a narrow piece of parafilm.

2. SALDI using GO, G and C_{60} surfaces

Ten microliters of GO, G, or C_{60} suspensions in acetonitrile was separately deposited on individual spots of a MALDI target and then 10 μL of the commercial polycrystalline bulk Sb_2Se_3 powder suspension (described above) was separately added on the surface of the GO, G, or C_{60} suspension.

3. Sb_2Se_3 covered with paraffin

Ten microliters of the Sb_2Se_3 powder suspension (described above) was deposited on a target and then covered with paraffin solution in xylene (1 cm^2 of parafilm dissolved in 1 ml xylene).

Results and Discussion

LDI of different materials was used to generate clusters while mass spectra were recorded in both positive and negative ionization modes by using a reflectron mass analyzer. This analysis revealed that a low number of clusters and low-intensity spectra were produced in the negative ion mode. Therefore, the results obtained in the positive ion mode are presented.

Effect of Laser Energy on Homemade Sb_2Se_3 Polycrystalline Material Mass Spectra

The effect of laser energy on intensity of clusters formed is shown in Figure 1. The high-intensity clusters were observed in the 300–450 *m/z* range; the intensities heightened as the laser energy increased. However, some low-intensity clusters were also observed in the 450–650 mass range (spectra not shown). This data indicates that the homemade Sb_2Se_3 polycrystalline material was rather easy to decompose even at relatively low laser energy (140 a.u.). Detailed analysis of the homemade Sb_2Se_3 polycrystalline material spectra is shown in Figure S1A. In addition to $SbSe_2^+$, $Sb_2Se_n^+$ (n = 1, 2) and $Sb_3Se_n^+$ (n = 1–3) clusters, Sb_m^+ (m = 2–4) species were also detected. Comparison of experimental and theoretical isotopic patterns concerning Sb_3Se^+ is provided in Figure S1B. Overall, they showed good agreement.

Effect of Laser Energy on Thin Film Mass Spectra

The effect of laser energy on thin film mass spectra (Figure S2A) was different from that of homemade Sb_2Se_3

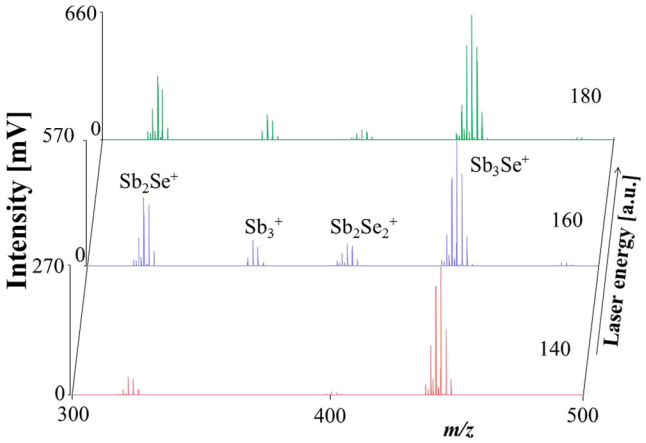

Figure 1. The effect of laser energy on the mass spectra from LDI of homemade Sb_2Se_3 polycrystalline material in the 300-500 *m/z* range in the positive ion mode

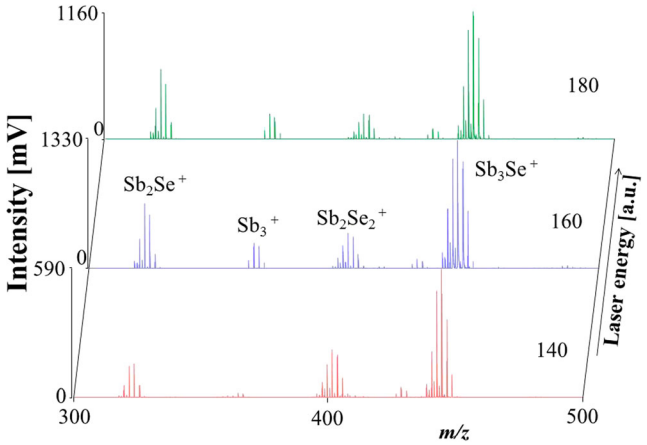

Figure 3. The effect of laser energy on the mass spectra from LDI of commercial Sb_2Se_3 polycrystalline bulk in the 300–500 *m/z* range in positive ion mode

polycrystalline material. At 140 a.u. laser energy, the cluster intensities reached their maxima. The mass spectra showed that the thin film was less stable against pulsed laser irradiation than the homemade Sb_2Se_3 polycrystalline material the thin films were easier to ablate. An example of a thin film mass spectrum is shown in Figure 2. The thin film mass spectra showed similar clusters to those formed from the homemade Sb_2Se_3 polycrystalline material. However, the $Sb_3Se_3^+$, $SbSe_2^+$, Sb_m^+ (m = 2–4), $Sb_2Se_n^+$ (n = 1, 2) and $Sb_3Se_n^+$ (n = 1, 2) clusters were not observed. There was good agreement between the theoretical and experimental isotopic patterns as exemplified for Sb_2Se^+cluster (Figure S2B).

Effect of Laser Energy on Commercial Sb_2Se_3 Polycrystalline Material Mass Spectra

Comparison of mass spectra generated from commercial Sb_2Se_3 polycrystalline bulk at different laser energies is shown in Figure 3. Even at low laser energy (120 a.u.), we observed several low-intensity clusters in the *m/z* range over 450. Figure S3A shows the result of detailed mass spectra analysis concerning commercial Sb_2Se_3 polycrystalline bulk material. Besides $SbSe_2^+$, $Sb_2Se_n^+$ (n = 1–4) and $Sb_3Se_n^+$ (n = 1–5), Sb_m^+ (m = 3, 4) clusters were also noted. Comparison of experimental and theoretical isotopic patterns for the $Sb_2Se_2^+$ cluster is provided in Figure S3B; there was good agreement between the experiment with the theoretical model.

Comparison of Amorphous Sb_2Se_3 Thin Film, Commercial and Homemade Polycrystalline Sb_2Se_3 Material Mass Spectra

Figure 4 shows thin film, commercial and home-made polycrystalline Sb_2Se_3 material mass spectra that were measured using the same laser energy (120 a.u.). At this

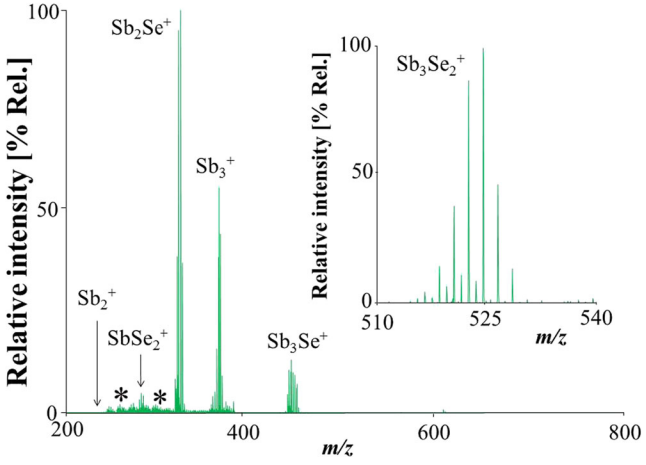

Figure 2. Mass spectra from LDI of amorphous Sb_2Se_3 thin film in the 200–800 *m/z* range. The inset shows the magnification of spectra in 510–540 *m/z* range. Conditions: positive ion mode; 120 a.u. laser energy; *refers to unidentified clusters

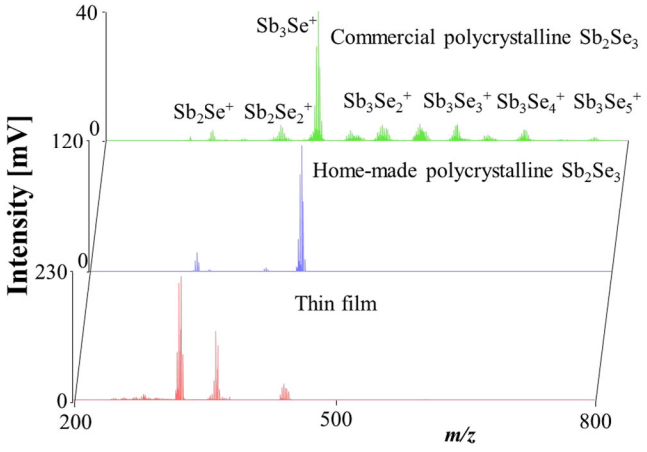

Figure 4. Mass spectra from LDI of commercial and home-made Sb_2Se_3 polycrystalline material as well as amorphous Sb_2Se_3 thin film in the 300–500*m/z* range. Conditions: positive ion mode; 120 a.u. laser energy

laser energy, the order of intensity was thin film, followed by homemade and finally commercial Sb_2Se_3 polycrystalline material, data that indicate the stability of the three materials with respect to laser pulse is increasing. In the homemade polycrystalline Sb_2Se_3 material and commercial Sb_2Se_3 polycrystalline bulk material mass spectra, the most intensive cluster was Sb_3Se^+. Contrary, in the thin film mass spectra, the Sb_2Se^+ cluster was the strongest. The most intense cluster, observed in the thin film mass spectrum at 140–180 a.u. laser energy, was Sb_3Se^+. Additionally, the commercial Sb_2Se_3 polycrystalline bulk produced more clusters (Figure 5).

Special Methods to Enhance Mass Spectra Intensity and Produce Higher-mass Clusters

Enhancement of cluster intensity GO, G, or C_{60} were previously used as a matrix for SALDI mass spectrometry [25–27]. We examined whether these materials can increase the intensity of Sb_2Se_3 mass spectra. Comparison of mass spectra for commercial Sb_2Se_3 polycrystalline bulk and the same material deposited on the surface of GO, C_{60}, or G at the same laser energy (120 a.u.) is shown in Figure 6. GO, G, and C_{60} enhanced the intensity of the most of the signals present in mass spectra. GO was the most effective material for enhancing the mass spectra intensity (nine times greater intensity compared to simple LDI), followed by C_{60} and then G.

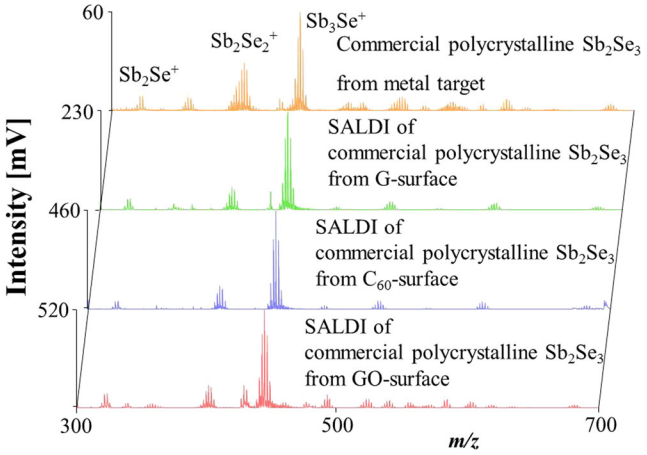

Figure 6. Mass spectra from LDI of commercial polycrystalline Sb_2Se_3 on the surface of GO, C_{60}, and G and on a common metal target in the 300–700 *m/z* range. Conditions: positive ion mode; 120 a.u. laser energy

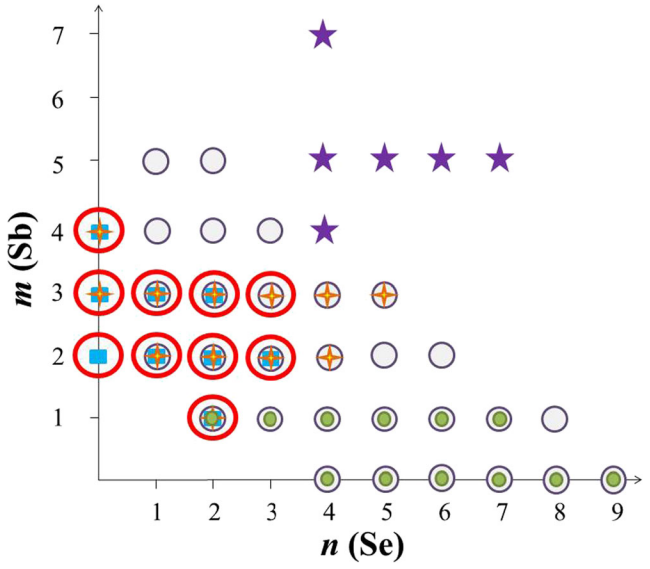

Figure 5. Overview of clusters observed by using paraffin and Sb_mSe_n cluster stoichiometry generated from commercial/homemade Sb_2Se_3 polycrystalline material, amorphous Sb_2Se_3 thin film, and mixtures of antimony with selenium (Sb/Se = 1:1 or 1:10). ★ New clusters by using paraffin; ○ Sb/Se = 1:10; ● Sb/Se = 1:1; ■ thin film; ✦ commercial polycrystalline $Sb2Se_3$; ○ home-made polycrystalline Sb_2Se_3

Effect of Paraffin Comparison of commercial Sb_2Se_3 polycrystalline bulk mass spectra with and without a paraffin cover at 160 a.u. laser energy is shown in Figure 7a–c. At the *m/z* range below 510, the cluster intensities produced solely by Sb_2Se_3 was higher than when Sb_2Se_3 was covered with paraffin. On the contrary, in the *m/z* range over 510, the intensity of the clusters originating in Sb_2Se_3 covered with paraffin was higher than that one produced by Sb_2Se_3 alone. Furthermore, we detected the formation of new clusters beyond *m/z* 800 ($Sb_4Se_4^+$, $Sb_5Se_{3\text{-}6}^+$, and $Sb_7Se_4^+$) from Sb_2Se_3 covered with paraffin. Comparison of experimental and theoretical isotopic patterns for one newly identified $Sb_5Se_6^+$ cluster is given in Figure S4; the data showed good agreement between the experimental results and theoretical model. The results obtained indicate that paraffin acts as a protective agent to diminish fragmentation. It is not easy to explain the effect of paraffin, as it can be very complex. First, because particles of materials are covered with paraffin layer which is absorbing part of the laser energy, the fragmentation is diminished. In addition, similarly to those of Ag^+ adducts with paraffin [28], we observed here the formation of $Sb_mSe_n^+$ cation adducts with paraffin ($C_4H_{10}{\cdot}Sb_2Se_3^+$ shown in Figure S5 A and $C_{18}H_{38}{\cdot}Sb_3Se^+$ shown in Figure S5B). Such formation of charged adducts can also decrease the fragmentation. An overview of the Sb_m, Se_n, and Sb_mSe_n clusters generated from all Sb_2Se_3 forms and Sb/Se mixtures (1:1 or 1:10) [23] is provided in Figure 5.

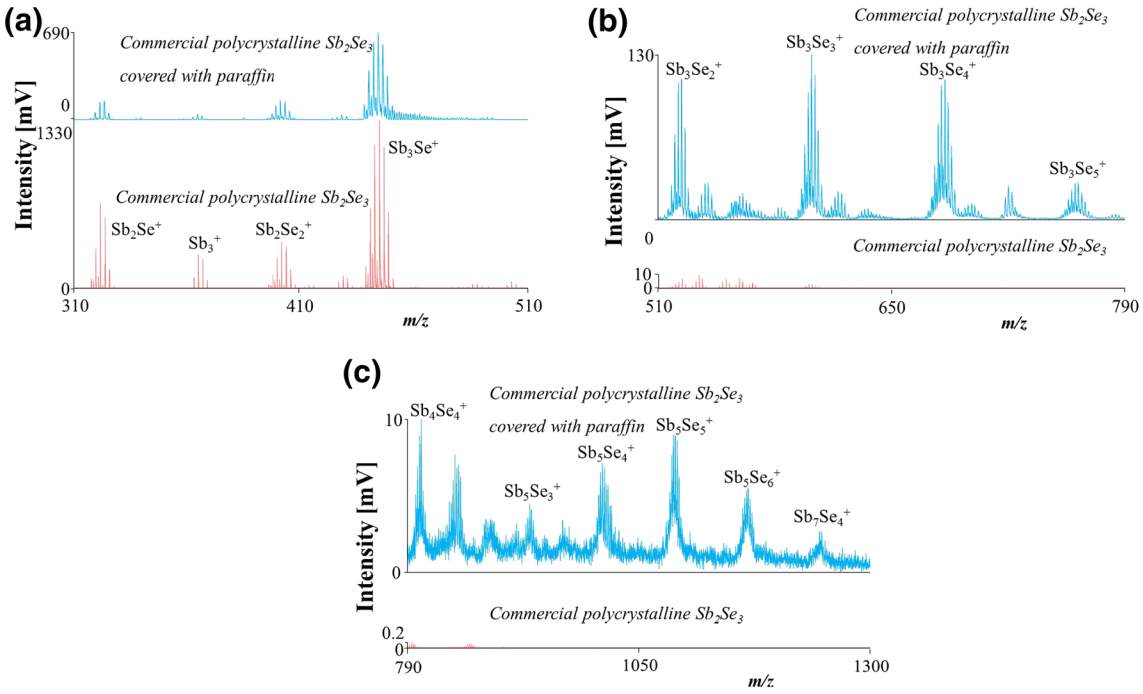

Figure 7. (**a**) Mass spectra from LDI of commercial polycrystalline Sb_2Se_3, and the same sample covered with paraffin, in the 310–510 *m/z* range. Conditions: positive ion mode; 160 a.u. laser energy. (**b**) Mass spectra from LDI of commercial polycrystalline Sb_2Se_3, and the same sample covered with paraffin, in the 510–790 *m/z* range. Conditions: positive ion mode; 160 a.u. laser energy. (**c**) Mass spectra from LDI of commercial polycrystalline Sb_2Se_3, and the same sample covered with paraffin, in the 790–1300 *m/z* range. Conditions: positive ion mode; 160 a.u. laser energy

Conclusions

LDI with quadrupole ion trap time-of-flight mass spectrometry was used to characterize different Sb_2Se_3 forms (commercial or home-made polycrystalline material or amorphous thin films). We showed that this technique is a powerful method to study the formation of binary Sb_mSe_n clusters. Homemade Sb_2Se_3 polycrystalline material produced the lowest number of clusters during LDI. Commercial Sb_2Se_3 polycrystalline bulk generated a higher number of detected Sb_mSe_n species. The amorphous Sb_2Se_3 thin film was easily ablated. We demonstrated that GO, C60, or G are suitable materials for SALDI in order to enhance the mass spectra intensity of the clusters produced from Sb_2Se_3 polycrystalline material. With the use of paraffin, some new clusters were detected in the high-mass part of the spectra.

Acknowledgements

This work was funded with the support from the Czech Science Foundation (Project No. 18-03823S).

References

1. Tideswell, N.W., Kruse, F.H., McCullough, J.D.: The crystal structure of antimony selenide, Sb_2Se_3. Acta Cryst. **10**, 99–102 (1957)
2. Voutsas, G.P., Papazoglou, A.G., Rentzeperis, P.J., Siapkas, D.: The crystal structure of antimony selenide, Sb_2Se_3. Z. Kristallogr. Cryst. Mater. **171**, 261–268 (1985)
3. Vadapoo, R., Krishnan, S., Yilmaz, H., Marin, C.: Electronic structure of antimony selenide (Sb_2Se_3) from GW calculations. Phys. Status Solidi B. **3**, 700–705 (2011)
4. Deringer, V.L., Stoffel, R.P., Wuttig, M., Dronskowski, R.: Vibrational properties and bonding nature of Sb_2Se_3 and their implications for chalcogenide materials. Chem. Sci. **6**, 5255–5262 (2015)
5. Itoh, K.: Short- and medium-range order in Sb-Se glasses. J. Solid State Chem. **233**, 368–373 (2016)
6. Holubová, H., Černošek, Z., Černosková, E.: The selenium based chalcogenide glasses with low content of As and Sb: DSC, StepScan DSC and Raman spectroscopy study. J. Non-Cryst. Solids. **355**, 2050–2053 (2009)
7. Kostadinova, O., Yannopoulos, S.N.: Raman spectroscopic study of Sb_xSe_{100-x} phase-separated bulk glasses. J. Non-Cryst. Solids. **355**, 2040–2044 (2009)
8. Halenkovič, T., Gutwirth, J., Němec, P., Baudet, E., Specht, M., Gueguen, Y., Sangleboeuf, J.-C., Nazabal, V.: Amorphous Ge-Sb-Se thin films fabricated by co-sputtering: properties and photosensitivity. J. Am. Ceram. Soc. **101**, 2877–2887 (2018)
9. Chen, C., Li, W.Q., Zhou, Y., Chen, C., Luo, M., Liu, X.S., Zeng, K., Yang, B., Zhang, C.W., Han, J.B., Tang, J.: Optical properties of amorphous and polycrystalline Sb_2Se_3 thin films prepared by thermal evaporation. Appl. Phys. Lett. **107**, 043905 (2015)
10. Němec, P., Olivier, M., Baudet, E., Kalendová, A., Benda, P., Nazabal, V.: Optical properties of $(GeSe_2)_{100-x}(Sb_2Se_3)_x$ glasses in near- and middle-infrared spectral regions. Mater. Res. Bull. **51**, 176–179 (2014)
11. Baudet, E., Gutierrez-Arroyo, A., Němec, P., Bodiou, L., Lemaitre, J., De Sagazan, O., Lhermitte, H., Rinnert, E., Michel, K., Bureau, B., Charrier,

J., Nazabal, V.: Selenide sputtered films development for MIR environmental sensor. Opt. Mater. Express. **6**, 2616–2627 (2016)
12. Olivier, M., Němec, P., Boudebs, G., Boidin, R., Focsa, C., Nazabal, V.: Photosensitivity of pulsed laser deposited Ge-Sb-Se thin films. Opt. Mater. Express. **5**, 781–793 (2015)
13. Baudet, E., Cardinaud, C., Boidin, R., Girard, A., Gutwirth, J., Němec, P., Nazabal, V.: X-ray photoelectron spectroscopy analysis of Ge–Sb–Se pulsed laser deposited thin films. J. Am. Ceram. Soc. **101**, 3347–3356 (2018)
14. Malligavathy, M., Ananth Kumar, R.T., Das, C., Asokan, S., Pathinettam Padiyan, D.: Growth and characteristics of amorphous Sb_2Se_3 thin films of various thicknesses for memory switching applications. J. Non-Crystal. Solids. **429**, 93–97 (2015)
15. Shylashree, N., Uma, B.V., Dhanush, S., Sagar, A., Nisarga, A., Aashith, K., Sangeetha, B.G.: Preparation and characterization of Sb_2Se_3 devices for memory applications. AIP Conference Proceedings. **1966**, 020032 (2018)
16. Zhang, X., Korolkov, I., Fan, B., Cathelinaud, M., Ma, H., Adam, J.-L., Merdrignac, O., Calvez, L., Lhermite, H., Le Brizoual, L., Pasquinelli, M., Simon, J.-J.: Chalcogenide glass-ceramic with self-organized heterojunctions: application to photovoltaic solar cells. EPJ Photovoltaics. **9**, 3 (2018)
17. Choi, Y., Mandal, T., Yang, W., Lee, Y., Im, S.H., Noh, J., Seok, S.: Sb_2Se_3-sensitized inorganic–organic heterojunction solar cells fabricated using a single-source precursor. Angew. Chem. **53**, 1329–1333 (2014)
18. Zeng, K., Xue, D.-J., Tang, J.: Antimony selenide thin-film solar cells. Semicond. Sci. Technol. **31**, 063001 (2016)
19. Hutter, O.S., Philips, L.J., Durose, K., Major, J.D.: 6.6% efficient antimony selenide solar cells using grain structure control and an organic contact layer. Sol. Energy Mater. Sol. Cells. **188**, 177–181 (2018)
20. Carey, J.J., Allen, J.P., Scanlon, D.O., Watson, G.W.: The electronic structure of the antimony chalcogenide series: prospects for optoelectronic applications. J. Solid State Chem. **213**, 116–125 (2014)
21. Xue, M.-Z., Fu, Z.-W.: Pulsed laser deposited Sb_2Se_3 anode for lithium-ion batteries. J. Alloys Compd. **458**, 351–356 (2008)
22. Ge, P., Cao, X., Hou, H., Li, S., Ji, X.: Rodlike Sb_2Se_3 wrapped with carbon: the exploring of electrochemical properties in sodium-ion batteries. ACS Appl. Mater. Interfaces. **9**, 34979–34989 (2017)
23. Huang, F., Prokeš, L., Havel, J.: Laser ablation synthesis of antimony selenide clusters with simultaneous laser desorption ionization (LDI) quadrupole ion trap mass spectrometry. J. Am. Soc. Mass Spectrom. **30**, 634–638 (2019)
24. Mawale, R.M., Ausekar, M.V., Prokeš, L., Nazabal, V., Baudet, E., Halenkovič, T., Bouška, M., Alberti, M., Němec, P., Havel, J.: Laser desorption ionization of As_2Ch_3 (Ch = S, Se, and Te) chalcogenides using quadrupole ion trap time-of-flight mass spectrometry: a comparative study. J. Am. Soc. Mass Spectrom. **28**, 2569–2579 (2017)
25. Dong, X.L., Cheng, J.S., Li, J.H., Wang, Y.S.: Graphene as a novel matrix for the analysis of small molecules by MALDI-TOF MS. Anal. Chem. **82**, 6208–6214 (2010)
26. Lee, G.B., Bae, S.-E., Huh, S., Cha, S.W.: Graphene oxide embedded sol–gel (GOSG) film as a SALDI MS substrate for robust metabolite fingerprinting. RSC Adv. **5**, 56455–56459 (2015)
27. Liu, J.A., Xiong, L., Zhang, S., Wei, J.C., Xiong, S.X.: C_{60} fluorine derivative as novel matrix for small molecule analysis by MALDI-TOF MS. Metabolomics. **S1**, 002 (2012)
28. Yang, M., Hashimoto, K., Fujino, T.: Silver nanoparticles loaded on ammonium exchanged zeolite as matrix for MALDI-TOF-MS analysis of short-chain n-alkanes. Chem. Phys. Lett. **706**, 525–532 (2018)

Appendix 2B

Fei HUANG, Lubomír PROKEŠ, Petr NĚMEC, Virginie NAZABAL, and Josef HAVEL: Comparison of Clusters Produced from Sb2Se3 Homemade Polycrystalline Material, Thin Films, and Commercial Polycrystalline Bulk Using Laser Desorption Ionization with Time of Flight Quadrupole Ion Trap Mass. *J. Am. Soc. Mass Spectrom*. **30**, 2756-2761 (2019).

Supporting information

(https://pubs.acs.org/doi/full/10.1007/s13361-019-02346-9)

Comparison Study of Clusters Produced from Sb_2Se_3 Home-made Polycrystalline Material, Thin Films, and Commercial Polycrystalline bulk. Laser Desorption Ionization with Time of Flight Quadrupole Ion Trap Mass Spectrometry

Fei Huang,[1] Lubomír Prokeš,[1,2,3] Petr Němec,[4] Virginie Nazabal,[4,5] and Josef Havel[1*]

[1]Department of Chemistry, Faculty of Science, Masaryk University, Kamenice 5/A14, 62500 Brno, Czech Republic

[2]Department of Physical Electronics, Faculty of Science, Masaryk University, Kotlářská 2, 61137 Brno, Czech Republic

[3]CEPLANT, R&D Centre for Low-Cost Plasma and Nanotechnology Surface Modification, Masaryk University, Kotlářská 2, 61137 Brno, Czech Republic

[4]Department of Graphic Arts and Photophysics, Faculty of Chemical Technology, University of Pardubice, Studentská 573, 53210 Pardubice, Czech Republic

[5]Institut des Sciences Chimiques de Rennes, UMR-CNRS 6226, Equipe Verres et Céramiques, Université de Rennes 1, 35042 Rennes, France

*Author to whom correspondence should be addressed. Email: havel@chemi.muni.cz

Phone: +420 549494114, Fax: +420 549492494

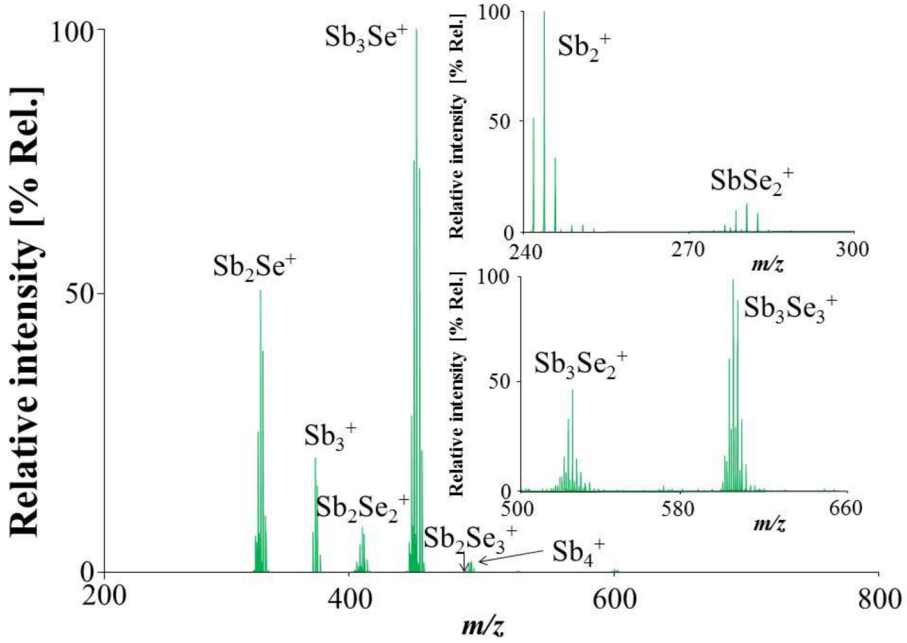

Figure S1A. Mass spectra from LDI of homemade Sb_2Se_3 polycrystalline material in the 200-800 *m/z* range. The insets show the magnification of spectra in the 240-300 and 500-650 *m/z* ranges. Conditions: positive ion mode; 120 a.u. laser energy.

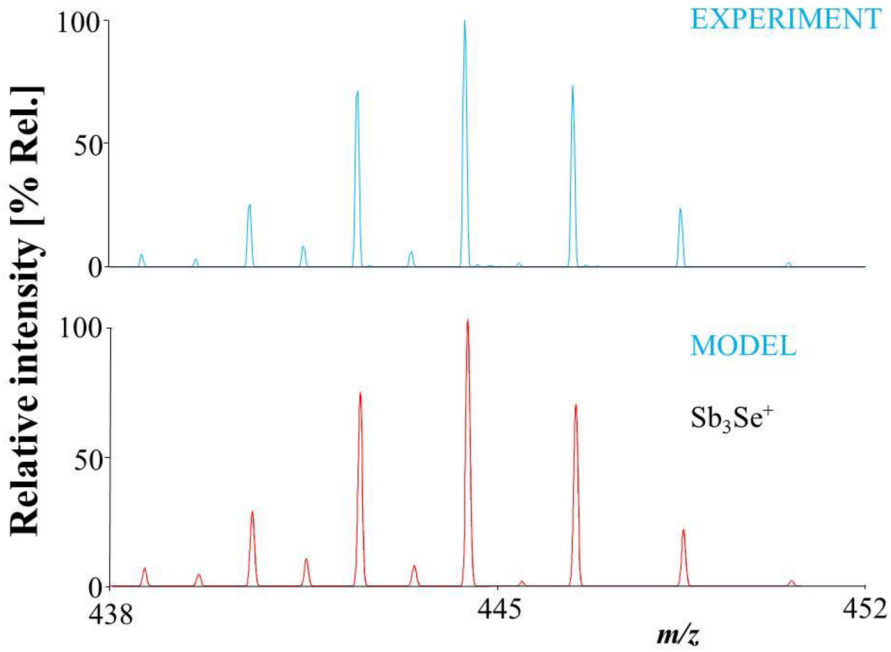

Figure S1B. Comparison of experimental and theoretical isotopic patterns for Sb_3Se^+ clusters. Conditions: positive ion mode; 120 a.u. laser energy.

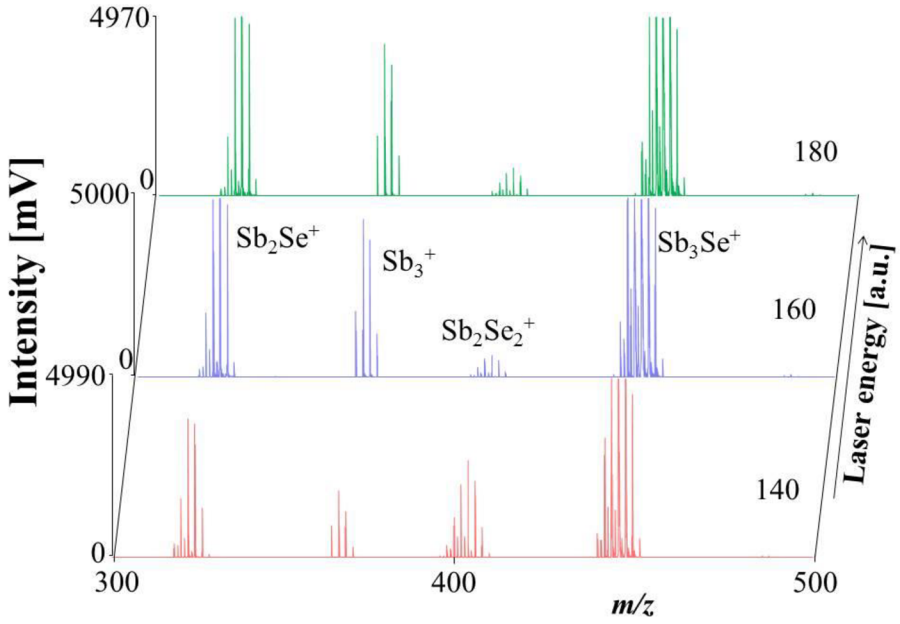

Figure S2A. The effect of laser energy on the mass spectra from LDI of thin film in the 300-500 *m/z* range in positive ion mode.

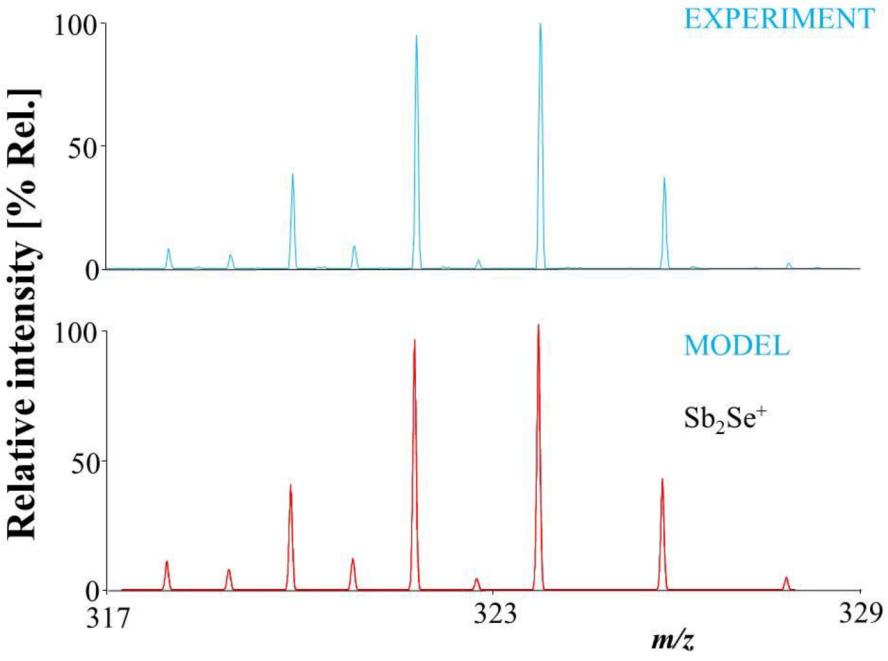

Figure S2B. Comparison of experimental and theoretical isotopic patterns for Sb_2Se^+ clusters. Conditions: positive ion mode; 120 a.u. laser energy.

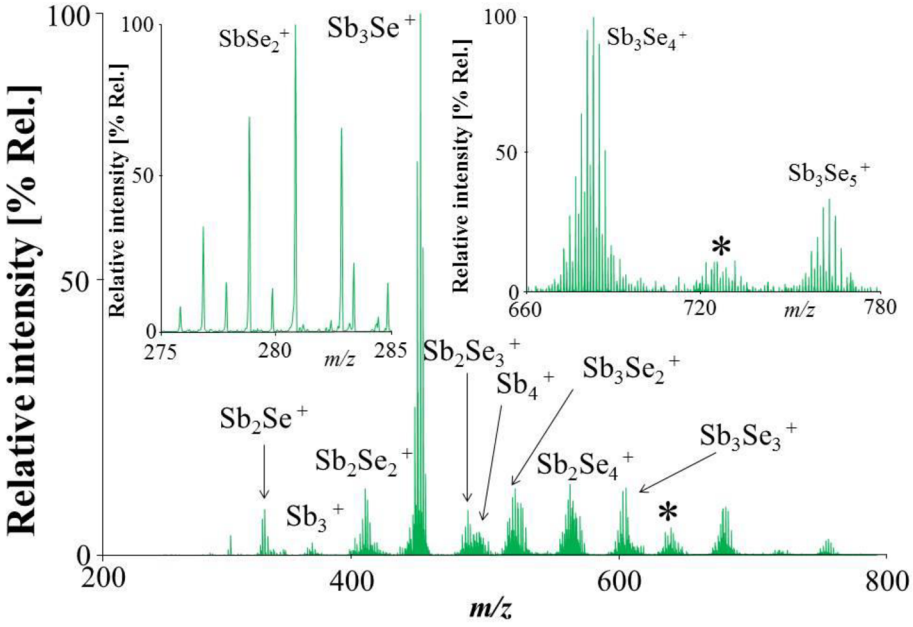

Figure S3A. Mass spectra from LDI of commercial Sb_2Se_3 polycrystalline bulk in the 200-800 *m/z* range. The insets show the magnification of spectra in two *m/z* ranges. Conditions: positive ion mode; 120 a.u. laser energy; * refers to unidentified clusters.

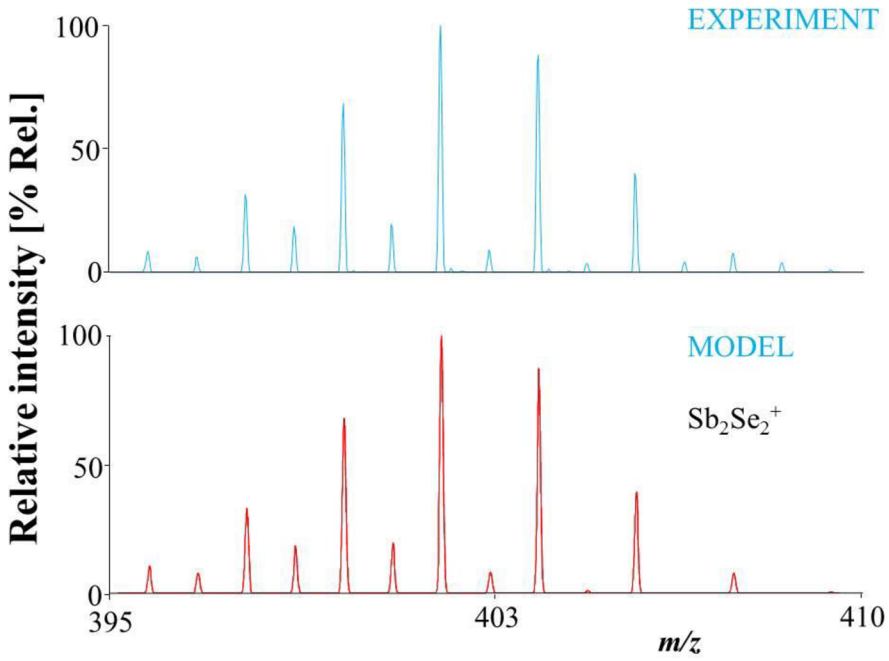

Figure S3B. Comparison of experimental and theoretical isotopic patterns for the $Sb_2Se_2^+$ cluster. Conditions: positive ion mode; 120 a.u. laser energy.

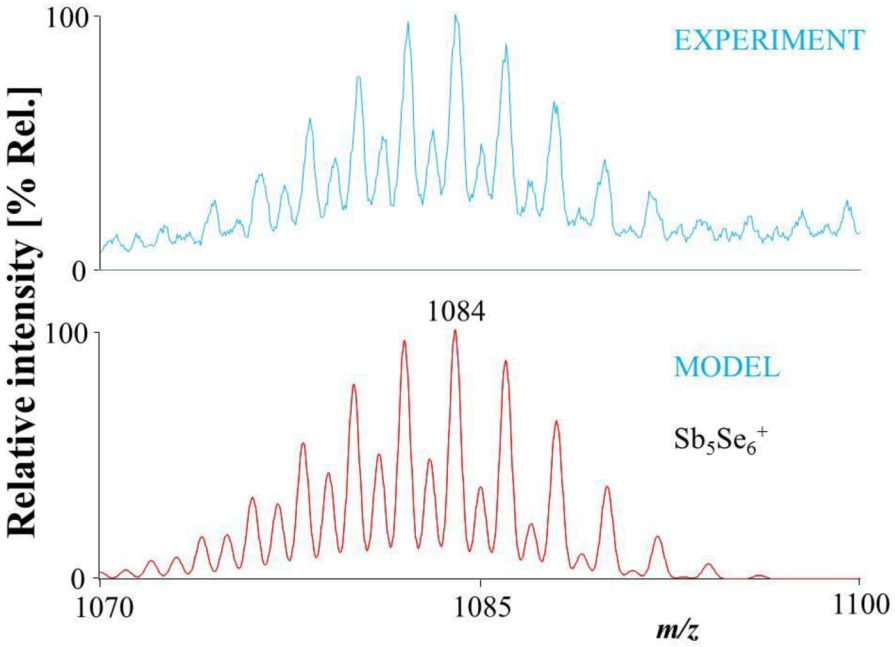

Figure S4. Comparison of experimental and theoretical isotopic patterns for $Sb_5Se_6^+$. Conditions: positive ion mode; 160 a.u. laser energy.

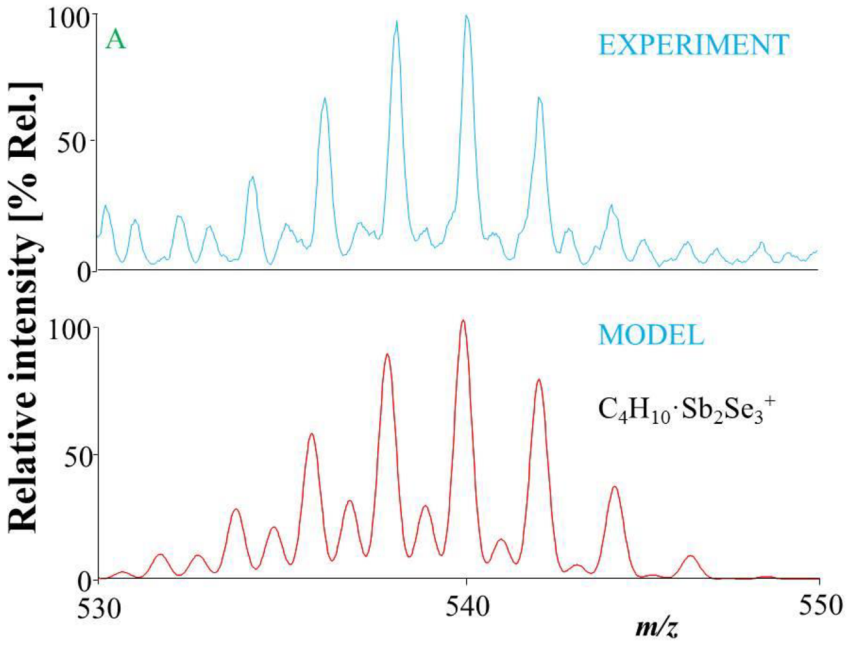

Figure S5A. Comparison of experimental and theoretical isotopic patterns for $C_4H_{10}\cdot Sb_2Se_3^+$. Conditions: positive ion mode; 160 a.u. laser energy.

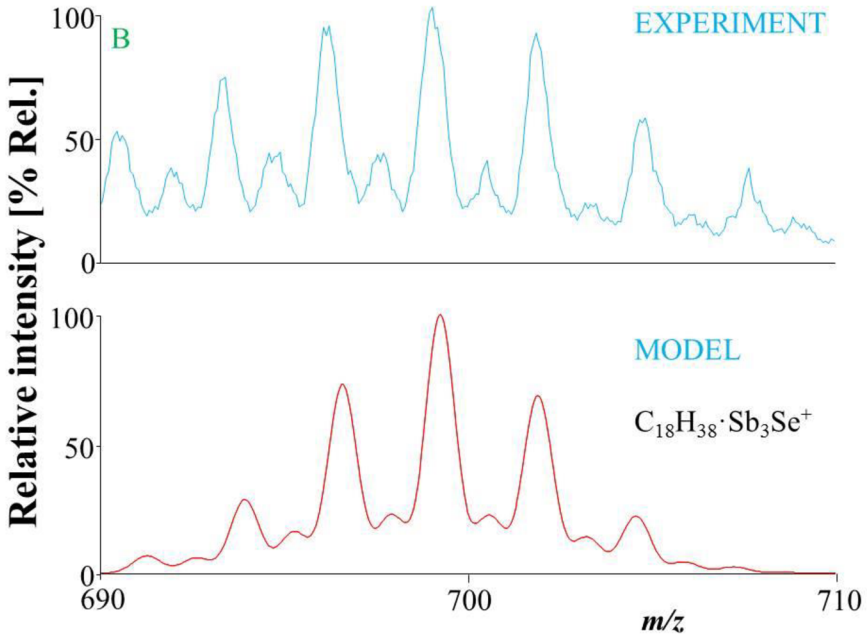

Figure S5B. Comparison of experimental and theoretical isotopic patterns for $C_{18}H_{38}\cdot Sb_3Se^+$.

Conditions: positive ion mode; 160 a.u. laser energy.

Appendix 3A

Fei HUANG, Tomáš WÁGNER, Božena FRUMAROVÁ, Max FRAENKL, Petr KOŠTÁL, and Josef HAVEL: Laser Desorption Ionization Time-of-Flight Mass Spectrometry of Silver-Doped $(GeS_2)_{50}(Sb_2S_3)_{50}$ Chalcogenide Glasses. *ACS Omega*. **5**, 28965-28971 (2020).

IF: 3.512, Quartile: Q2

(https://pubs.acs.org/doi/full/10.1021/acsomega.0c02561)

This is an open access article published under an ACS AuthorChoice License, which permits copying and redistribution of the article or any adaptations for non-commercial purposes.

ACS OMEGA

http://pubs.acs.org/journal/acsodf

Article

Laser Desorption Ionization Time-of-Flight Mass Spectrometry of Silver-Doped $(GeS_2)_{50}(Sb_2S_3)_{50}$ Chalcogenide Glasses

Fei Huang, Tomáš Wágner, Božena Frumarová, Max Fraenkl, Petr Koštál, and Josef Havel*

Cite This: *ACS Omega* 2020, 5, 28965−28971

Read Online

ACCESS | Metrics & More | Article Recommendations | Supporting Information

ABSTRACT: Mass spectra of $(GeS_2)_{50}(Sb_2S_3)_{50}$ glass and Ag-doped glasses [5% Ag $(GeS_2)_{50}(Sb_2S_3)_{50}$ and 15% Ag $(GeS_2)_{50}(Sb_2S_3)_{50}$] obtained using laser desorption ionization (LDI) time-of-flight coupled with quadrupole ion trap mass spectrometry were studied. The analysis of the mass spectra indicated the formation of $Ag_aGe_bSb_cS_d$ clusters. In addition to the SbS_d^+ (d = 1 and 2), $Sb_2S_d^+$ (d = 1−3), $Sb_3S_d^+$ (d = 1−5), $Sb_4S_d^+$ (d = 3 and 4), $Sb_5S_2^+$, and Sb_c^+ (c = 3 and 5) clusters, various clusters containing Ag, such as Ag_a^+ (a = 1 and 2), $AgGeS^+$, $AgSb_c^+$ (c = 1, 2, and 4), $AgSbS^+$, $AgSb_2S_d^+$ (d = 1−5), $AgSb_3S_3^+$, $AgSb_4S_4^+$, $Ag_2Sb_3S_d^+$ (d = 4 and 5), $Ag_4Sb_2S_3^+$, and $Ag_5SbS_3^+$, were generated. Moreover, in spite of the five-ninth purity of all glass components, several hydrogenated clusters ($SbS_3H_8^+$, $Sb_4S_2H^+$, $Ag_2H_{11}^+$, $Ag_2Sb_3H_4^+$, $Ag_3Sb_2H_4^+$, $Ag_4Sb_2H_2^+$, and $Ag_4S_3H_8^+$) and some low-intensity oxidized clusters, such as Sb_3O^+ and $Sb_3O_5^+$, were also detected. When applying LDI on $(GeS_2)_{50}(Sb_2S_3)_{50}$ glass, no Ge-containing clusters were detected in the positive ion mode, and just one Ge-containing cluster was observed after doping the glass with Ag. Hydrogen plays an important role in the glasses studied. The knowledge gained concerning cluster stoichiometry contributes to the elucidation of the structure of Ag-doped Ge−Sb−S chalcogenide glasses. It should be noted that some of the clusters were considered to be structural fragments. Furthermore, mass spectrometry was complemented with Raman spectroscopy.

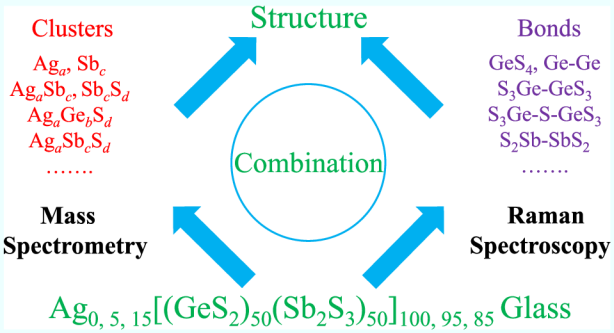

INTRODUCTION

Crystalline and amorphous chalcogenides are high-tech materials that have strategic importance.[1] The Ge−Sb−S system is an important member of the chalcogenide glass family. The properties of Ge−Sb−S glasses have already been studied, including their optical,[2] mechanical,[3] and structural[4] properties. Ag-doped materials are already widely used in many fields.[5−9] The incorporation of Ag into Ge−Sb−S materials changes their optical transmittances, optical gaps, reflectivity, and so forth. Higher indexes of refraction, decreased sensitivities to alkaline etching, and red-shifted absorptions have been observed in such glasses in comparison with silver-free chalcogenide glasses.[10] Ag-doped Ge−Sb−S glasses are utilized in RAM memory and are also widely used in many other fields, for example, as solid electrolytes,[11] optical waveguides,[12] holographic devices,[13] and electrochemical sensors.[14] Inorganic hydrides represent a wide class of compounds that have been described extensively.[15] The role of hydrogen in impairing the optical and emission properties of chalcogenide glass fibers has been studied.[16,17] When hydrogenated chalcogenide glasses were deliberately prepared, they show some unique and improved properties.[18,19] Because Ag acts to form a high number of hydrides,[20] the formation of silver hydrides in glasses follows. Recently, the thermokinetic behaviors of Ag-doped $(GeS_2)_{50}(Sb_2S_3)_{50}$ glasses have been studied,[21] along with the influence of Ag on their structures and physical properties.[22]

The aim of the present study is to use mass spectrometry (MS) to elucidate the chemistry of these materials, especially in terms of their basic structural items, via the study of the clusters generated by laser desorption ionization (LDI) in both undoped and silver-doped $(GeS_2)_{50}(Sb_2S_3)_{50}$ chalcogenide glasses. Complementary structural information on these glasses was acquired via Raman spectroscopy.

RESULTS AND DISCUSSION

The formation of clusters generated from $(GeS_2)_{50}(Sb_2S_3)_{50}$ glass, as well as from the same glass doped with 5 or 15% Ag via LDI, was studied. A reflectron or linear mode was employed to record the mass spectra in both positive and negative ion modes. It was shown that the clusters produced in the positive ion mode were of high intensity, and mass spectra indicated that they

Received: May 30, 2020
Accepted: October 27, 2020
Published: November 9, 2020

Downloaded via MASARYK UNIV on October 1, 2021 at 09:26:42 (UTC).
See https://pubs.acs.org/sharingguidelines for options on how to legitimately share published articles.

© 2020 American Chemical Society

occurred in higher numbers than the clusters in the negative ion mode. Therefore, the discussion to follow will be based largely on the results from the positive ion mode.

LDI of $(GeS_2)_{50}(Sb_2S_3)_{50}$ Chalcogenide Glass. An example of the mass spectra of $(GeS_2)_{50}(Sb_2S_3)_{50}$ chalcogenide glass generated via LDI at laser energy 170 a.u. is given in Figure S1. SbS_d^+ (d = 1 and 2), $Sb_2S_d^+$ (d = 1−3), $Sb_3S_d^+$ (d = 1−5), $Sb_4S_d^+$ (d = 3 and 4), $Sb_5S_2^+$, and Sb_c^+ (c = 3 and 5); low-intensity oxidized Sb_3O^+ and $Sb_3O_5^+$; and hydrogenated $SbS_3H_8^+$ clusters were detected. Some hydrogenated clusters containing antimony, sulfur, or both elements, for example, $SbS_3H_8^+$, were also identified. No clusters containing Ge were detected in the positive ion mode. However, $GeSbS_3^-$, $GeSbS_4^-$, and $GeSbS_5^-$ clusters were observed in the negative ion mode, as shown in Figure 1. A comparison of the experimental and theoretical isotopic patterns demonstrated that the most intensive cluster was Sb_3S^+, as shown in Figure S2, and a good agreement between the experimental and theoretical mass spectra was observed.

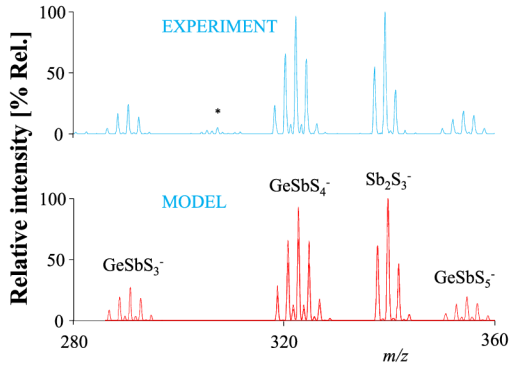

Figure 1. Comparison of experimental and theoretical isotopic patterns for mass spectra of $(GeS_2)_{50}(Sb_2S_3)_{50}$ glass. Conditions: negative ion mode; laser energy 170 a.u. * indicates that the isotopic pattern is too complex or the spectra intensity is too low for the identification of clusters.

LDI of 5% Ag-Doped $(GeS_2)_{50}(Sb_2S_3)_{50}$ Chalcogenide Glass. An example of the mass spectra of the clusters generated via LDI of 5% Ag-doped $(GeS_2)_{50}(Sb_2S_3)_{50}$ chalcogenide glass at laser energy (170 a.u.) is given in Figure S3. It is observed that, in addition to the SbS_d^+ (d = 1 and 2), $Sb_2S_d^+$ (d = 1−3), $Sb_3S_d^+$ (d = 1−5), and Sb_c^+ (c = 1, 2, 3, and 5) clusters, which are also seen in nondoped glass, Ag_a^+ (a = 1 and 2), $AgGeS^+$, $AgSb_c^+$ (c = 1, 2, and 4), $AgSbS^+$, $AgSb_2S_d^+$ (d = 1−5), $AgSb_3S_3^+$, $AgSb_4S_4^+$, $Ag_2Sb_3S_d^+$ (d = 4 and 5), $Ag_4Sb_2S_3^+$, and $Ag_5SbS_3^+$ clusters, as well as the hydrogenated clusters $Sb_4S_2H^+$, $Ag_2Sb_3H_4^+$, $Ag_3Sb_2H_4^+$, $Ag_4Sb_2H_2^+$, and $Ag_4S_3H_8^+$, were generated. With the exception of $Sb_4S_2H^+$ cluster, all the clusters containing hydrogen also contained silver. Only one cluster, namely, $AgGeS^+$, containing Ge was observed. The good agreement of the theoretical isotopic overlap pattern for the $AgGeS^+$ and Ag_2^+ clusters with the experimental one is demonstrated in Figure S4.

LDI of 15% Ag-Doped $(GeS_2)_{50}(Sb_2S_3)_{50}$ Chalcogenide Glass. An example of the LDI mass spectra generated by 15% Ag-doped $(GeS_2)_{50}(Sb_2S_3)_{50}$ chalcogenide glass at laser energy (170 a.u.) is given in Figure S5. No hydrogenated clusters were detected in the mass range studied. The following clusters were identified: SbS_d^+ (d = 1 and 2), $Sb_2S_d^+$ (d = 1−3), $Sb_3S_d^+$ (d = 1−5), Sb_c^+ (c = 1, 2, 3, and 5), Ag_a^+ (a = 1 and 2), $AgGeS^+$, $AgSb_c^+$ (c = 1, 2, and 4), $AgSbS^+$, $AgSb_2S_d^+$ (d = 1−4), $AgSb_3S_3^+$, $AgSb_4S_4^+$, $Ag_2Sb_3S_d^+$ (d = 4 and 5), $Ag_4Sb_2S_3^+$, $Ag_5SbS_3^+$, $Ag_2H_{11}^+$, $Ag_3Sb_2H_4^+$, and $Ag_4Sb_2H_2^+$. Only one cluster containing Ge, namely, $AgGeS^+$, was detected. A comparison of the experimental and theoretical isotopic patterns for the overlap of $AgSb^+$ and hydrogenated $Ag_2H_{11}^+$ clusters is given in Figure S6, and there is good agreement between the two patterns.

Comparison of $(GeS_2)_{50}(Sb_2S_3)_{50}$, 5% Ag-Doped $(GeS_2)_{50}(Sb_2S_3)_{50}$, and 15% Ag-Doped $(GeS_2)_{50}(Sb_2S_3)_{50}$ Mass Spectra. Figure 2A−D shows the mass spectra of (i) $(GeS_2)_{50}(Sb_2S_3)_{50}$, (ii) 5% Ag-doped $(GeS_2)_{50}(Sb_2S_3)_{50}$, and (iii) 15% Ag-doped $(GeS_2)_{50}(Sb_2S_3)_{50}$ glasses measured at the same laser energy (160 a.u.). In the 100−160 m/z range, it was observed that when silver is incorporated into $(GeS_2)_{50}(Sb_2S_3)_{50}$ glass and its percentage is increasing from 5 to 15%, the intensities of the mass spectra also increase (indicating the decreasing stability of silver-doped chalcogenide glass). In the 160−410 m/z range, the most intense peak for nondoped glass was found for the Sb_3S^+ cluster, while the most intense peak corresponded to the Sb_2S^+ cluster for the 5% silver-doped material and the $AgSbS^+$ cluster for 15% silver-doped glass. In the 410−500 m/z range, the clusters $AgSb_2S_4^+$ and $Sb_3S_4^+$ were observed after conducting LDI on 5% Ag-doped glass, but they were not detected for 15% silver-doped glass. Most of the hydrogenated clusters were observed in the 500−800 m/z range. The intensities of the mass spectra for the 5% Ag-doped glass were higher than those for the 15% Ag-doped glass (which is opposite to what was observed in the 100−160 m/z range).

Effect of Laser Energy on 5% Ag-Doped $(GeS_2)_{50}(Sb_2S_3)_{50}$ Chalcogenide Glass in Negative Ion Mode. A comparison of the mass spectra generated for 5% Ag-doped $(GeS_2)_{50}(Sb_2S_3)_{50}$ chalcogenide glass at different laser energies is shown in Figure S7. The spectra for the negative ion mode differ from those for the positive ion mode. The most intense peak in the negative ion mode was for $AgSb_2S_4^-$, which contrasts with the findings for the positive ion mode, where Sb_3S^+ had the most intense peak (cf. Figure S3). In this mass range, with the exception of $AgSb_2^-$, $Sb_2S_d^-$ (d = 2, 3), $Sb_3S_d^-$ (d = 3−5), and $AgSb_2S_d^-$ (d = 3−5) clusters, which were also generated in the positive ion mode, the other clusters are missing. The spectra below 250 and over 550 m/z at low intensity are not provided (only two clusters, namely, $Ag_2Sb_3S_5^-$ and $Ag_4Sb_2S_3^-$, were detected). Figure S7 demonstrates that the intensities of the clusters increase when the laser energy increases from 150 to 160 a.u., but the same intensities decrease when the laser energy is further increased to 170 a.u., except in the case of $AgSb_2S_4^-$. A comparison of the experimental and theoretical isotopic patterns for the $AgSb_2S_4^-$ cluster is given in Figure S8, and there is good agreement between the experimental results and the theoretical model.

In conclusion, the glasses' structural disorder allows the random formation of homopolar bonds (Ge−Ge, Sb−Sb, and S−S). It is also clear that silver reacts with sulfur and forms preferential Ag−S bonds, which results in sulfur depletion and the formation of Ge−Ge and Sb−Sb bonds. The LDI technique is powerful enough to ionize all the Ge−Ge and Sb−Sb bonds.

Hydrogen Presence in Clusters. Even though the studied materials were made from elements (Ag, Ge, Sb, and S) with five-ninths (5N) purity, several hydrogenated clusters, namely, $SbS_3H_8^+$, $Sb_4S_2H^+$, $Ag_2H_{11}^+$, $Ag_2Sb_3H_4^+$, $Ag_3Sb_2H_4^+$, $Ag_4Sb_2H_2^+$, and $Ag_4S_3H_8^+$, were detected. The hydrogen detected in the studied glasses is most probably from elements used for synthesis. Even when 5N purity standards are used, traces of hydrogen can be present because H_2 is used as a reduction agent during the preparation of the pure elements.

https://dx.doi.org/10.1021/acsomega.0c02561
ACS Omega 2020, 5, 28965−28971

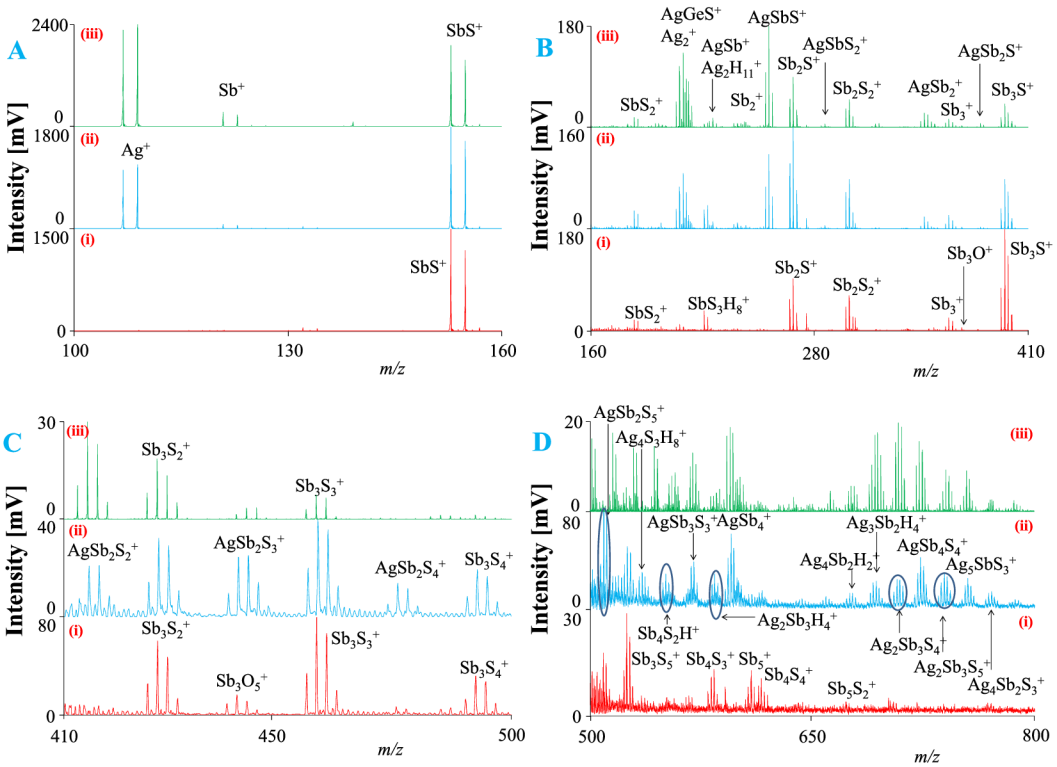

Figure 2. (A–D) Comparison of mass spectra generated via LDI for (i) $(GeS_2)_{50}(Sb_2S_3)_{50}$, (ii) 5% Ag-doped $(GeS_2)_{50}(Sb_2S_3)_{50}$, and (iii) 15% Ag-doped $(GeS_2)_{50}(Sb_2S_3)_{50}$ glass in the *m/z* ranges: A (100–160), B (160–410), C (410–500), and D (500–800). Conditions: positive ion mode; laser energy 160 a.u.

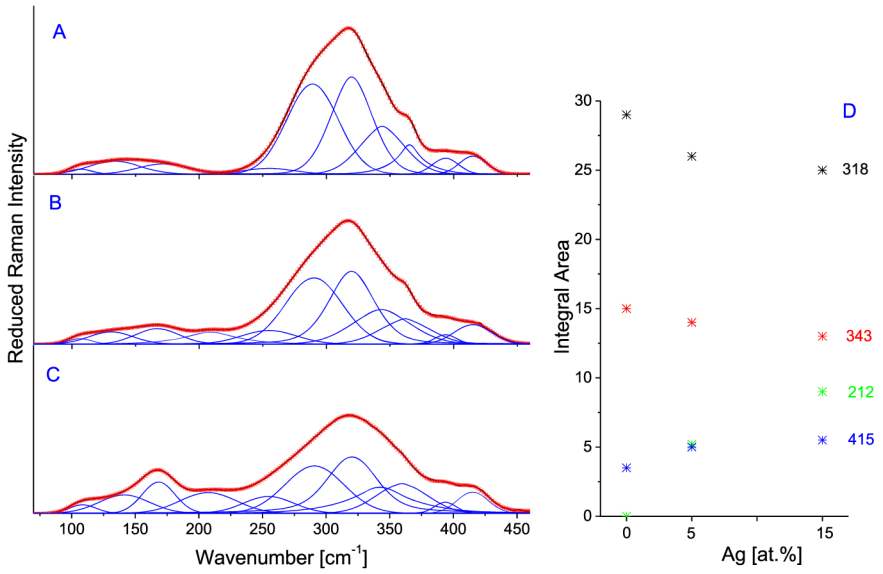

Figure 3. Raman spectra of (A) $(GeS_2)_{50}(Sb_2S_3)_{50}$, (B) 5% Ag-doped glass, and (C) 15% Ag- doped glass and (D) comparison of the integral intensities of the Raman bands at 212, 318, 343, and 415 cm^{-1}.

Raman Spectra of Glasses. The Raman spectra of prepared undoped and Ag-doped $(GeS_2)_{50}(Sb_2S_3)_{50}$ glass samples are shown in Figure 3. All Raman spectra were scaled by area and decomposed into a series of Raman peaks. Raman spectroscopy was performed to analyze the structures in a nondestructive way, unlike MS. Moreover, MS was not able to detect any structural units of clusters related to −Ge−S− or Ge−Ge in undoped Ge−S glass. These structural units were identified via Raman spectroscopy.

The Raman spectra of $(GeS_2)_{50}(Sb_2S_3)_{50}$ glass are shown in Figure 3A. These spectra are in good agreement with those for similar glasses in the Ge−Sb−S system.[23−26] The Raman band between 200 and 450 cm^{-1} can be decomposed into seven bands with maxima near 250, 290, 318, 343, 360, 390, and 415 cm^{-1}.

https://dx.doi.org/10.1021/acsomega.0c02561
ACS Omega 2020, 5, 28965−28971

Table 1. Clusters Generated from $(GeS_2)_{50}(Sb_2S_3)_{50}$ and Its Ag-Doped Chalcogenide Glasses[a]

nondoped	SbS^+	SbS_2^+			
	Sb_2S^+	$Sb_2S_2^+$	$Sb_2S_3^+$		
	Sb_3S^+	$Sb_3S_2^+$	$Sb_3S_3^+$	$Sb_3S_4^+$	$Sb_3S_5^+$
	$Sb_4S_3^+$	$Sb_4S_4^+$			
	$Sb_5S_2^+$				
	Sb_3^+	Sb_5^+			
	Sb_3O^+	$Sb_3O_5^+$			
	$SbS_3H_8^+$				
5% Ag doping	SbS^+	SbS_2^+			
	Sb_2S^+	$Sb_2S_2^+$	$Sb_2S_3^+$		
	Sb_3S^+	$Sb_3S_2^+$	$Sb_3S_3^+$	$Sb_3S_4^+$	$Sb_3S_5^+$
	Sb^+	Sb_2^+	Sb_3^+	Sb_5^+	
	Ag^+	**Ag_2^+**			
	$AgGeS^+$				
	$AgSb^+$	**$AgSb_2^+$**	**$AgSb_4^+$**		
	$AgSbS^+$				
	$AgSb_2S^+$	**$AgSb_2S_2^+$**	**$AgSb_2S_3^+$**	**$AgSb_2S_4^+$**	**$AgSb_2S_5^+$**
	$AgSb_3S_3^+$				
	$AgSb_4S_4^+$				
	$Ag_2Sb_3S_4^+$	**$Ag_2Sb_3S_5^+$**			
	$Ag_4Sb_2S_3^+$				
	$Ag_5SbS_3^+$				
	$Sb_4S_2H^+$	*$Ag_2Sb_3H_4^+$*	*$Ag_3Sb_2H_4^+$*	*$Ag_4Sb_2H_2^+$*	*$Ag_4S_3H_8^+$*
15% Ag doping	SbS^+	SbS_2^+			
	Sb_2S^+	$Sb_2S_2^+$	$Sb_2S_3^+$		
	Sb_3S^+	$Sb_3S_2^+$	$Sb_3S_3^+$	$Sb_3S_4^+$	
	Sb^+	Sb_2^+	Sb_3^+	Sb_5^+	
	Ag^+	**Ag_2^+**			
	$AgGeS^+$				
	$AgSb^+$	**$AgSb_2^+$**	**$AgSb_4^+$**		
	$AgSbS^+$				
	$AgSb_2S^+$	**$AgSb_2S_2^+$**	**$AgSb_2S_3^+$**	**$AgSb_2S_4^+$**	
	$AgSb_3S_3^+$				
	$AgSb_4S_4^+$				
	$Ag_2Sb_3S_4^+$	**$Ag_2Sb_3S_5^+$**			
	$Ag_4Sb_2S_3^+$				
	$Ag_5SbS_3^+$				
	$Ag_2H_{11}^+$	*$Ag_3Sb_2H_4^+$*	*$Ag_4Sb_2H_2^+$*		

[a]**Bold**: clusters containing silver; *Italics*: clusters containing both silver and hydrogen.

The main Raman bands, which are located at 343, 318, and 290 cm^{-1}, have been attributed to the symmetric stretching vibrations of corner−sharing $[GeS_4]$ tetrahedra and asymmetric and symmetric stretching vibrations of $[SbS_3]$ pyramids. The smaller bands at 360, 390, and 415 cm^{-1} can be ascribed to edge-shared $[GeS_4]$ tetrahedral symmetric stretching vibrations, asymmetric stretching vibrations of corner-shared $[GeS_4]$ tetrahedra, and bridging sulfur vibrations in the $S_3Ge−S−GeS_3$ structural units, respectively. Finally, the band at 250 cm^{-1} can be assigned to vibrations of the Ge−Ge bonds in the $[S_3Ge−GeS_3]$ ethane-like structural units.

The low-intensity broad band in the region 100−200 cm^{-1} can be decomposed into three bands at 110, 140, and 170 cm^{-1} corresponding to bending vibrations (ν_2 and ν_4 mode) of GeS_4 tetrahedra and Sb−Sb vibrations in $(S_2)Sb−Sb(S_2)$ bipyramidal units.

The addition of silver to $(GeS_2)_{50}(Sb_2S_3)_{50}$ glass causes several changes:

1 The addition of silver at 5% (Figure 3B,D): The intensity of the band connected to the vibrations of the SbS_3 pyramids (318 cm^{-1}) decreases, while the intensity of the band corresponding to the vibrations of the Sb−Sb bonds (170 cm^{-1}) increases. The new band at 212 cm^{-1} appears when the silver is added to the glass matrix. This band indicates the formation of Ag−S bonds dispersed in glass structure. A similar band was found in the Raman spectra of Ag_2S amorphous thin film.[27]

2 The addition of silver at 15% (Figure 3C,D): The intensity of the band at 318 cm^{-1} decreases progressively, while the intensities of the bands corresponding to the corner-sharing $[GeS_4]$ tetrahedra (343 and 390 cm^{-1}) decrease slightly. The intensities of the bands at 170, 212, 250, 360, and 415 cm^{-1} increase.

We assume that silver is first incorporated into the host structure via its interactions with the sulfur atoms in the $[SbS_3]$ pyramids. Thus, the concentration of Sb−Sb bonds grows. The intense growth of the band at 250 cm^{-1} shows that more ethane-like structural units have been formed. The reduction of the band near 343 cm^{-1} and the growth of bands at 360 and 415 cm^{-1} indicates that the addition of silver leads to the breaking of Ge−S−Ge bridges and the creation of nonbridging sulfur $Ge−S^-$ terminal bonds [pyro-$(GeS_{3.5}{}^{3-})$, meta-$(GeS^{2-}{}_3)$, and di-

https://dx.doi.org/10.1021/acsomega.0c02561
ACS Omega 2020, 5, 28965−28971

($GeS^{-}_{2.5}$) thiogermanate tetrahedra].[28−30] The presence of metathiogermanate tetrahedra can indicate the formation of the Ag_2GeS_3 amorphous phase, which then becomes an inherent part of the amorphous network.[29] Our results are in good agreement with those given in Fraenkle et al.[22]

Another aim of this work was to study the silver doping of glasses using MS. LDI time-of-flight MS decomposes glass into ionic fragments in contrast to Raman spectroscopy, which is a nondestructive technique. The identified fragments (clusters) are listed in Table 1. In contrast to the similar ($GeSe_2$) (Sb_2Se_3) system,[31] there were no Ge-containing clusters detected when LDI was applied to generate the mass spectra of nondoped glasses in the positive ion mode. A possible explanation could be the fact that the bond energy of Ge−S is higher than that of Sb−S (Ge−S = 534 kJ/mol, Sb−S = 199 kJ/mol)[32] and also higher than the bond energy of Ge−Ge and Sb−S (Ge−Ge = 188 kJ/mol). Another possible explanation is that the electronegativity of S is greater than that of Se. Regardless, the presence of Ge-containing structural units and Ge−S and Sb−S bonds was confirmed by Raman spectroscopy, which also clearly identified Ge−Ge and Sb−Sb bonds when silver was added to the glass structure. Comparison of the results of Raman spectroscopy with MS is shown in Table 2. Germanium-contained structural units were detected by Raman spectroscopy but not observed by MS. This might be because these structural units are too stable (tetrahedral structure and high bond energy of Ge−Ge or Ge−S bonds) to be decomposed by MS. There are no Ag−S−Sb structural units detected by Raman, but they were observed by MS. This is, for example, because of the possible reactions that happened between the ions in the plasma plume. In conclusion, while Raman spectroscopy detects the basic structural units, MS shows mostly their fragments. Thus, the combination of these two techniques provides a more complex image of the glass structure and bond strengths when the glass is exposed to laser beams with different energies and intensities.

Table 2. Comparison of the Results of Raman Spectroscopy with MS

structural units detected by Raman spectroscopy	band position cm^{-1}	fragments[a] detected by MS
Ge−Ge	250	no fragments detected
corner-shared GeS_4 tetrahedral	343 and 390	
edge-shared GeS_4 tetrahedral	360	
$S_3Ge−GeS_3$ ethane-like structure	250	
$S_3Ge−S−GeS_3$	415	
Sb−Sb	170	Sb^+ $Sb−Sb^+$ Sb_3^+ Sb_5^+
SbS_3 pyramids	290 and 318	SbS^+ SbS_2^+ Sb_2S^+ $Sb_2S_2^+$ $Sb_2S_3^+$ Sb_3S^+ $Sb_3S_2^+$
$S_2Sb−SbS_2$ bipyramidal	170	Sb_3S^+ $Sb_3S_2^+$ $Sb_3S_3^+$ $Sb_3S_4^+$ $Sb_3S_5^+$ $Sb_4S_3^+$ $Sb_4S_4^+$ $Sb_5S_2^+$
Ag−S	212	Ag^+ Ag_2^+
Ag_2GeS_3 amorphous phase	not detected	$AgGeS^+$
Ag−S−Sb structural units	not detected	$AgSb^+$ $AgSb_2^+$ $AgSb_4^+$
		$AgSbS^+$ $AgSb_2S^+$ $AgSb_2S_2^+$ $AgSb_2S_3^+$ $AgSb_2S_4^+$ $AgSb_2S_5^+$ $AgSb_3S_3^+$ $AgSb_4S_4^+$ $Ag_2Sb_3S_4^+$ $Ag_2Sb_3S_5^+$ $Ag_4Sb_2S_3^+$ $Ag_5SbS_3^+$

[a]Fragments might also be including reaction products formed in plasma plume.

■ CONCLUSIONS

LDI can generate clusters in Ge−Sb−S and its Ag-doped chalcogenide glasses efficiently, and the simultaneous use of a time-of-flight mass spectrometer yields mass spectra that can be analyzed to provide cluster compositions. This methodology has been shown to be a powerful method for studying the formation of various clusters in inorganic compounds. No Ge-containing clusters were detected when LDI of nondoped $(GeS_2)_{50}(Sb_2S_3)_{50}$ glass was done. When $(GeS_2)_{50}(Sb_2S_3)_{50}$ glass was doped with silver, only one Ge-containing cluster was generated. Because of a trace concentration of hydrogen, Raman spectroscopy was not detecting any hydrogenated clusters. The hydrogen in the studied glasses most probably originated from the elements used for the syntheses of these glasses. Although 5N purity standards were used, traces of hydrogenated clusters are detectable by MS.

Raman scattering results are helpful in understanding the structure of the original material prior to MS. Raman spectroscopy observes the structure in short-range order, and all bonds, for example, Ag−S, Sb−Sb, Ge−Ge, Ge−S, and Sb−S bonds, in identified structural units agree well with those structural units and fragments identified by MS, with the exception that no Ge−Ge and Ge−S units in undoped glasses were identified via MS. The results enable an understanding of the structural motifs of the Ag-doped Ge−Sb−S chalcogenide glasses, and the findings could contribute to proposals of new thin films to be manufactured by pulsed laser deposition. Such films could lead to more efficient conductive bridge RAM memory materials and devices.

■ EXPERIMENTAL SECTION

Chemicals. Acetonitrile was purchased from Sigma-Aldrich (Steinheim, Germany). Germanium, antimony, sulfur, and silver of 5N purity were purchased from VUK Panenské Břežany s.r.o. (Panenské Břežany, Czech). Ultrapure double-distilled water was produced with a quartz apparatus from Heraeus Quarzschmelze (Hanau, Germany). All other reagents were of analytical grade purity.

Samples of $Ag_x((GeS_2)_{50}(Sb_2S_3)_{50})_{100-x}$ glass for x = 0, 5, and 15 were prepared. Appropriate amounts of elements (Ge, Sb, S, and Ag) of 5N purity were sealed in an evacuated silica ampule. Each batch weighed about 10 g. The syntheses were done in a rocking furnace at a temperature of 970 °C for 36 h. Then, the temperature was decreased to 700 °C, and the samples were quenched in water and annealed for 3 h ca. 20 °C under glass transition temperature. The compositions and glass homogeneities were tested via a scanning electron microscopy microscope Lyra 3 (Tescan) equipped with the energy-dispersive X-ray analyzer AZtec X-Max 20 (Oxford Instruments).

Mass Spectrometry. Mass spectra were recorded in both the positive and negative ion modes via AXIMA Resonance or CFR mass spectrometers from Kratos Analytical Ltd. (Manchester, UK). Both instruments were equipped with a nitrogen laser (337 nm) and coupled with time-of-flight detection. The AXIMA Resonance mass spectrometer had a quadruple ion trap. The laser repetition rate was set to 5 Hz with a pulse time width of 3 ns. The maximum laser pulse energy was 250 μJ.

https://dx.doi.org/10.1021/acsomega.0c02561
ACS Omega 2020, 5, 28965−28971

Software and Computations. The stoichiometries of the clusters were determined via comparisons of theoretical and experimental isotopic envelopes on Launchpad software (Kompact version 2.9.3, 2011) from Kratos Analytical Ltd. (Manchester, UK).

Sample Preparation for MS and Raman Spectroscopy. Selected pieces were powdered in an agate mortar in a nitrogen atmosphere, and the powders were then suspended in acetonitrile (1 mg/mL). Next, 2.5 μL of each suspension was deposited on a target, dried, and used to measure mass spectra. Pieces of bulk glasses were used to measure Raman spectra.

Raman Spectroscopy. The room-temperature Raman spectra were measured by a MultiRam Raman spectrophotometer (Bruker). Spectra were excited with a laser operating at 785 nm (the output power was 1 mW). For the correction of the temperature-dependent population of phonon levels, the intensities of the bands in Raman spectra were reduced using the Gammon−Shuker formula.[33] Raman spectra band deconvolution was performed using the PSVoigt2 method in the Peak Fitting Module of the Origin program. All parameters were fixed, with only changes in band areas and the ratios between the Gauss and Lorentz parts allowed, and individual bands were attributed to structural units.

■ ASSOCIATED CONTENT

Supporting Information

The Supporting Information is available free of charge at https://pubs.acs.org/doi/10.1021/acsomega.0c02561.

Mass spectra of $(GeS_2)_{50}(Sb_2S_3)_{50}$ glass; comparison of experimental and theoretical isotopic patterns; mass spectra of 5% and 15% Ag-doped $(GeS_2)_{50}(Sb_2S_3)_{50}$ glass; effect of laser energy; and experimental and theoretical isotopic patterns (PDF)

■ AUTHOR INFORMATION

Corresponding Author

Josef Havel − *Department of Chemistry, Faculty of Science, Masaryk University, 62500 Brno, Czech Republic;* orcid.org/0000-0002-6675-5671; Phone: +420 549494114; Email: havel@chemi.muni.cz; Fax: +420 549492494

Authors

Fei Huang − *Department of Chemistry, Faculty of Science, Masaryk University, 62500 Brno, Czech Republic*

Tomáš Wágner − *Department of General and Inorganic Chemistry, Faculty of Chemical Technology and Center of Materials and Nanotechnologies, Faculty of Chemical Technology, University of Pardubice, 53210 Pardubice, Czech Republic;* orcid.org/0000-0001-6445-5395

Božena Frumarová − *Center of Materials and Nanotechnologies, Faculty of Chemical Technology, University of Pardubice, 53002 Pardubice, Czech Republic*

Max Fraenkl − *Center of Materials and Nanotechnologies, Faculty of Chemical Technology, University of Pardubice, 53002 Pardubice, Czech Republic*

Petr Koštál − *Department of General and Inorganic Technology, Faculty of Chemical Technology, University of Pardubice, 53210 Pardubice, Czech Republic*

Complete contact information is available at: https://pubs.acs.org/10.1021/acsomega.0c02561

Notes

The authors declare no competing financial interest.

■ ACKNOWLEDGMENTS

The authors are grateful for the grants they received from the Ministry of Education, Youth and Sports of the Czech Republic (grant LM2018103), the European Regional Development Fund-Project "Modernization and upgrade of the CEMNAT" (no. CZ.02.1.01/0.0/0.0/16_013/0001829), the project NANOMAT (no. CZ.02.1.01/0.0/0.0/17_048/0007376), and the Faculty of Chemical Technology, University Pardubice "Excellent teams" 2020 project. F.H. is grateful for the financial support from Project no. MUNI/A/1421/2019 for the Analytical and Physical and Chemical methods for Geological, Biological and Synthetic Materials. Our appreciation goes to Dr. L. Prokes for his help with MS measurements.

■ REFERENCES

(1) Frumar, M.; Wágner, T.; Shimakawa, K.; Frumarova, B. Crystalline and amorphous chalcogenides, High−Tech materials with structural disorder and many important applications. In *Nanomaterials and Nanoarchitectures, A complex review of current hot topics and their applications*, 1st ed.; Bardošová, M.; Wágner, T., Eds.; Springer Netherlands: Dordrecht, 2015; pp 151−238.

(2) Choi, J. W.; Han, Z.; Sohn, B. U.; Chen, G. F. R.; Smith, C.; Kimerling, L. C.; Richardson, K. A.; Agarwal, A. M.; Tan, D. T. H. Nonlinear characterization of GeSbS chalcogenide glass waveguides. *Sci. Rep.* **2016**, *6*, 39234.

(3) Petit, L.; Carlie, N.; Adamietz, F.; Couzi, M.; Rodriguez, V.; Richardson, K. C. Correlation between physical, optical and structural properties of sulfide glasses in the system Ge-Sb-S. *Mater. Chem. Phys.* **2006**, *97*, 64−70.

(4) Lin, C.; Li, Z.; Ying, L.; Xu, Y.; Zhang, P.; Dai, S.; Xu, T.; Nie, Q. Network structure in GeS_2-Sb_2S_3 chalcogenide glasses: Raman spectroscopy and phase transformation study. *J. Phys. Chem. C* **2012**, *116*, 5862−5867.

(5) Chao, H. E.; Yun, Y. U.; Xingfang, H. U.; Larbot, A. Effect of silver doping on the phase transformation and grain growth of sol-gel titania powder. *J. Eur. Ceram. Soc.* **2003**, *23*, 1457−1464.

(6) Ecclestone, L. J.; Reaney, I. M.; Lee, W. E. Correlation of microstructures with electrical performance of Ag-based metal electrode−PZT electroceramic interfaces. *J. Eur. Ceram. Soc.* **2005**, *25*, 1647−1655.

(7) Xu, J.; Liu, B.; Song, Z.; Feng, S.; Chen, B. Crystallization and C-RAM application of Ag-doped Sb_2Te_3 material. *Mat. Sci. Eng. B.* **2006**, *127*, 228−232.

(8) Esteban-Tejeda, L.; Cabal, B.; Malpartida, F.; López-Piriz, R.; Torrecillas, R.; Saiz, E.; Tomsia, A. P.; Moya, J. S. Soda-lime glass-coating containing silver nanoparticleson Ti−6Al−4V alloy. *J. Eur. Ceram. Soc.* **2012**, *32*, 2723−2729.

(9) Reddy, M. V.; Pathak, M. Sol-gel combustion synthesis of Ag doped $CaSiO_3$: in vitro bioactivity, antibacterial activity and cytocompatibility studies for biomedical applications. *Mater. Technol.* **2018**, *33*, 38−47.

(10) Frumar, M.; Wágner, T. Ag doped chalcogenide glasses and their applications. *Curr. Opin. Solid State Mater. Sci.* **2003**, *7*, 117−126.

(11) Rau, C.; Armand, P.; Pradel, A.; Varsamis, C. P. E.; Kamitsos, E. I.; Granier, D.; Ibanez, A.; Philippot, E. Mixed cation effect in chalcogenide glasses Rb_2S-Ag_2S-GeS_2. *Phys. Rev. B: Condens. Matter Mater. Phys.* **2001**, *63*, 184201−184204.

(12) Fick, J.; Nicolas, B.; Rivero, C.; Elshot, K.; Irwin, R.; Richardson, K. A.; Fischer, M.; Vallée, R. Thermally activated silver diffusion in chalcogenide thin films. *Thin Solid Films* **2002**, *418*, 215−221.

(13) Mitkova, M. Applications of Non-Crystalline Materials-C. Real time optical recording on thin films of amorphous semiconductors. In *Insulating and Semiconducting Glasses*, 1st ed.; Boolchand, P., Ed.; World Scientific Publishing Co. Pte. Ltd: Cincinnati, 2000; pp 813−843.

(14) Schubert, J.; Schöning, M. J.; Mourzina, Y. G.; Legin, A. V.; Vlasov, Y. G.; Zander, W.; Lüth, H. Multicomponent thin films for electrochemical sensor applications prepared by pulsed laser deposition. *Sens. Actuators, B* **2001**, *76*, 327−330.
(15) Shaw, B. L. *Inorganic Hydrides*, 1st ed.; Shaw, B. L., Ed.; Elsevier Ltd: Leeds, 1967; pp 1−152.
(16) Devyatykh, G. G.; Churbanov, M. F.; Scripachev, I. V.; Dianov, E. M.; Plotnichenko, V. G. The Role Of Impurities In The Optical Losses Of Chalcogenide Glass Fibers. *Infrared Fiber Opt.* **1989**, *1048*, 80−84.
(17) Churbanov, M. F.; Velmuzhov, A. P.; Sukhanov, M. V.; Snopatin, G. E.; Skripachev, I. V.; Plotnichenko, V. G. Arsenic-sulfide glasses with low content of hydrogen impurity for fiber optics. *Opt. Mater.* **2018**, *77*, 87−92.
(18) Meng, D.; Sakata, M.; Shimizu, K.; Iijima, Y.; Saitoh, H.; Sato, T.; Takagi, S.; Orimo, S. Superconductivity of the hydrogen-rich metal hydride Li_5MoH_{11} under high pressure. *Phys. Rev. B* **2019**, *99*, 024508.
(19) Fritzsche, H.; Šmíd, V.; Ugur, H.; Gaczi, P. Plasma-deposited hydrogenated chalcogenide glasses. *J. Phys. Colloq.* **1981**, *42*, 699−702.
(20) Zhao, S.; Liu, Z.-P.; Li, Z.-H.; Wang, W.-N.; Fan, K.-N. Density Functional Study of Small Neutral and Charged Silver Cluster Hydrides. *J. Phys. Chem. A* **2006**, *110*, 11537−11542.
(21) Svoboda, R.; Fraenkl, M.; Frumarová, B.; Wágner, T.; Málek, J. Thermokinetic behaviour of Ag-doped $(GeS_2)_{50}(Sb_2S_3)_{50}$ glasses. *J. Non-Cryst. Solids* **2016**, *449*, 12−19.
(22) Fraenkl, M.; Frumarová, B.; Podzemná, V.; Slang, S.; Benes, L.; Vlcek, M.; Wágner, T. How silver influences the structure and physical properties of chalcogenide glass $(GeS_2)_{50}(Sb_2S_3)_{50}$. *J. Non-Cryst. Solids* **2018**, *499*, 412−419.
(23) Koudelka, L.; Frumar, M.; Pisárčik, M. Raman Spectra of Ge-Sb-S System Glasses in the S-Rich Region. *J. Non-Cryst. Solids* **1980**, *41*, 171−178.
(24) Petit, L.; Carlie, N.; Adamietz, F.; Couzi, M.; Rodriguez, V.; Richardson, K. C. Correlation between physical, optical and structural properties of sulfide glasses in the system Ge−Sb−S. *Mat. Chem. Phys.* **2006**, *97*, 64−70.
(25) Frumarová, B.; Frumar, M.; Oswald, J.; Kincl, M.; Vlcek, M. Structure and optical properties of chalcohalide glasses doped with Pr3+ and Yb3+ ions. *J. Non-Cryst. Solids* **2009**, *355*, 1865−1868.
(26) Frumarová, B.; Němec, P.; Frumar, M.; Oswald, J.; Vlček, M. Synthesis and optical properties of the Ge−Sb−S: PrCl3 glass system. *J. Non-Cryst. Solids* **1999**, *256*−*257*, 266−270.
(27) Minceva-Sukarova, B.; Najdoski, M.; Grozdanov, I.; Chunnilall, C. J. Raman spectra of thin solid films of some metal sulfides. *J. Mol. Struct.* **1997**, *410*−*411*, 267−270.
(28) Kamitsos, E. I.; Kapoutsis, J. A.; Chryssikos, G. D.; Taillades, G.; Pradel, A.; Ribes, M. Structure and Optical Conductivity of Silver Thiogermanate Glasses. *J. Solid State Chem.* **1994**, *112*, 255−261.
(29) Mitkova, M.; Kozicki, M. N. Ag-photodoping in Ge-chalcogenide amorphous thin films-Reaction products and their characterization. *J. Phys. Chem. Solids* **2007**, *68*, 866−872.
(30) Balakrishnan, M.; Kozicki, M. N.; Poweleit, C. D.; Bhagat, S.; Alford, T. L.; Mitkova, M. Crystallization effects in annealed thin GeS_2 films photodiffused with Ag. *J. Non-Cryst. Solids* **2007**, *353*, 1454−1459.
(31) Šútorová, K.; Prokeš, L.; Nazabal, V.; Bouška, M.; Havel, J.; Němec, P. Laser Desorption Ionisation Time-of-Flight Mass Spectrometry of Chalcogenide Glasses from $(GeSe_2)_{100-x}(Sb_2Se_3)_x$ System. *J. Am. Ceram. Soc.* **2015**, *98*, 4107−4110.
(32) Popescu, M. A. Physico-Chemical Properties of Chalcogens and Binary Chalcogenide Glasses. In *Non-Crystalline Chalcogenides*, 1st ed.; Popescu, M. A., Ed.; Springer Netherlands: Dordrecht, 2002; pp 103−208.
(33) Shuker, R.; Gammon, R. W. Raman-Scattering Selection-Rule Breaking and the Density of States in Amorphous Materials. *Phys. Rev. Lett.* **1970**, *25*, 222−225.

https://dx.doi.org/10.1021/acsomega.0c02561
ACS Omega 2020, 5, 28965−28971

Appendix 3B

Fei HUANG, Tomáš WÁGNER, Božena FRUMAROVÁ, Max FRAENKL, Petr KOŠTÁL, and Josef HAVEL: Laser Desorption Ionization Time-of-Flight Mass Spectrometry of Silver-Doped $(GeS_2)_{50}(Sb_2S_3)_{50}$ Chalcogenide Glasses. *ACS Omega*. **5**, 28965-28971 (2020).

Supporting information

(https://pubs.acs.org/doi/full/10.1021/acsomega.0c02561)

Supporting Information

Laser Desorption Ionization Time-of-Flight Mass Spectrometry of Silver-Doped $(GeS_2)_{50}(Sb_2S_3)_{50}$ Chalcogenide Glasses

Fei Huang,[1] Tomáš Wágner,[2,3] Božena Frumarová,[3] Max Fraenkl,[3] Petr Koštál,[4] and Josef Havel[1*]

[1]**Fei Huang and Josef Havel -** *Department of Chemistry, Faculty of Science, Masaryk University, Kamenice 5/A14, 62500 Brno, Czech Republic*

[2]**Tomáš Wágner -** *Department of General and Inorganic Chemistry, Faculty of Chemical Technology, University of Pardubice, Studentská 573, 53210 Pardubice, Czech Republic*

[3]**Tomáš Wágner, Božena Frumarová, and Max Fraenkl** - *Center of Materials and Nanotechnologies, Faculty of Chemical Technology, University of Pardubice, Nám. Čs. Legií 565, 53002 Pardubice, Czech Republic*

[4]**Petr Koštál -** *Department of General and Inorganic Technology, Faculty of Chemical Technology, University of Pardubice, Doubravice 41, 53210 Pardubice, Czech Republic*

*Correspondence should be addressed. Email: havel@chemi.muni.cz

Phone: +420 549494114, Fax: +420 549492494

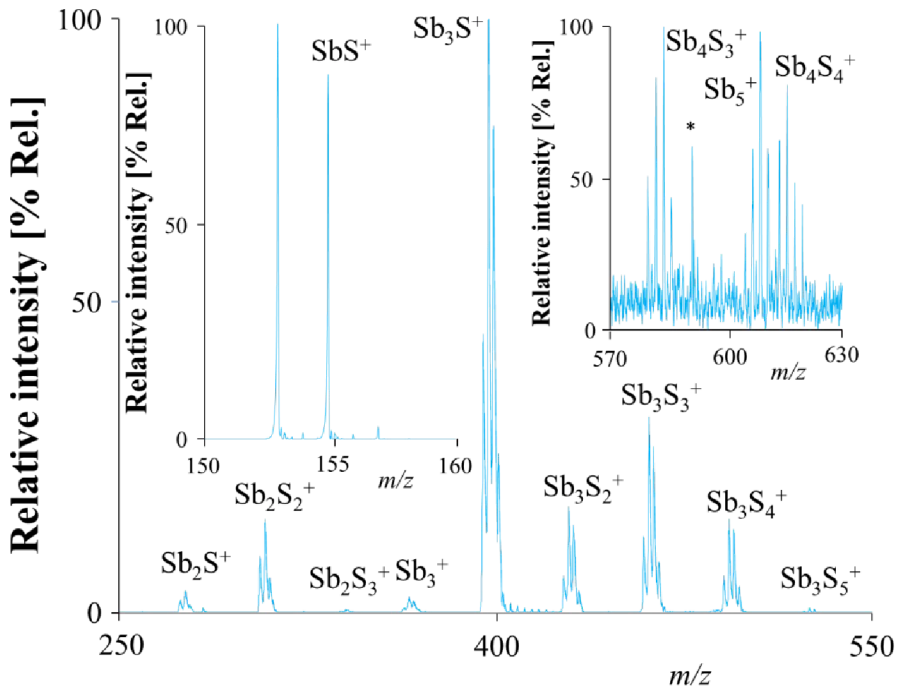

Figure S1. Mass spectra of $(GeS_2)_{50}(Sb_2S_3)_{50}$ glass. Insets show the mass spectra in 150-160 and 570-630 *m/z* range. Conditions: positive ion mode; laser energy 170 a.u. * means the isotopic pattern is too complex or the spectra intensity is too low to identify clusters.

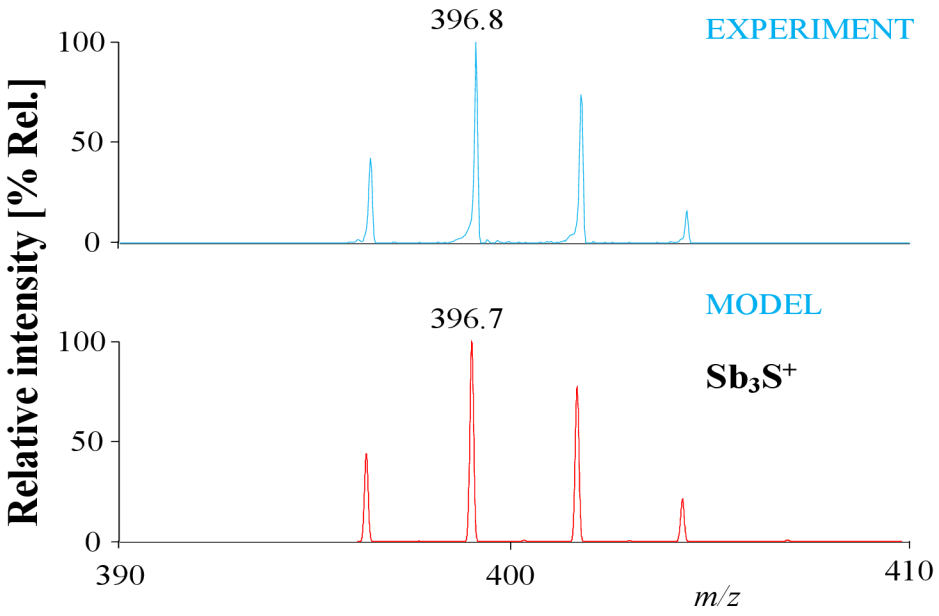

Figure S2. Comparison of experimental and theoretical isotopic patterns for Sb_3S^+ cluster. Conditions: positive ion mode; laser energy 170 a.u.

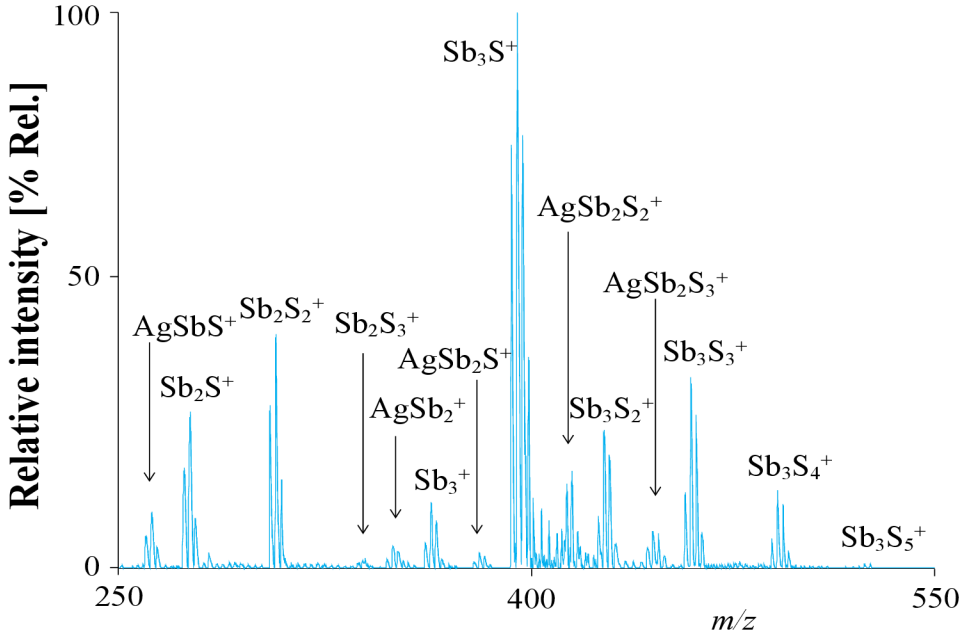

Figure S3. Mass spectra of 5% Ag dopped $(GeS_2)_{50}(Sb_2S_3)_{50}$ glass. Conditions: positive ion mode; laser energy 170 a.u.

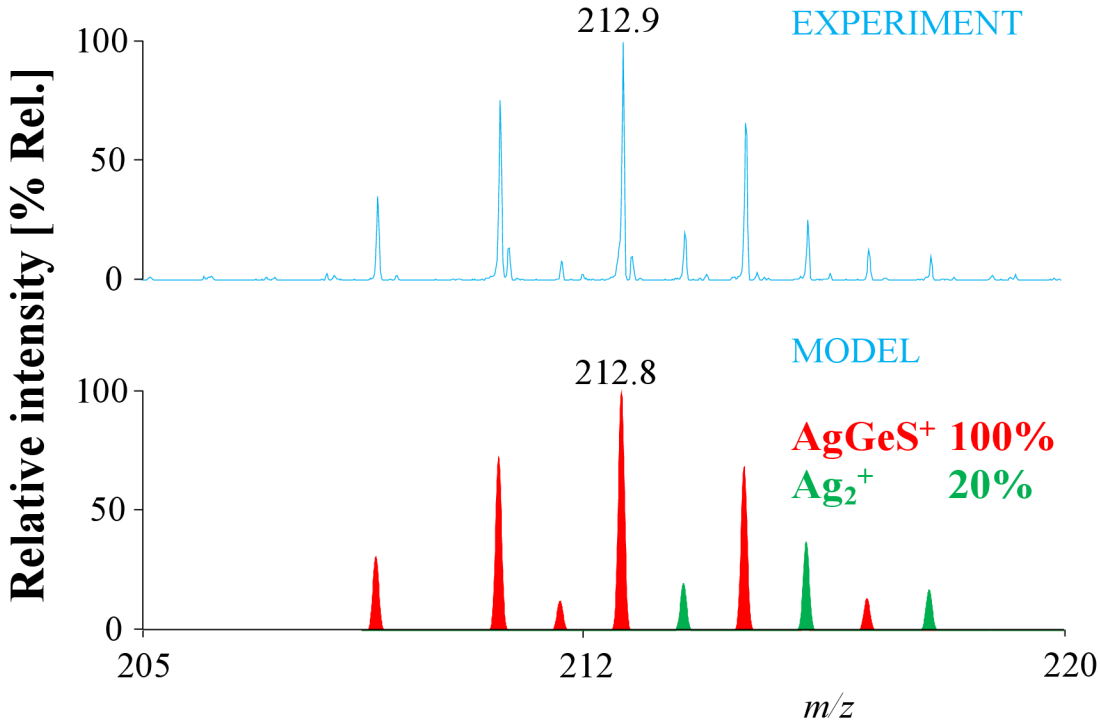

Figure S4. Comparison of experimental and theoretical isotopic patterns for overlap of $AgGeS^+$ and Ag_2^+ clusters. Conditions: positive ion mode; laser energy 170 a.u.

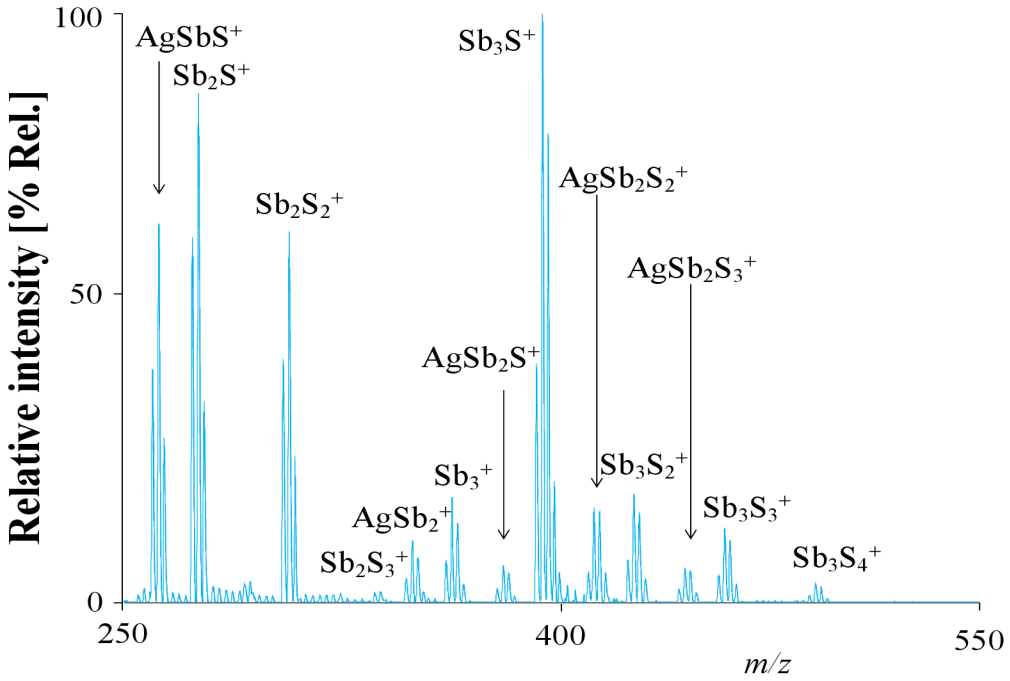

Figure S5. Mass spectra of 15% Ag dopped $(GeS_2)_{50}(Sb_2S_3)_{50}$ glass. Conditions: positive ion mode; laser energy 170 a.u.

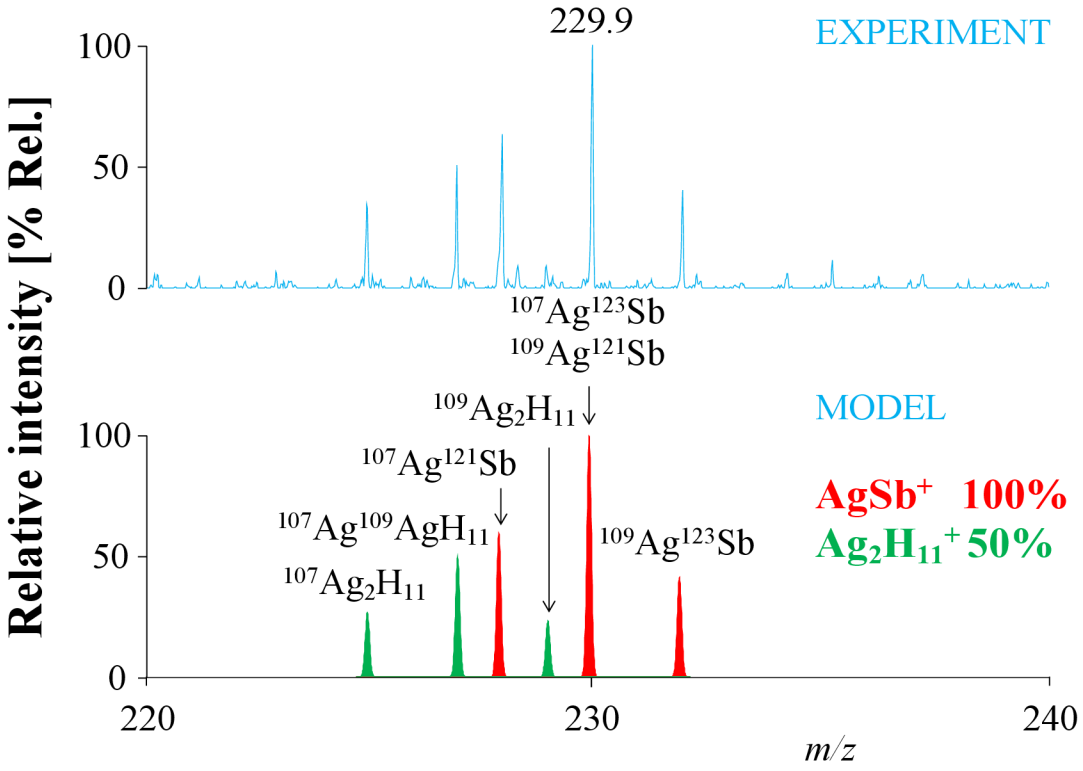

Figure S6. Comparison of experimental and theoretical isotopic patterns for overlap of $AgSb^+$ and $Ag_2H_{11}^+$ clusters. Conditions: positive ion mode; laser energy 170 a.u.

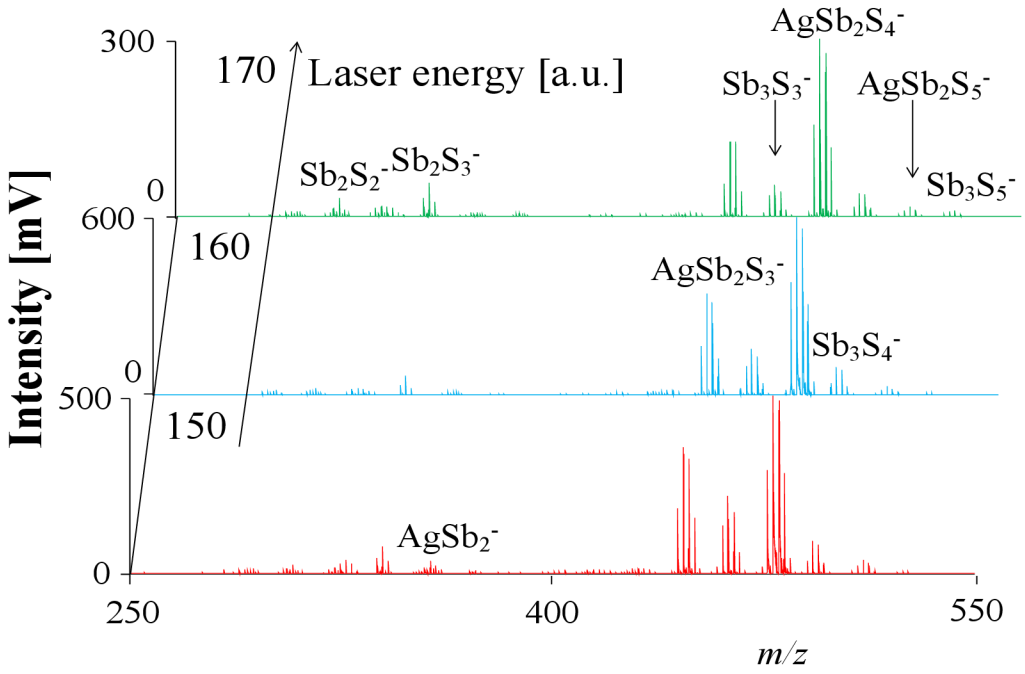

Figure S7. The effect of laser energy on the mass spectra generated via LDI of 5% Ag dopped chalcogenide glass in the 250-550 *m/z* range in the negative ion mode.

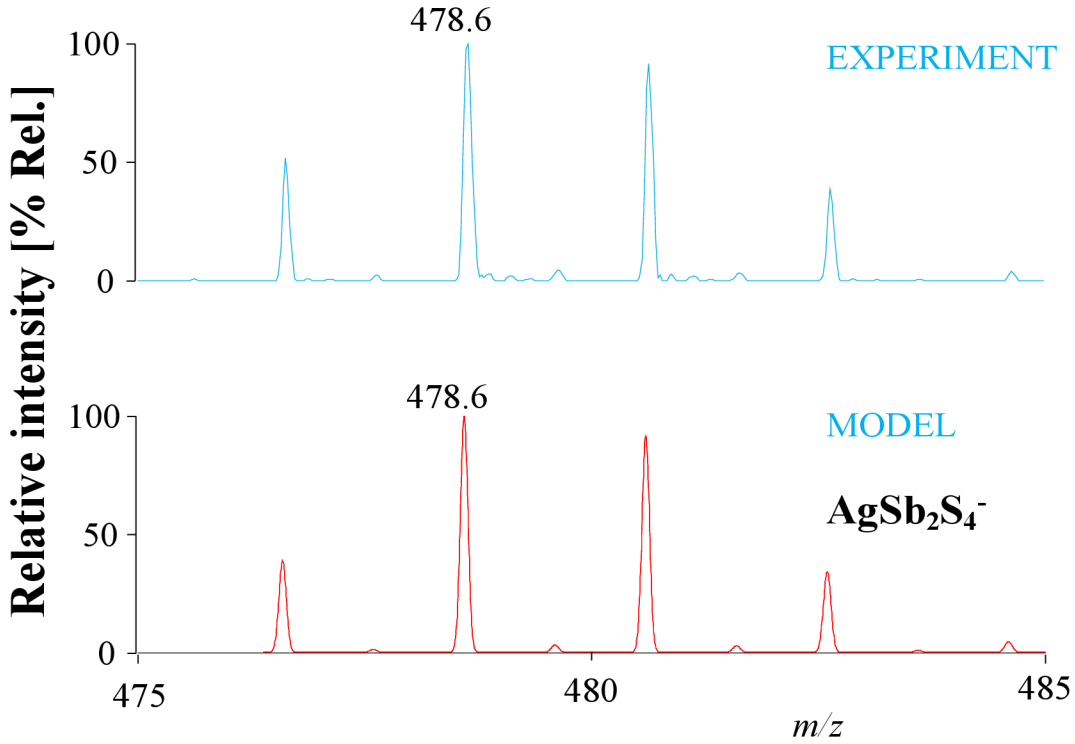

Figure S8. Comparison of experimental and theoretical isotopic patterns for negative charged $AgSb_2S_4^-$ cluster. Conditions: negative ion mode; laser energy 170 a.u.

Appendix 4A

Fei HUANG, Tomáš HALENKOVIČ, Marion BAILLIEUL, Virginie NAZABAL, Petr NĚMEC, and Josef HAVEL: Germanium-antimony-selenium-tellurium thin films: Clusters formation by laser ablation and comparison with clusters from mixtures of elements. *J. Am. Ceram. Soc.* **105,** 1992-2000 (2022).

IF: 3.784, Quartile: Q1

(https://ceramics.onlinelibrary.wiley.com/doi/full/10.1111/jace.18228)

Check for updates

Received: 17 August 2021 | Revised: 26 October 2021 | Accepted: 30 October 2021

DOI: 10.1111/jace.18228

Journal of the American Ceramic Society

RESEARCH ARTICLE

Germanium-antimony-selenium-tellurium thin films: Clusters formation by laser ablation and comparison with clusters from mixtures of elements

Fei Huang[1] | **Tomáš Halenkovič**[2] | **Marion Baillieul**[2] | **Virginie Nazabal**[2,3] | **Petr Němec**[2] | **Josef Havel**[1]

[1] Department of Chemistry, Faculty of Science, Masaryk University, Brno, Czech Republic

[2] Department of Graphic Arts and Photophysics, Faculty of Chemical Technology, University of Pardubice, Pardubice, Czech Republic

[3] Institut des Sciences Chimiques de Rennes UMR 6226, Centre nationale de la recherche scientifique, ScanMAT UMS 2001, Université de Rennes 1, Rennes, France

Correspondence
Josef Havel, Department of Chemistry, Faculty of Science, Masaryk University, Kamenice 5/A14, 62500 Brno, Czech Republic.
Email: havel@chemi.muni.cz

Funding information
the Grant Agency of the Czech Republic, Grant/Award Numbers: 19–24516S, LM2018103; Ministry of Education, Youth and Sports of the Czech Republic, Grant/Award Number: MUNI/A/1390/2020

Abstract

Quaternary germanium-antimony-selenium-tellurium (Ge-Sb-Se-Te) thin films deposited from $Ge_{19.4}Sb_{16.7}Se_{63.9-x}Te_x$ (x = 5, 10, 15, and 20) glass-ceramics targets by radio frequency magnetron sputtering were studied using laser ablation quadrupole ion trap time of flight mass spectrometry. Binary, ternary, and quaternary $Ge_aSb_bSe_cTe_d$ clusters were formed and their stoichiometry was determined. By comparison of the clusters obtained from quaternary Ge-Sb-Se-Te thin films and those from ternary Ge-Sb-Te materials, we found that Ge-Te species are not detected from the quaternary system. Furthermore, Ge-Se and Se-Te species are missing in mass spectra generated from Ge-Sb-Se-Te thin films. From the Ge-Sb-Se-Te thin films, 16 clusters were detected while ternary Ge-Sb-Se glasses yielded 26 species. This might be considered as a signal of higher stability of Ge-Sb-Se-Te thin films which is increasing with a higher content of Te. The missing (Se_2^+, Ge_aSb^+ (a = 1–4), and $GeSe_c^+$ (c = 1, 2)) and new (Ge^+ and Sb_bTe^+ (b = 1–3)) clusters may indicate that some of the structural features of the films ($Ge_2Se_{6/2}$ and $Se_2Sb\text{-}SbSe_2$) were replaced by ($GeSe_{4-x}Te_x$ and $SbSe_{3-x}Te_x$) ones. In addition, when comparing the stoichiometry of clusters formed from Ge-Sb-Se-Te thin films with those from the mixtures of the elements, only Sb_3^+ and $SbSe^+$ were observed in both cases. The knowledge gained concerning clusters stoichiometry contributes to the elucidation of the processes proceeding during plasma formation used for the chalcogenide thin films deposition.

KEYWORDS

amorphous chalcogenides, clusters, Ge-Sb-Se-Te, laser ablation, magnetron sputtering, mass spectrometry, thin films

1 | INTRODUCTION

Chalcogenide glasses and amorphous thin films are widely used[1–4] because of their unique advantages of broad transmission window in infrared (IR) spectral region, high refractive index, and photosensitivity to light exposure.[5–9] Moreover, chalcogenide glasses exhibit huge Kerr nonlinearities at a femtosecond time scale which can reach values of several orders of magnitude larger than that of silica glass, variable two-photon absorption depending on their bandgap, and insignificant free carrier absorption.[10] Given the above-mentioned properties, the application of

chalcogenide glasses in all-optical signal processing based on nonlinear effects for telecommunication systems has been studied.[2]

Ternary germanium-antimony-selenium (Ge-Sb-Se) glasses are important members of the chalcogenide group of glasses; their physicochemical properties have been intensively studied.[8,11–14] Furthermore, Ge-Sb-Se amorphous thin films fabricated using different physical vapor deposition techniques are in the center of interest of several research groups.[15–19]

The attention of some authors has been already attracted by modifying of Ge-Sb-Se glasses by tellurium (Te). The substitution of Se by heavier Te atoms may lead to the decrease of phonon energies which may result in a broadening of IR transparency. Besides that, the increasing Te concentration may cause the increase of the (non)linear refractive index which can make Ge-Sb-Se-Te glasses and thin films promising materials for nonlinear optical applications. In fact, the quaternary Ge-Sb-Se-Te system was studied from the point of view of glass-forming ability,[20] structures,[21] thermal properties,[22] optical, and other properties.[23–24] Finally, thin films from the Ge-Sb-Se-Te quaternary system might be considered as a promising alternative to Ge-Sb-Te layers in phase-change memory applications as proposed recently by Wang[25] and Zhang.[26]

It has been shown that exposure of amorphous chalcogenides (in both bulk and thin-film forms) with a pulsed laser, having high enough pulse energy density, leads to laser ablation (LA). The plasma plume, which is formed due to LA, contains many clusters which can be detected by time-of-flight mass spectrometry (TOF-MS). Indeed, this technique can be used to elucidate the composition of the structural fragments present in the plasma generated during the interaction of high-energy laser pulses with chalcogenide glasses[27] or amorphous thin films.[28]

The aim of this paper is to evaluate the changes in amorphous Ge-Sb-Se-Te thin films when Se is partially replaced by Te by studying the chemistry of clusters formed by LA. In parallel, the comparison of the stoichiometry's of clusters detected by LA of thin films with those of the species generated via LA synthesis (LAS) from binary, ternary, and quaternary mixtures of the elements (i.e., Ge-Sb, Ge-Te, Sb-Te, Se-Te, and Ge-Sb-Se-Te) was performed.

2 | EXPERIMENTAL PROCEDURE

2.1 | Chemicals

Acetonitrile and (Ge, Sb, Se, and Te of 99.999% purity) were purchased from Sigma-Aldrich (Steinheim, Germany). A quartz apparatus from Heraeus Quarzschmelze (Hanau, Germany) was used to produce ultrapure double distilled water. All the other reagents were of analytical-grade purity.

2.2 | Thin films fabrication and characterization

Glass-ceramics $Ge_{19.4}Sb_{16.7}Se_{63.9-x}Te_x$ (x = 5, 10, 15, and 20) sputtering targets, whose basic composition ($Ge_{19.4}Sb_{16.7}Se_{63.9}$) corresponds to $(GeSe_2)_{70}(Sb_2Se_3)_{30}$ identified earlier (from the point of view of its nonlinear optical properties and photostability) as promising glass composition in $(GeSe_2)_{100-x}(Sb_2Se_3)_x$ pseudobinary system,[8] were fabricated by a conventional melt-quenching technique as described elsewhere.[29] Thin films with thickness in the 780–840 nm range were deposited at room temperature by radio frequency (13.56 MHz) magnetron sputtering onto single crystalline silicon < 100 > substrates employing the MPE600 multichamber deposition system (Plassys-Bestek, France). The deposition conditions varied in terms of electrical power applied on targets (10 or 15 W) and argon pressures (0.5 or 1 Pa).

The chemical composition of thin films was determined through energy-dispersive X-ray analysis connected with a scanning electron microscope (JSM 6400-OXFORD Link INCA; JEOL Ltd., Japan). The amorphous state of the layers was confirmed by the X-ray diffraction measurements.

2.3 | Sample preparation for MS

Ge, Sb, Se, and Te were separately crushed into powder using an agate mortar and then suspended in acetonitrile (1 mg/ml). From the suspensions, 1 μl sample was deposited on a target and dried. When the thin films were analyzed, a narrow piece of parafilm was used to fix the Ge-Sb-Se-Te thin films on the target.

2.4 | Mass spectrometry

Mass spectra were recorded using either an AXIMA curved-field reflectron or AXIMA resonance mass spectrometer, both from Kratos Analytical Ltd (Manchester, UK), in both positive and negative ion modes. Both instruments were coupled with a TOF detection and equipped with a nitrogen laser (337 nm). The AXIMA Resonance was equipped with a Quadruple Ion Trap. The laser repetition rate was set to 5 Hz with a pulse time width of 3 ns. Mass spectra were obtained by accumulating 1000 laser shots. The laser energy was scaled in arbitrary units (a.u.) from 0 to 180; this relative scale will be used hereafter. The irradi-

TABLE 1 The summary of deposition parameters of germanium-antimony-selenium-tellurium (Ge-Sb-Se-Te) thin films. Chemical composition (±1 at. %) was determined by energy-dispersive X-ray analysis (EDS)

Film Nr.	Sputtering target	Power (W)	Ar pressure (Pa)	Composition (at. %)
1	$Ge_{19.4}Sb_{16.7}Se_{58.9}Te_5$	10	0.5	$Ge_{22.0}Sb_{16.9}Se_{54.6}Te_{6.5}$
2		10	1	$Ge_{19.5}Sb_{16.6}Se_{56.5}Te_{7.4}$
3		15	0.5	$Ge_{20.7}Sb_{17.3}Se_{55.0}Te_{6.9}$
4		15	1	$Ge_{19.3}Sb_{17.0}Se_{56.4}Te_{7.4}$
5	$Ge_{19.4}Sb_{16.7}Se_{53.9}Te_{10}$	10	0.5	$Ge_{21.7}Sb_{17.9}Se_{49.8}Te_{10.7}$
6		10	1	$Ge_{19.3}Sb_{17.4}Se_{51.2}Te_{12.1}$
7		15	0.5	$Ge_{20.5}Sb_{18.1}Se_{50.1}Te_{11.3}$
8		15	1	$Ge_{20.0}Sb_{17.7}Se_{50.9}Te_{11.4}$
9	$Ge_{19.4}Sb_{16.7}Se_{48.9}Te_{15}$	10	0.5	$Ge_{21.3}Sb_{18.1}Se_{45.6}Te_{15.0}$
10		10	1	$Ge_{19.9}Sb_{17.6}Se_{46.4}Te_{16.2}$
11		15	0.5	$Ge_{19.4}Sb_{19.1}Se_{45.0}Te_{16.6}$
12		15	1	$Ge_{19.1}Sb_{17.9}Se_{46.0}Te_{16.9}$
13	$Ge_{19.4}Sb_{16.7}Se_{43.9}Te_{20}$	10	0.5	$Ge_{19.1}Sb_{17.4}Se_{42.1}Te_{21.4}$
14		10	1	$Ge_{17.8}Sb_{19.8}Se_{39.8}Te_{22.7}$
15		15	0.5	$Ge_{18.7}Sb_{20.2}Se_{39.3}Te_{21.7}$
16		15	1	$Ge_{17.7}Sb_{19.7}Se_{40.0}Te_{22.6}$

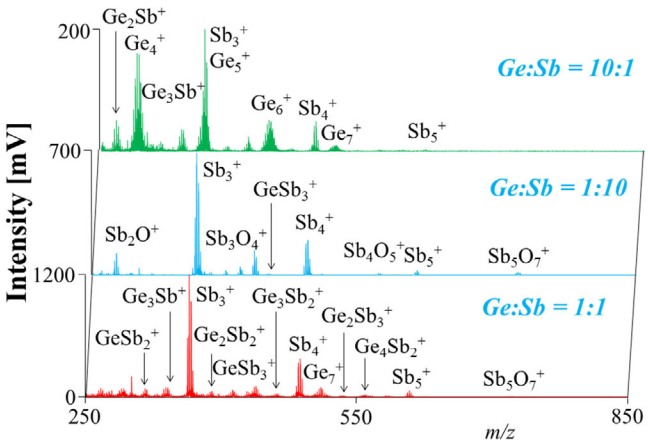

FIGURE 1 Mass spectra from laser ablation synthesis (LAS) of germanium-antimony mixtures with different molar ratios in the 250–650 *m/z* range. Conditions: positive ion mode; laser energy 120 a.u.

ated spot size was approximately 150 μm in diameter. The maximum laser pulse energy was 250 μJ. The laser fluence was ~1 J/cm^2.

2.5 | Software and computation

The stoichiometry of clusters was determined via a comparison of theoretical and experimental isotopic envelopes using Launchpad software (Kompact version 2.9.3, 2011) from Kratos Analytical Ltd.

3 | RESULTS

An overview of the thin films deposition parameters with resulting thin films chemical composition is given in Table 1. We note that there is good agreement between the nominal chemical composition of deposited thin films and corresponding sputtering targets.

The mass spectra were recorded in both positive and negative ion modes by using the reflectron mode. The formation of clusters generated from mixtures of elements and thin films via LA was studied. It was shown that in positive ion mode, mass spectra were of higher intensity compared to the negative ion mode and a higher number of species was observed. Therefore, the results presented here are for the positive ion mode. We note that LAS of Sb-Se and Ge-Se mixtures with different ratios have already been studied.[30–31]

3.1 | LAS of Ge-Sb clusters from Ge:Sb = 1:1, 1:10, and 10:1 mixtures

A comparison of mass spectra of Ge-Sb mixtures with different molar ratios is shown in Figure 1. For the ratio with a high excess of Sb, $GeSb_3^+$ was the only Ge-Sb cluster observed apart from Sb_b^+ (b = 2–4) species. In addition, low-intensity Sb_bO^+ (b = 2, 3), $Sb_3O_4^+$, $Sb_4O_5^+$, and $Sb_5O_7^+$ clusters were also identified. For the 1:1 ratio of Ge to Sb, or for high content of Ge, there were many Ge-Sb clusters detected such as $GeSb_b^+$ (b = 2–4), $Ge_2Sb_b^+$ (b = 1–

3), $Ge_3Sb_b^+$ ($b = 1$–3), $Ge_4Sb_b^+$ ($b = 1, 2$), and Ge_6Sb^+ and also Ge unary species Ge_a^+ ($a = 1$–7) were found. A comparison of experimental and theoretical isotopic patterns demonstrating the overlap of $GeSb_4^+$ and Ge_6Sb^+ clusters is shown in Figure S1. As seen in the figure, there is a good agreement between experimental and theoretical mass spectra.

3.2 | LAS of Ge-Te clusters from Ge:Te = 1:1, 1:10, and 10:1 mixtures

A comparison of mass spectra for Ge-Te mixtures in different ratios at the laser energy of 120 a.u. is shown in Figure S2A. It can be seen that the spectra features are similar. The $GeTe_d^+$ ($d = 2$, 3) clusters are the Ge-Te species observed (in the mass spectrum of a mixture with a large excess of Ge (Ge:Te = 10:1)). In addition to the Ge_4^+, Ge_5^+, Te_d^+ ($d = 2$–6), $GeTe_d^+$ ($d = 2$, 3), and $Ge_2Te_d^+$ ($d = 2$, 3) clusters, some oxidized Te_dO^+ ($d = 2$–4) and hydroxylated Te_dOH^+ ($d = 2, 3$) species were also generated. A good agreement of the theoretical isotopic pattern of the $GeTe_2^+$ cluster with the experimental pattern can be seen in Figure S2B.

3.3 | LAS of Sb-Te clusters from Sb:Te = 1:1, 1:10, and 10:1 mixtures

Figure S3A shows a comparison of mass spectra for Sb-Te mixtures at different ratios measured at the same laser energy (120 a.u.). It is shown that only for the ratio with high Sb concentrations, Sb-Te clusters like $SbTe_d^+$ ($d = 1$, 2), Sb_2Te^+, and Sb_3Te^+ were observed, while Te_d^+ ($d = 2$–6) species were observed in all spectra. In addition to the clusters mentioned, Sb_b^+ ($b = 3$–6) and oxidized Sb_bO^+ ($b = 2$, 3), $Sb_2O_2^+$, $Sb_3O_4^+$, and $Sb_3TeO_6^+$ species were also detected. A comparison of experimental and theoretical isotopic patterns for Sb_3Te^+ provided in Figure S3B shows that they are in good agreement.

3.4 | LAS of Se-Te clusters from Se:Te = 1:1, 1:10, and 10:1 mixtures

An example of LAS mass spectra for Se-Te mixtures (concerning the generation of $Se_bTe_d^+$ clusters) is shown in Figure S4A. For the ratio in which the Te was in high excess over Se, the intensity of the spectra features was high. When the Te concentration was higher than or equal to Se, Se_c^+ ($c = 2$–8), Te_d^+ ($d = 2$–5), Se_cTe^+ ($c = 1$–6), and $Se_cTe_2^+$ ($c = 1$, 3) clusters were observed. Even

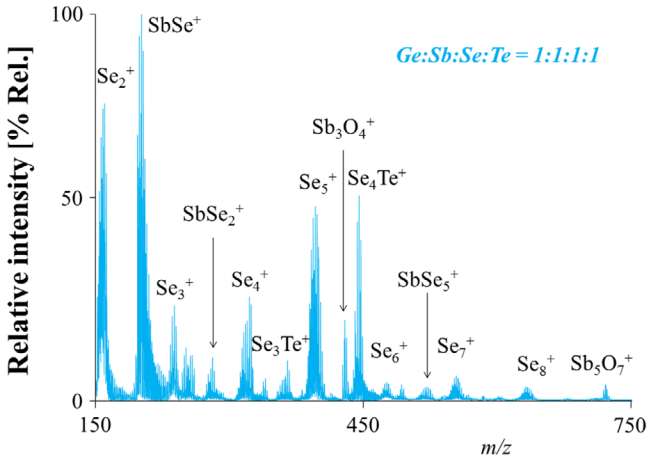

FIGURE 2 Mass spectra from laser ablation synthesis (LAS) of germanium-antimony-selenium-tellurium mixtures with the molar ratio of 1:1:1:1 in the 150–750 *m/z* range. Conditions: positive ion mode; laser energy 120 a.u.

when the Se was in high excess to Te, besides Se_c^+ ($c = 2$–8), only the $SeTe_4^+$ cluster was detected. The good agreement between the experimental and theoretical mass spectra related to the formation of $SeTe_4^+$ is shown in Figure S4B.

3.5 | LAS of Ge-Sb-Se-Te clusters from Ge:Sb:Se:Te = 1:1:1:1 mixtures

An example of mass spectra for the clusters generated from the quaternary element mixture is shown in Figure 2. In addition to Sb_3^+, Te_2^+, Ge_3Sb^+, $Se_3Te_2^+$, Se_c^+ ($c = 2$–8), $SbSe_c^+$ ($c = 1$, 2, 5), and Se_cTe^+ ($c = 3$, 4, 6, and 7) clusters, some low-intensity $Sb_3O_4^+$, $Sb_4O_{5-6}^+$, and $Sb_5O_7^+$ species were also observed. Arbitrary, signal corresponding Se_4Te^+ species was selected and it is shown in Figure S5; the experimental and theoretical isotopic patterns for the Se_4Te^+ cluster are in good agreement.

3.6 | LA TOF-MS of Ge-Sb-Se-Te thin films with different Se:Te ratio

A comparison of LA TOF-MS data of four selected thin films (No. 3, 7, 11, and 15) at the same laser energy (150 a.u.) is shown in Figure 3. It was observed that when Te is incorporated into thin films and its content increases, the stability of the thin film increases. This is deduced from the fact of decreased intensities of the spectra with the increased content of Te. The clusters produced from the 16 quaternary Ge-Sb-Se-Te thin films are the same.

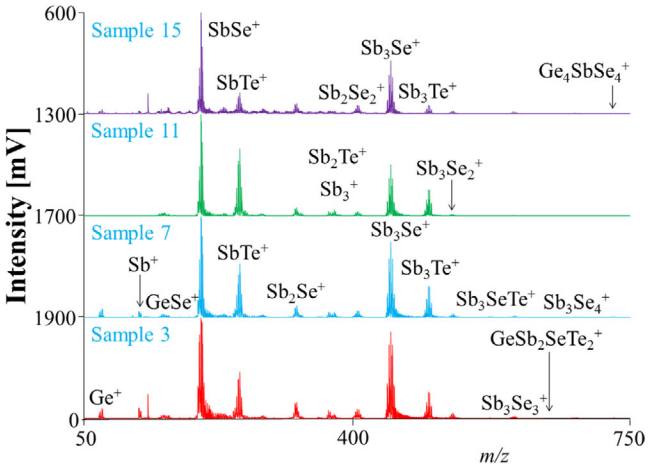

FIGURE 3 Laser ablation time-of-flight mass spectrometry (LA TOF-MS) data of Ge-Sb-Se-Te thin films in the 50–750 *m/z* range. Conditions: positive ion mode; laser energy 150 a.u.

In addition to the Ge^+, Sb^+, Sb_3^+, and binary Sb_bSe^+ (b = 1–3), $Sb_2Se_2^+$, $Sb_3Se_c^+$ (c = 2–4), Sb_bTe^+ (b = 1–3) clusters, ternary Sb_3SeTe^+, $Ge_4SbSe_4^+$, and quaternary $GeSb_2SeTe_2^+$ species were also observed. A comparison of experimental and theoretical isotopic patterns for the ternary Sb_3SeTe^+ cluster is given in Figure S6, showing a good agreement of the experiment with the theoretical model. The clusters formed from quaternary Ge-Sb-Se-Te thin films are from more than 50% the same as the clusters detected from ternary Ge-Sb-Se glasses (nine Sb_b^+ (b = 1, 3), $SbSe^+$, $Sb_2Se_c^+$ (c = 1, 2), and $Sb_3Se_c^+$ (c = 1–4) species are identical).[27] Contrary, the clusters originating from quaternary Ge-Sb-Se-Te thin films were mostly different from those generated from the ternary Ge-Sb-Te system.[32] For example, only three species are common (Ge^+, Sb_2Te^+, and Sb_3Te^+).

4 | DISCUSSION

A review of the species identified in LA TOF-MS data of mixtures of elements and those detected from thin films is provided in Tables 2 and 3. When comparing the stoichiometry of the clusters generated from quaternary system Ge-Sb-Se-Te to those generated from ternary Ge-Sb-Te materials,[32] it was found that Ge-Te clusters are missing. This can be explained that Te was at least partially replaced by Se in the structure. It was also observed that no Ge-Se clusters were detected from the quaternary system. Probably it is because the bond energy Ge-Se is higher than Ge-Sb, Ge-Te, Se-Se, and Sb-Se (Ge-Se = 2.44 eV, Ge-Sb = 1.48 eV, Ge-Te = 1.87 eV, Se-Se = 2.14 eV, and Sb-Se = 2.25 eV).[33–34] While Se-Te clusters were not detected from the quaternary system, many of them were generated during the LAS of the mixtures of elements. The missing Se-Te species is probably because that the entity $SbSe_{3-x}Te_x$[35] is present in the structure (bond energy of Se-Te = 2.00 eV is higher than Sb-Te = 1.73 eV), so we observed not Se-Te but Sb-Te species. On the other hand, Sb-Se clusters were detected from Ge-Sb-Se-Te layers which demonstrate that Se is the most probably bonded to Sb in the structure of studied quaternary materials.

When comparing the stoichiometry of the clusters obtained from Ge-Sb-Se-Te thin films to those observed from ternary Ge-Sb-Se glasses,[27] it was found that

(i) A lower number of clusters is formed. Furthermore, for Te doped thin films, it is demonstrated that the formation of binary and ternary clusters is diminished. A review of the species (Ge-Sb, Ge-Se, Sb-Se, and Ge-Sb-Se) detected both in Ge-Sb-Se and Ge-Sb-Se-Te is given in Table 4. These indicate that the quaternary system shows greater stability than the ternary system.

(ii) Sb_b^+ (b = 1, 3) and the most of Sb-Se clusters ($SbSe^+$, $Sb_2Se_c^+$ [c = 1, 2], and $Sb_3Se_c^+$ species [c = 1–4]) are the same. Comparing LAS of mixtures of elements, Sb-Se mixtures are the easiest ones to form clusters. Indeed, these bonds are high-energy bonds, and once they are formed it is not easy to incorporate other elements especially when there have some lower energy bonds that coexist in the system.

(iii) Se_2^+, Ge_aSb^+ (a = 1–4), and $GeSe_c^+$ (c = 1, 2) clusters are missing whereas Ge^+ and Sb_bTe^+ (b = 1–3) clusters were generated. The $SbSe_{3/2}$ pyramids, $GeSe_{4/2}$ tetrahedra, $Ge_2Se_{6/2}$ entities, and Se_2Sb-$SbSe_2$ species form the structure of Ge-Sb-Se glasses. From the point of view of chemical boding, homopolar Ge-Ge, Sb-Sb, and Se-Se bonds, as well as heteropolar Ge-Se and Sb-Se (perhaps also Ge-Sb) bonds, are present in the structure.[8] We suggest that $SbSe_{3/2}$ pyramidal and $GeSe_{4/2}$ tetrahedral are too stable (pyramidal, tetrahedral structure, and high bond energy of Sb-Se or Ge-Se bonds) to be decomposed by MS. A similar observation was observed for sulfides.[36] This probably means that the entities ($Ge_2Se_{6/2}$ and Se_2Sb-$SbSe_2$) were replaced by the entities ($GeSe_{4-x}Te_x$ and $SbSe_{3-x}Te_x$),[35] and thus the reactions in the plasma plume changed. In addition, when comparing the stoichiometry of the clusters generated from Ge-Sb-Se-Te mixtures of elements with those generated from Ge-Sb-Se-Te thin films, only two clusters (Sb_3^+ and $SbSe^+$) are common. The Se_c^+ (c = 2–8) clusters were not observed in thin films. The bond energies of Ge-Se, Sb-Se, and Se-Te are higher than Ge-Sb, Ge-Te, and Sb-Te, which leads

TABLE 2 Clusters generated from mixtures of elements (the molar ratio of elements in the binary mixture was 1:1, 1:10, and 10:1)

System	Clusters							References
Ge-Sb	Ge^+	Ge_2^+	Ge_3^+	Ge_4^+	Ge_5^+	Ge_6^+	Ge_7^+	This work
	Sb_2^+	Sb_3^+	Sb_4^+	Sb_5^+				
	$GeSb_2^+$	$GeSb_3^+$	$GeSb_4^+$					
	Ge_2Sb^+	$Ge_2Sb_2^+$	$Ge_2Sb_3^+$					
	Ge_3Sb^+	$Ge_3Sb_2^+$	$Ge_3Sb_3^+$					
	Ge_4Sb^+	$Ge_4Sb_2^+$						
	Ge_6Sb^+							
Ge-Te	Ge_4^+	Ge_5^+						This work
	Te_2^+	Te_3^+	Te_4^+	Te_5^+	Te_6^+			
	$GeTe_2^+$	$GeTe_3^+$						
	$Ge_2Te_2^+$	$Ge_2Te_3^+$						
Ge-Se	Ge_4^+							31
	Se_2^+	Se_3^+	Se_4^+	Se_5^+	Se_6^+	Se_7^+	Se_8^+	
	$GeSe_2^+$	$GeSe_3^+$	$GeSe_4^+$	$GeSe_5^+$	$GeSe_6^+$	$GeSe_7^+$	$GeSe_8^+$	$GeSe_2$
	$Ge_2Se_4^+$	$Ge_2Se_6^+$						
	Ge_4Se^+	$Ge_4Se_2^+$	$Ge_4Se_3^+$	$Ge_4Se_4^+$				
	Ge_5Se^+	$Ge_5Se_2^+$	$Ge_5Se_3^+$	$Ge_5Se_5^+$				
Sb-Se	Se_4^+	Se_5^+	Se_6^+	Se_7^+	Se_8^+	Se_9^+		30
	$SbSe_2^+$	$SbSe_3^+$	$SbSe_4^+$	$SbSe_5^+$	$SbSe_6^+$	$SbSe_7^+$	$SbSe_8^+$	
	Sb_2Se^+	$Sb_2Se_2^+$	$Sb_2Se_3^+$	$Sb_2Se_4^+$	$Sb_2Se_5^+$	$Sb_2Se_6^+$		
	Sb_3Se^+	$Sb_3Se_2^+$	$Sb_3Se_3^+$	$Sb_3Se_4^+$	$Sb_3Se_5^+$			
	Sb_4Se^+	$Sb_4Se_2^+$	$Sb_4Se_3^+$					
	Sb_5Se^+	$Sb_5Se_2^+$						
Sb-Te	Sb_3^+	Sb_4^+	Sb_5^+	Sb_6^+				This work
	Te_2^+	Te_3^+	Te_4^+	Te_5^+	Te_6^+			
	$SbTe^+$	$SbTe_2^+$						
	Sb_2Te^+							
	Sb_3Te^+							
Se-Te	Se_2^+	Se_3^+	Se_4^+	Se_5^+	Se_6^+	Se_7^+	Se_8^+	This work
	Te_2^+	Te_3^+	Te_4^+	Te_5^+				
	$SeTe^+$	$SeTe_2^+$	$SeTe_4^+$					
	Se_2Te^+							
	Se_3Te^+	$Se_3Te_2^+$						
	Se_4Te^+							
	Se_5Te^+							
	Se_6Te^+							
Ge-Sb-Se-Te1:1:1:1	Sb_3^+							This work
	Se_2^+	Se_3^+	Se_4^+	Se_5^+	Se_6^+	Se_7^+	Se_8^+	
	Te_2^+							
	Ge_3Sb^+							
	$SbSe^+$	$SbSe_2^+$	$SbSe_5^+$					
	$TeSe_3^+$	$TeSe_4^+$	$TeSe_6^+$	$TeSe_7^+$				

TABLE 3 Clusters generated from germanium-antimony-selenium (Ge-Sb-Se) bulk glasses, germanium-antimony-tellurium (Ge-Sb-Te) thin layers/bulk glasses, and germanium-antimony-selenium-tellurium (Ge-Sb-Se-Te) thin films

System	Clusters					References
Ge-Sb-Se	Se_2^+					27
	Sb^+	Sb_3^+				
	$GeSb_3^+$	$Ge_2Sb_3^+$	$Ge_3Sb_3^+$	$Ge_4Sb_3^+$		
	$GeSe^+$	$GeSe_2^+$				
	$SbSe^+$	$SbSe_2^+$				
	Sb_2Se^+	$Sb_2Se_2^+$	$Sb_2Se_3^+$	$Sb_2Se_4^+$		
	Sb_3Se^+	$Sb_3Se_2^+$	$Sb_3Se_3^+$	$Sb_3Se_4^+$	$Sb_3Se_5^+$	
	$GeSbSe_2^+$	$GeSb_4Se^+$	$GeSb_5Se^+$			
	$Ge_9Sb_2Se_5^+$	$Ge_9Sb_2Se_6^+$	$Ge_9Sb_2Se_7^+$			
Ge-Sb-Te	Ge^+	Ge_2^+				32
	Te_2^+	Te_3^+				
	$GeTe^+$	$GeTe_2^+$				
	$SbTe_2^+$					
	Sb_2Te^+	$Sb_2Te_3^+$				
	Sb_3Te^+					
	$GeSbTe_2^+$	$GeSbTe_3^+$				
Ge-Sb-Se-Te	Ge^+					This work
	Sb^+	Sb_3^+				
	$SbSe^+$					
	Sb_2Se^+	$Sb_2Se_2^+$				
	Sb_3Se^+	$Sb_3Se_2^+$	$Sb_3Se_3^+$	$Sb_3Se_4^+$		
	$TeSb^+$	$TeSb_2^+$	$TeSb_3^+$			
	Sb_3SeTe^+					
	$Ge_4SbSe_4^+$					
	$GeSb_2SeTe_2^+$					

TABLE 4 The number of clusters observed from ternary germanium-antimony-selenium (Ge-Sb-Se) glasses and from thin films analyzed in this work

	27	This work
Ge-Sb	4	0
Ge-Se	2	0
Sb-Se	11	7
Ge-Sb-Se	6	1

to the difficult decomposition of the Se-containing species.

5 | CONCLUSION

Laser ablation with quadrupole ion trap time of flight mass spectrometric analysis was used to characterize Ge-Sb-Se-Te thin films. The LAS of the clusters from the elements was found to be a suitable method to follow Te incorporation, i.e. the replacement of Se by Te in ternary Ge-Sb-Se system. It was demonstrated that the replacement of Se with Te is causing that fewer clusters are produced which might indicate greater stability of the quaternary Ge-Sb-Se-Te thin films. Furthermore, it was observed that when the percentage of Te is increasing, the stability of the thin films increases. The species present in the plasma originating from quaternary Ge-Sb-Se-Te thin films were discussed. It was found that (Se_2^+ and Ge containing clusters Ge_aSb^+ (a = 1–4), and $GeSe_c^+$ (c = 1, 2) are missing), (Ge^+ and Sb_bTe^+ (b = 1–3) clusters are new), and (nine clusters (Sb_b^+ (b = 1, 3), $SbSe^+$, $Sb_2Se_c^+$ (c = 1, 2), and $Sb_3Se_c^+$ (c = 1–4)) are the same) when comparing the clusters to those generated from ternary Ge-Sb-Se glasses. These observations indicate some chemical/structural changes induced by Te incorporation. Besides, the comparison of quaternary Ge-Sb-Se-Te layers and ternary Ge-Sb-Te materials demonstrating the chemistry changes was discussed. In addition, comparing the stoichiometry of clusters observed from Ge-Sb-Se-Te thin films with those from mixtures of its constituting elements was described. These results would enable a better understanding of the plasma processes for

Ge-Sb-Se-Te thin films deposition as well as a description of structural motifs and chemical bonding in the plasma plume.

ACKNOWLEDGMENTS

This work was funded with support from the Grant Agency of the Czech Republic (Project No. 19–24516S). The authors appreciate the financial support from the LM2018103 project funded by the Ministry of Education, Youth and Sports of the Czech Republic. Fei Huang is grateful for the financial support from Project no. MUNI/A/1390/2020 for the analytical, physical, and chemical methods for geological, biological, and synthetic materials. Our appreciation goes to Dr. L. Prokes for his help with mass spectrometry measurements.

ORCID

Petr Němec https://orcid.org/0000-0003-2426-3078
Josef Havel https://orcid.org/0000-0002-6675-5671

REFERENCES

1. Zakery A, Elliott SR. Optical properties and applications of chalcogenide glasses: a review. J Non-Cryst Solids. 2003;330:1–12.
2. Eggleton BJ, Luther-Davies B, Richardson K. Chalcogenide photonics. Nat Photonics. 2011;5:141–8.
3. Adam JL, Zhang XH (editors). Chalcogenide glasses: preparation, properties and application. Oxford: Woodhead Publishing; 2014.
4. Wuttig M, Bhaskaran H, Taubner T. Phase-change materials for non-volatile photonic applications. Nat Photonics. 2017;11:465–76.
5. Lucas P, Yang Z, Fah MK, Luo T, Jiang S, Boussard-Pledel C, et al. Telluride glasses for far infrared photonic applications. Opt Mater Express. 2013;3:1049–58.
6. Meneghini C, Villeneuve A. As_2S_3 photosensitivity by two-photon absorption: holographic gratings and self-written channel waveguides. J Opt Soc Am B. 1998;15:2946–50.
7. Shimakawa K, Kolobov A, Elliott S. Photoinduced effects and metastability in amorphous semiconductors and insulators. Adv Phys. 1995;44:475–588.
8. Olivier M, Tchahame J, Němec P, Chauvet M, Besse V, Cassagne C, et al. Structure, nonlinear properties, and photosensitivity of $(GeSe_2)_{100-x}(Sb_2Se_3)_x$ glasses. Opt Mater Express. 2014;4:525–40.
9. Calvez L, Yang Z, Lucas P. Light-induced matrix softening of Ge-As-Se network glasses. Phys Rev Lett. 2008;101:177402.
10. Sanghera J, Florea C, Shaw L, Pureza P, Nguyen V, Bashkansky M, et al. Non-linear properties of chalcogenide glasses and fibers. J Non-Cryst Solids. 2008;354:462–7.
11. Němec P, Olivier M, Baudet E, Kalendova A, Benda P, Nazabal V. Optical properties of $(GeSe_2)_{100-x}(Sb_2Se_3)_x$ glasses in near-and middle-infrared spectral regions. Mater Res Bull. 2014;51:176–9.
12. Varshneya AK, Mauro DJ. Microhardness, indentation toughness, elasticity, plasticity, and brittleness of Ge–Sb–Se chalcogenide glasses. J Non-Cryst Solids. 2007;353:1291–7.
13. Wei WH, Wang RP, Shen X, Fang L, Luther-Davies B. Correlation between structural and physical properties in Ge–Sb–Se Glasses. J Phys Chem C. 2013;117:16571–6.
14. Giridhar A, Narasimham P, Mahadevan S. Density and microhardness of Ge-Sb-Se glasses. J Non-Cryst Solids. 1981;43:29–35.
15. Chen Y, Shen X, Wang RP, Wang GX, Dai SX, Xu TF, et al. Optical and structural properties of Ge–Sb–Se thin films fabricated by sputtering and thermal evaporation. J Alloys Comp. 2013;548:155–60.
16. Olivier M, Němec P, Boudebs G, Boidin R, Focsa C, Nazabal V. Photosensitivity of pulsed laser deposited Ge-Sb-Se thin films. Opt Mater Express. 2015;5:781–93.
17. Lin L, Wang GX, Shen X, Dai SX, Xu TF, Nie QH. Photo-induced structural changes in Ge-Sb-Se films. Infrared Phys Technol. 2017;81:59–63.
18. Halenkovič T, Gutwirth J, Kuriakose T, Bouška M, Chauvet M, Renversez G, et al. Linear and nonlinear optical properties of co-sputtered Ge-Sb-Se amorphous thin films. Opt Lett. 2020;45:1523–6.
19. Baudet E, Sergent M, Němec P, Cardinaud C, Rinnert E, Michel K, et al. Experimental design approach for deposition optimization of RF sputtered chalcogenide thin films devoted to environmental optical sensors. Sci Rep. 2017;7:3500.
20. Bordas S, Casas-Vazquez J, Clavaguera N, Clavagura-Mora M. Glass-forming ability in the Ge-Sb-Te-Se quaternary system. Thermochim Acta. 1979;28:387–93.
21. Fabian M, Svab E, Pamukchieva V, Szekeres A, Todorova K, Vogel S, et al. Reverse Monte Carlo modeling of the neutron and X-ray diffraction data for new chalcogenide Ge–Sb–S (Se)–Te glasses. J Phys Chem Solids. 2013;74:1355–62.
22. Svoboda R, Málek J. Thermal behavior of Se-rich $GeSb_2Se_{(4-y)}Te_y$ (glassy) system. J Alloys Compd. 2016;670:222–8.
23. Yin N, Xu J, Chang F, Jian Z, Gao C. Effect of Te proportion on the properties of $Ge_{25}Sb_{10}Se_{65-x}Te_x$ chalcogenide glasses. Infrared Phys Technol. 2019;96:361–5.
24. Sharma N, Sharda S, Katyal SC, Sharma V, Sharma P. Effect of Te on linear and non-linear optical properties of new quaternary Ge-Se-Sb-Te chalcogenide glasses. Electron Mater Lett. 2014;10:101–6.
25. Wang H, Guo TQ, Xue Y, Lv SL, Yao DN, Zhou ZG, et al. The phase change memory features high-temperature characteristic based on Ge-Sb-Se-Te alloys. Mater Lett. 2019;254:182–5.
26. Zhang YF, Chou JB, Li JY, Li HS, Du QY, Yadav A, et al. Broadband transparent optical phase change materials for high-performance nonvolatile photonics. Nat Commun. 2019;10:4279.
27. Šútorová K, Prokeš L, Nazabal V, Bouška M, Havel J, Němec P. Laser desorption ionisation time-of-flight mass spectrometry of chalcogenide glasses from $(GeSe_2)_{100-x}(Sb_2Se_3)_x$ System. J Am Ceram Soc. 2015,98:4107–10.
28. Mawale R, Halenkovič T, Bouška M, Gutwirth J, Nazabal V, Bora PL, et al. Mass spectrometric investigation of amorphous Ga-Sb-Se thin films, Sci Rep. 2019;9:10213.

29. Baudet E, Gutierrez-Arroyo A, Němec P. Bodiou L, Lemaitre J, De Sagazan O, et al. Selenide sputtered films development for MIR environmental sensor. Opt Mater Express. 2016;6:2616-27.
30. Huang F, Prokeš L, Havel J. Laser ablation synthesis of antimony selenide clusters with simultaneous laser desorption ionization (LDI) quadrupole ion trap mass spectrometry. J Am Soc Mass Spectrom. 2019;30:634–8.
31. Mawale R, Halenkovič T, Bouška M, Gutwirth J, Nazabal V, Takáts V, et al. Laser desorption ionization time-of-flight mass spectrometry of Ge_xSe_{1-x} chalcogenide glasses, their thin films, and Ge:Se mixtures. J Non-Cryst Solids. 2019;509:65–73.
32. Houška J, Peña-Méndez EM, Kolář J, Přikryl J, Pavlišta M, Frumar M, et al. Laser desorption time-of-flight mass spectrometry of atomic switch memory $Ge_2Sb_2Te_5$ bulk materials and its thin films. Rapid Commun Mass Spectrom. 2014;28: 699–704.
33. Rao KJ, Mohan R. Chemical bond approach to determining conductivity band gaps in amorphous chalcogenides and pnictides. Solid State Commun. 1981;39:1065–8.
34. Lee JH, Lee WH, Park JK, Yi JH, Shin SY, Park BJ, et al. Thermal properties of ternary Ge–Sb–Se chalcogenide glass for use in molded lens applications. J Non-Cryst Solids. 2016;431:41–6.
35. Abdellaoui N, Starecki F, Boussard-Pledel C, Shpotyuk Y, Doualan JL, Braud A, et al. Tb^{3+} doped $Ga_5Ge_{20}Sb_{10}Se_{65-x}Te_x$ (x = 0–37.5) chalcogenide glasses and fibers for MWIR and LWIR emissions. Opt Mater Express. 2018;8:2887–900.
36. Huang F, Wágner T, Frumarová B, Fraenkl M, Koštál P, Havel J. Laser desorption ionization time-of-flight mass spectrometry of silver-doped $(GeS_2)_{50}(Sb_2S_3)_{50}$ chalcogenide glasses. ACS Omega. 2020;5:28965–71.

SUPPORTING INFORMATION

Additional supporting information may be found in the online version of the article at the publisher's website.

How to cite this article: Huang F, Halenkovič T, Baillieul M, Nazabal V, Němec P, Havel J. Germanium-antimony-selenium-tellurium thin films: Clusters formation by laser ablation and comparison with clusters from mixtures of elements. J Am Ceram Soc. 2022;105:1992–2000. https://doi.org/10.1111/jace.18228

Appendix 4B

Fei HUANG, Tomáš HALENKOVIČ, Marion BAILLIEUL, Virginie NAZABAL, Petr NĚMEC, and Josef HAVEL: Germanium-antimony-selenium-tellurium thin films: Clusters formation by laser ablation and comparison with clusters from mixtures of elements. *J. Am. Ceram. Soc.* **105,** 1992-2000 (2022).

Supporting information

(https://ceramics.onlinelibrary.wiley.com/doi/full/10.1111/jace.18228)

Ge-Sb-Se-Te Thin Films: Clusters Formation by Laser Ablation and Comparison with Clusters from Mixtures of Elements.

Fei Huang,[1] Tomáš Halenkovič,[2] Marion Baillieul,[2] Virginie Nazabal,[2,3] Petr Němec,[2] and Josef Havel[1*]

[1]Department of Chemistry, Faculty of Science, Masaryk University, Kamenice 5/A14, 62500 Brno, Czech Republic

[2]Department of Graphic Arts and Photophysics, Faculty of Chemical Technology, University of Pardubice, Studentská 573, 53210 Pardubice, Czech Republic

[3]Univ Rennes, CNRS, ISCR UMR6226, ScanMAT UMS 2001, F-35000 Rennes, France

*Author to whom correspondence should be addressed. Email: havel@chemi.muni.cz

Phone: +420 549494114, Fax: +420 549492494

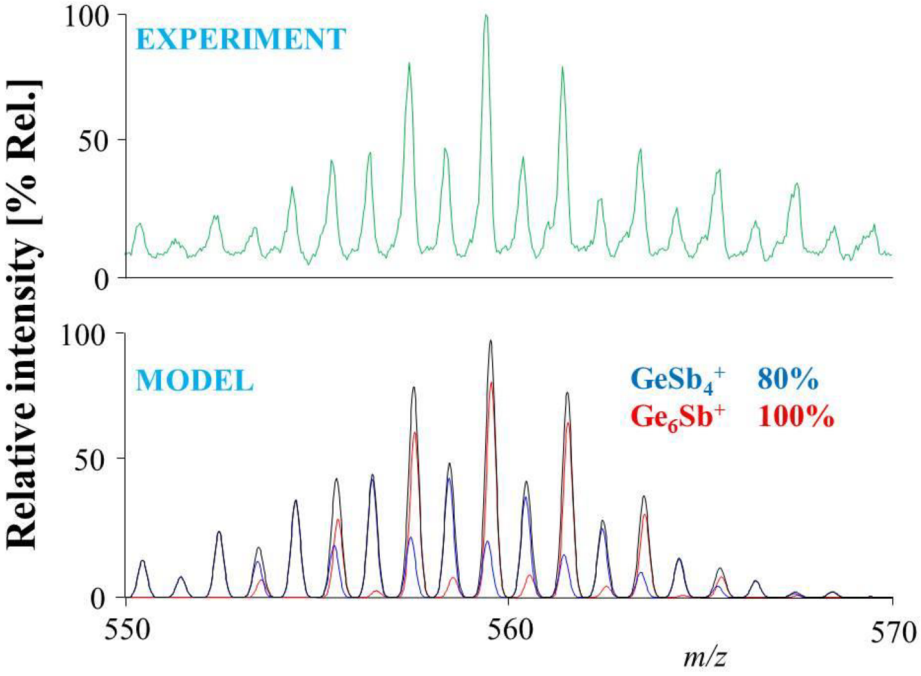

FIGURE S1 Comparison of experimental and theoretical isotopic patterns for the overlap clusters $GeSb_4^+$ and Ge_6Sb^+. Conditions: positive ion mode; laser energy 120 a.u.

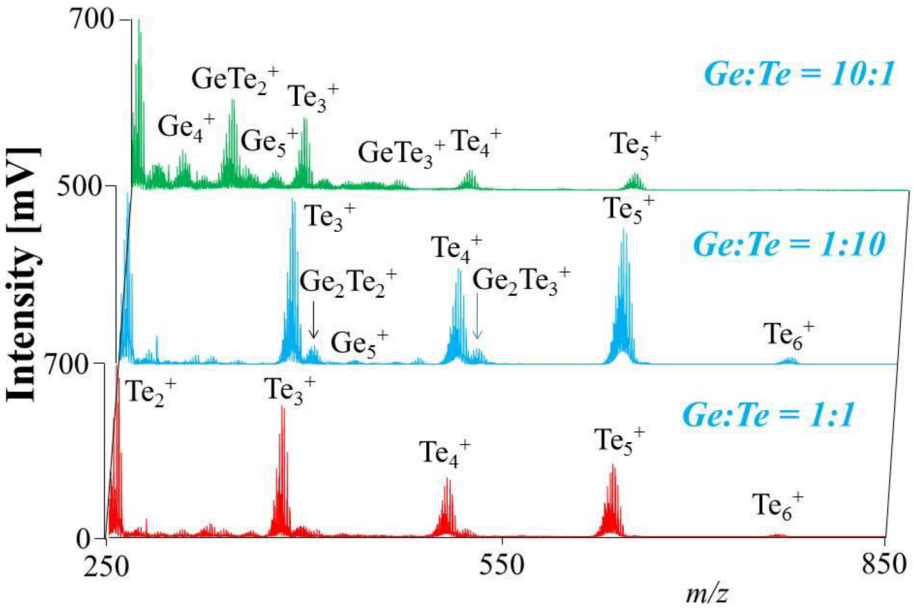

FIGURE S2A. Mass spectra from LAS of germanium-tellurium mixtures with different molar ratios in the 250-650 *m/z* range. Conditions: positive ion mode; laser energy 120 a.u.

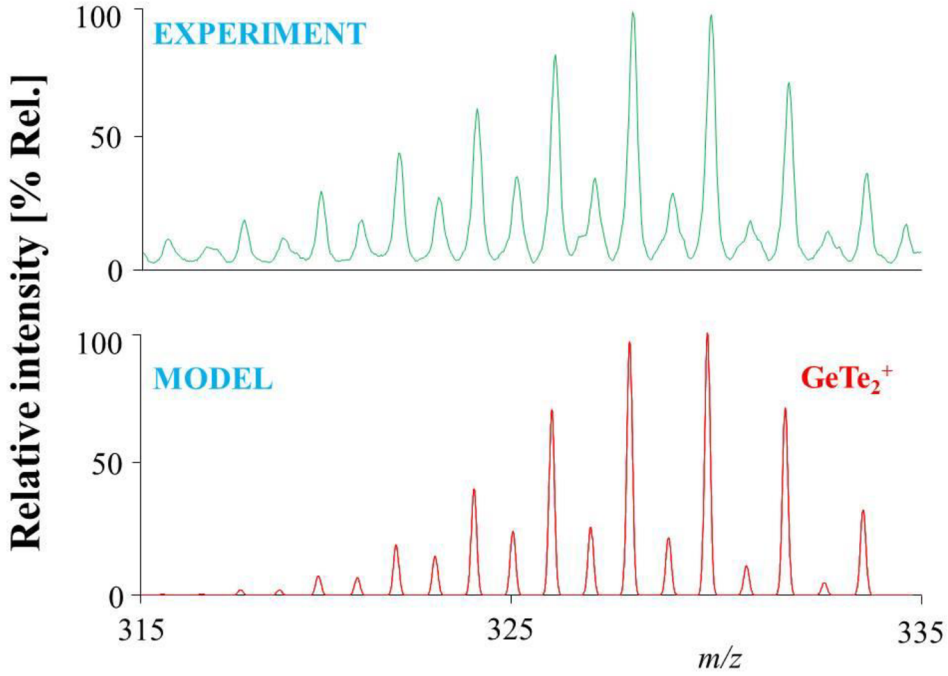

FIGURE S2B. Comparison of experimental and theoretical isotopic patterns for the $GeTe_2^+$ cluster. Conditions: positive ion mode; laser energy 120 a.u.

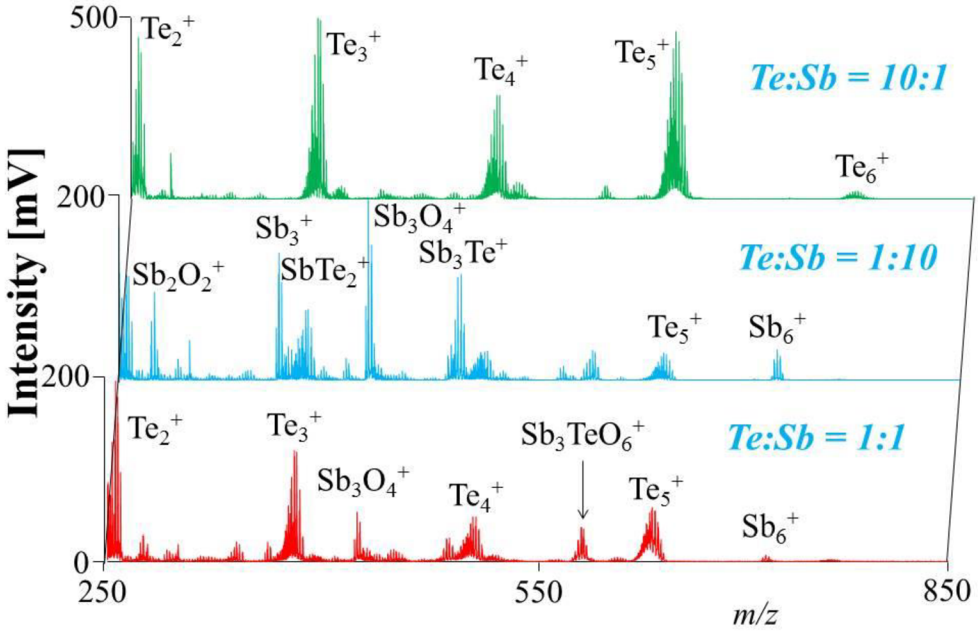

FIGURE S3A. Mass spectra from LAS of antimony-tellurium mixtures with different molar ratios in the 250-650 *m/z* range. Conditions: positive ion mode; laser energy 120 a.u.

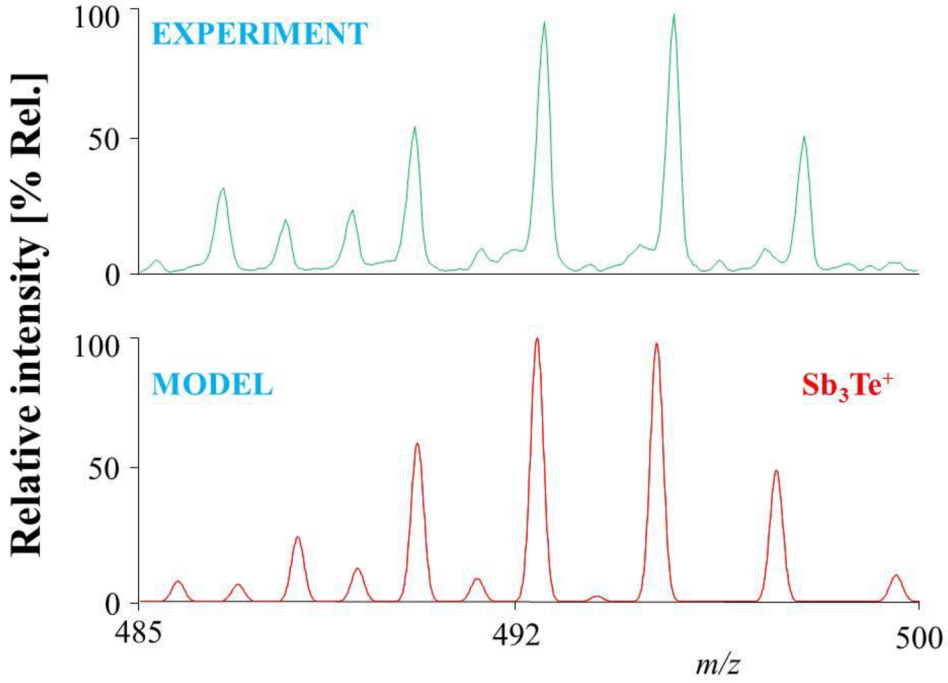

FIGURE S3B. Comparison of experimental and theoretical isotopic patterns for the Sb_3Te^+ cluster. Conditions: positive ion mode; laser energy 120 a.u.

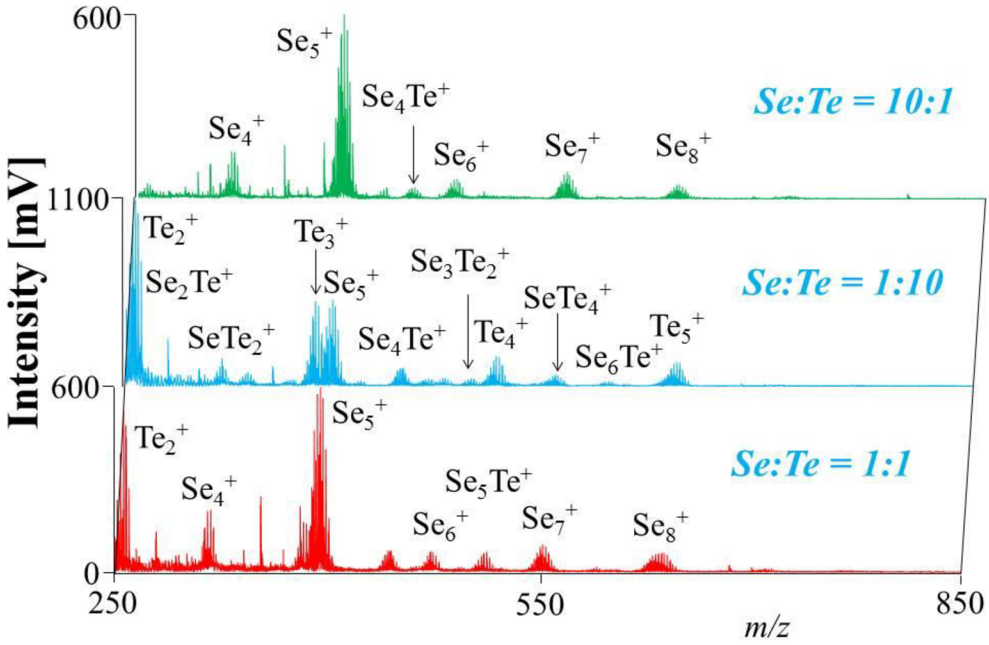

FIGURE S4A. Mass spectra from LAS of selenium-tellurium mixtures with different molar ratios in the 250-650 *m/z* range. Conditions: positive ion mode; laser energy 120 a.u.

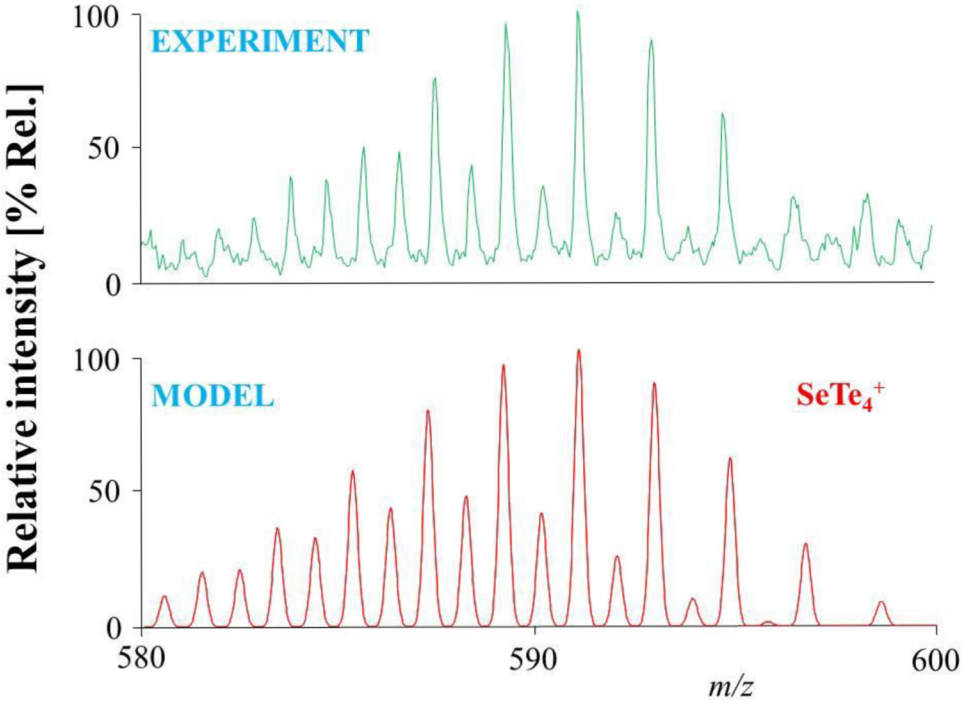

FIGURE S4B. Comparison of experimental and theoretical isotopic patterns for the $SeTe_4^+$ cluster. Conditions: positive ion mode; laser energy 120 a.u.

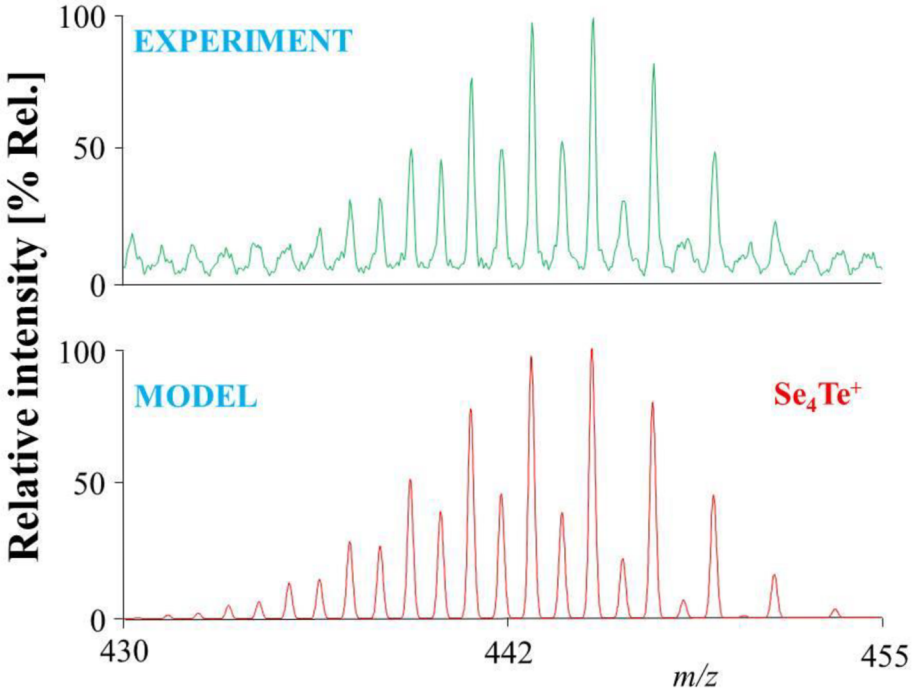

FIGURE S5. Comparison of experimental and theoretical isotopic patterns for the Se_4Te^+ cluster. Conditions: positive ion mode; laser energy 120 a.u.

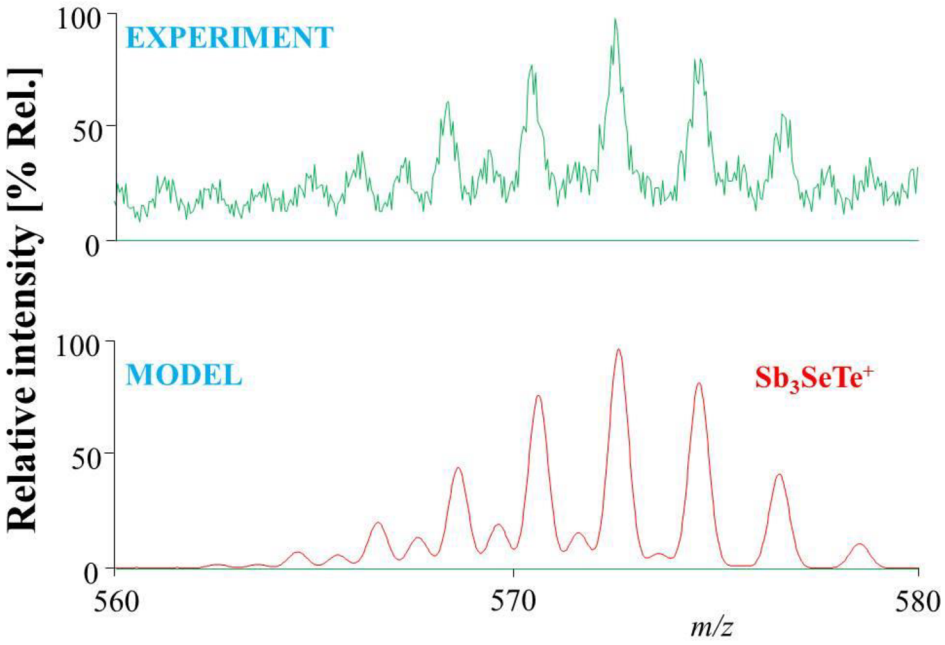

FIGURE S6. Comparison of experimental and theoretical isotopic patterns for the Sb_3SeTe^+ cluster. Conditions: positive ion mode; laser energy 150 a.u.

9. List of Posters

Appendix 5 **Fei HUANG**, Ravi. MAWALE, Petr NĚMEC, Lubomír PROKEŠ, Virginie NAZABAL, and Josef HAVEL: Formation of $Ge_mSe_n^{+/-}$ clusters via laser ablation synthesis from Ge-Se mixtures-a way to understand structure of Ge-Se glasses: Laser Desorption Ionization time-of-flight Quadrupole Ion Trap Mass Spectrometry. 15th International Conference on Nanoscience & Nanotechnologies, Thessaloniki, Greece, July 3-6, 2018.

Appendix 6 **Fei HUANG**, Lubomír PROKEŠ, and Josef HAVEL: Laser ablation synthesis of antimony selenides clusters with simultaneous laser desorption ionization (LDI) quadrupole ion trap mass spectrometry. The 2018 International Conference on Nanoscience + Technology (ICN+T), Brno, Czech Republic, July 22-27, 2018.

Appendix 7 **Fei HUANG**, Lubomír PROKEŠ, and Josef HAVEL: Laser Ablation Synthesis (LAS) of Ge-Sb, Ge-Te, and Sb-Te clusters. 3rd Global Summit & Expo on Nanotechnology and Nanomedicine, Barcelona, Spain, September 18-20, 2019.

Appendix 5

Fei HUANG, Ravi. MAWALE, Petr NĚMEC, Lubomír PROKEŠ, Virginie NAZABAL, and Josef HAVEL: Formation of $Ge_mSe_n^{+/-}$ clusters via laser ablation synthesis from Ge-Se mixtures-a way to understand structure of Ge-Se glasses: Laser Desorption Ionization time-of-flight Quadrupole Ion Trap Mass Spectrometry.

15th International Conference on Nanoscience & Nanotechnologies, Thessaloniki, Greece, July 3-6, 2018.

Formation of $Ge_mSe_n^{+/-}$ clusters via laser ablation synthesis from Ge-Se mixtures-a way to understand structure of Ge-Se glasses: Laser Desorption Ionization time-of-flight Quadrupole Ion Trap Mass Spectrometry

Fei Huang[1], Ravi Mawale[2], Petr Němec[2], Lubomír Prokeš[1,2,3], Virginie Nazabal[2,5], Josef Havel[1]

[1]Department of Chemistry, Faculty of Science, Masaryk University, Kamenice 5/A14, 62500 Brno, Czech Republic, email: 478620@email.muni.cz

[2]Department of Graphic Arts and Photophysics, Faculty of Chemistry Technology, University of Pardubice, Studentská 573, 53201 Pardubice, Czech Republic

[3]Department of Physical Electronics, Faculty of Science, Masaryk University, Kotlářská 2, 61137 Brno, Czech Republic

[4]CEPLANT, R&D Centre for Low-Cost Plasma and Nanotechnology Surface Modification, Masaryk University, Kotlářská 2, 61137 Brno, Czech Republic

[5]ISCR, Glasses and Ceramics team, UMR-CNRS 6226, University of Rennes 1, 35042 Rennes, France

Introduction

Chalcogenide glasses are extensively studied due to their important applications in photonics, ultrafast switching, ultra-high-density phase-change memories, integrated fiber optics, biosensors, *etc* [1-3]. Germanium-selenium glasses present one of the classical examples of chalcogenide glasses [4-6].

The main goal of this study is the identification of species present in the plasma originating from the interaction of laser pulses with solid state materials from Ge-Se system in the form of Ge-Se mixtures as well as Ge_xSe_{100-x} (x=10, 20, 30, 33) glasses.

Preparation of samples

1) 5N solid germanium mixed with selenium powder in different molar ratio (Ge/Se=1:1, Ge/Se=3:1, Ge/Se=5:1, Ge/Se=10:1).
2) The mixtures were powdered in agate mortar. Finally, germanium, and germanium-selenium mixtures were prepared as suspension in acetonitrile (1 mg/ml). The suspension was deposited to a target and dried.

Laser ablation synthesis

Ge_mSe_n clusters were generated (Fig. 1) and mass spectra were recorded in both positive and negative ion modes using mass spectrometer of AXIMA Resonance from Kratos Analytical Ltd (Manchester, UK) equipped with a nitrogen laser (337 nm) from Laser Science Inc. (Franklin, MA, USA). The laser power was scaled in arbitrary units from 0 to 180 a.u. External calibration was carried out using red phosphorus clusters. Examples of the spectra are given (Fig. 2-6).

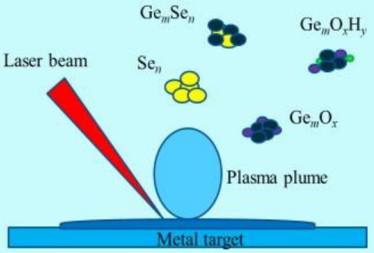

Fig. 1 Scheme of laser ablation.

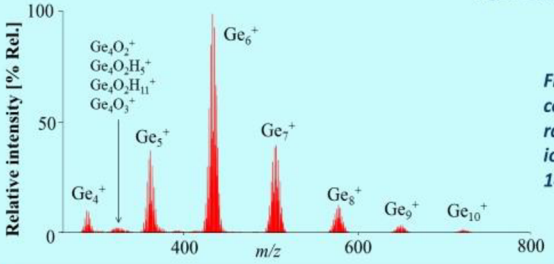

Fig. 2. Part of mass spectra concerning LDI of Ge in the range 250 – 800 in positive ion mode with laser energy 140 a.u.

Results

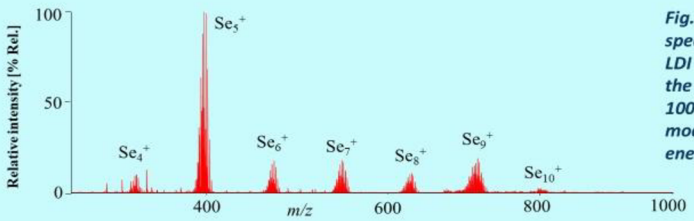

Fig. 3. Part of mass spectra concerning LDI of Ge:Se=1:1 in the range 250 – 1000 in positive ion mode with laser energy 140 a.u.

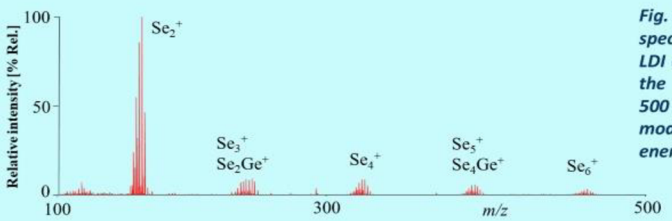

Fig. 4. Part of mass spectra concerning LDI of Ge:Se=3:1 in the range 100 – 500 in positive ion mode with laser energy 140 a.u.

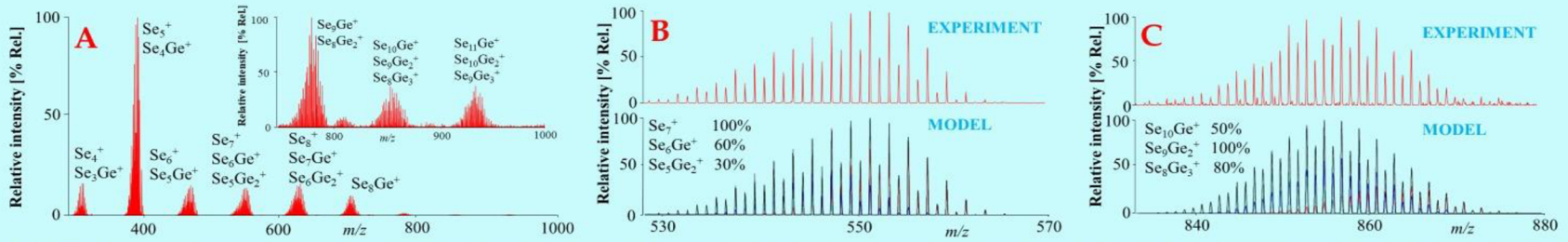

Fig. 5. Part of mass spectra concerning LDI of Ge:Se = 5:1 in the range 300 – 1000 in positive ion mode with laser energy 140 a.u (A) and comparison of experimental and theoretical isotopic patterns concerning overlay Se_7^+, Se_6Ge^+, $Se_5Ge_2^+$ (B), and $Se_{10}Ge^+$, $Se_9Ge_2^+$, $Se_8Ge_3^+$ (C) .

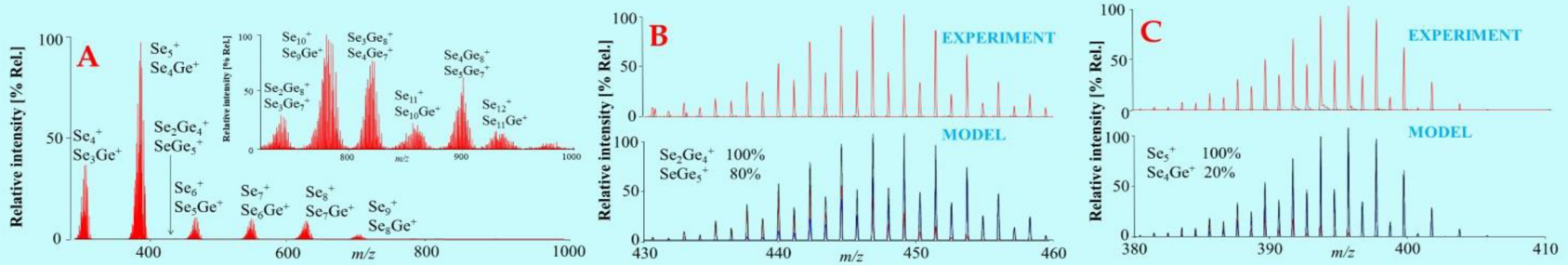

Fig. 6. Part of mass spectra concerning LDI of Ge:Se = 10:1 in the range 300 – 1000 in positive ion mode with laser energy 140 a.u (A) and comparison of experimental and theoretical isotopic patterns concerning overlay $Se_2Ge_4^+$, $SeGe_5^+$ (B) , and Se_5^+, Se_4Ge^+ (C) .

References

[1] R. Mawale, M. Ausekar, L. Prokeš, V. Nayabal, E. Baudet, T. Halenkovič, M. Bouška, M. Alberti, P. Němec, J. Havel, JASMS 28 (2017) 2569-2579.

[2] S. D. Pangavhane, P. Němec, V. Nazabal, A. Moreac, P. Jovári, J. Havel, RCMS 28 (2014) 1221-1232.

[3] J. L. Adam, X. H. Zhang, Chalcogenide glasses: preparation, properties and applications. Woodhead Publishing, Cambridge, (2014).

[4] K. C. Klavetter, J. Pedro de Souza, A. Heller, C. Buddie Mullins, JMCA 11 (2015) 5829-5834.

[5] P. Nemec, S. Zhang, V. Nazabal, K. Fedus, G. Boudebs, A. Moreac, M. Cathelinaud, X.-H. Zhang, OE 18 (2010) 22944-22957.

[6] K. Šútorová, P. Hawlová, L. Prokeš, P. Němec, R. Boidin, J. Havel, RCMS 29 (2015) 408-414.

Conclusions

The formation of Ge_mSe_n clusters generated by laser ablation synthesis from Ge-Se mixtures was studied and stoichiometry of clusters was determined. The results obtained can contribute to proposal to fabricate new, more efficient phase-change memories materials.

Acknowledgments

We gratefully acknowledge the financial support of the Czech Science Foundation (No.18-03823S) and Project CZ.1.07/2.3.00/30.0058 of the Ministry of Education, Youth and Sports of the Czech Republic and CEPLANT, CZ.1.05/2.1.00/03.0086 funding by European Regional Development Fund.

Appendix 6

Fei HUANG, Lubomír PROKEŠ, and Josef HAVEL: Laser ablation synthesis of antimony selenides clusters with simultaneous laser desorption ionization (LDI) quadrupole ion trap mass spectrometry.

The 2018 International Conference on Nanoscience + Technology (ICN+T), Brno, Czech Republic, July 22-27, 2018.

Laser ablation synthesis of antimony selenides clusters with simultaneous laser desorption ionization (LDI) quadrupole ion trap mass spectrometry

Fei Huang[1], Lubomír Prokeš[1,2,3], Josef Havel[1]

[1]Department of Chemistry, Faculty of Science, Masaryk University, Kamenice 5/A14, 625 00 Brno, Czech Republic, e-mail: 478620@mail.muni.cz
[2]CEPLANT, R&D Centre for Low-Cost Plasma and Nanotechnology Surface Modification, Masaryk University, , Kotlářská 2, 61137 Brno, Czech Republic
[3]Department of Physical Electronics, Faculty of Science, Masaryk University, Kotlářská 2, 61137 Brno, Czech Republic

INTRODUCTION

Antimony-selenium glasses are important chalcogenides which has been already widely used in fields of rewritable optical discs, phase-change memories, and so on[1-4].
In this work binary system Sb-Se is to be studied via laser ablation synthesis (LAS) generating new Sb_mSe_n clusters in both positive and negative ion modes using antimony-selenium powdered mixtures of elements at various ratios.

chalcogenide glasses

rewritable optical discs

phase-change memories

Sample preparation for mass spectrometry

1) Solid antimony in pellets was cleaned by applying five-minutes soliciting with 0.1M hydrochloric acid, then the pellets were washed with double distilled water, acetonitrile, then mixed with selenium powder at different molar ratio (Sb:Se=1:1, Sb:Se=1:10, Sb:Se=10:1).
2) The mixtures of Sb-Se were powdered in agate mortar. Finally, antimony, selenium and antimony-selenium mixtures were prepared as suspension in acetonitrile (1 mg/ml) and was deposited to a target and dried.

Instrumentation

Sb_mSe_n clusters were generated (Fig. 1) and mass spectra were recorded in both positive and negative ion modes using mass spectrometer of AXIMA Resonance from Kratos Analytical Ltd (Manchester,

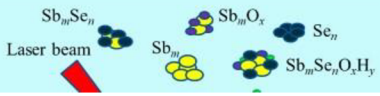

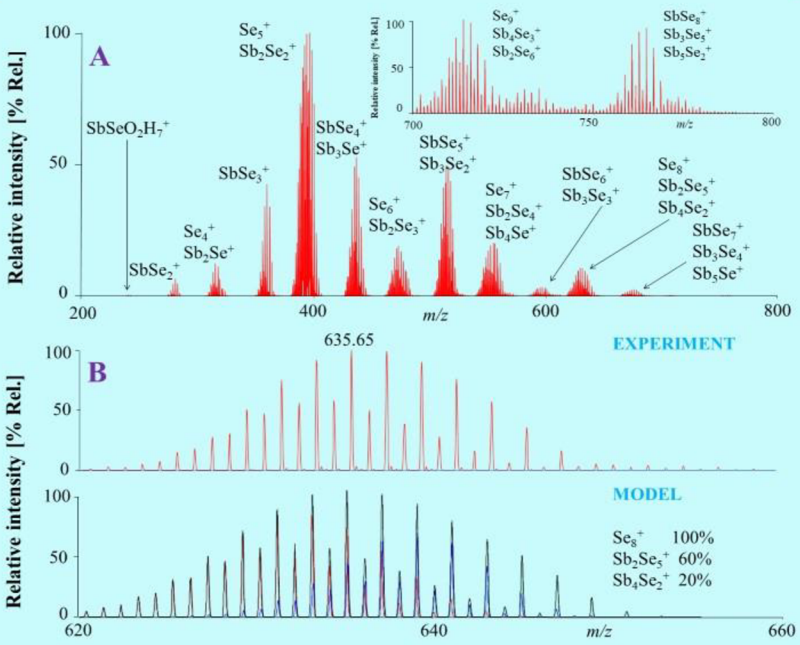

Fig. 4. Part of mass spectrum concerning LDI of Sb:Se =1:10 (A) in positive ion mode with laser energy 180 a.u. and comparison of experimental and theoretical isotopic patterns concerning overlay Se_8^+, $Sb_2Se_5^+$, and $Sb_4Se_2^+$ (B).

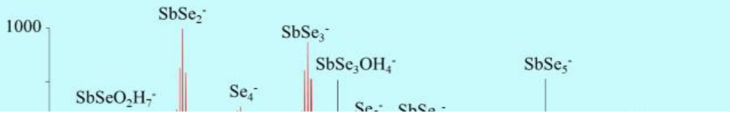

UK) equipped with a nitrogen laser (337 nm) from Laser Science Inc. (Franklin, MA, USA). The laser power was scaled in arbitrary units from 0 to 180 a.u. External calibration was carried out using red phosphorus clusters.

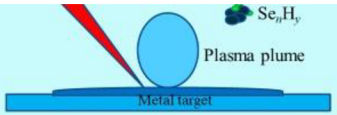

Fig. 1 Scheme of laser ablation.

Results

Examples of the spectra are given in Fig. 2-5.

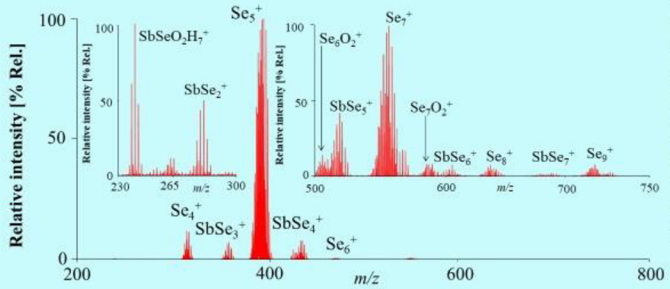

Fig. 2. Part of mass spectra concerning LDI of Sb:Se =1:1 in positive ion mode with laser energy 130 a.u. Insets are showing magnification of spectra in m/z ranges 230-300, 500 – 750.

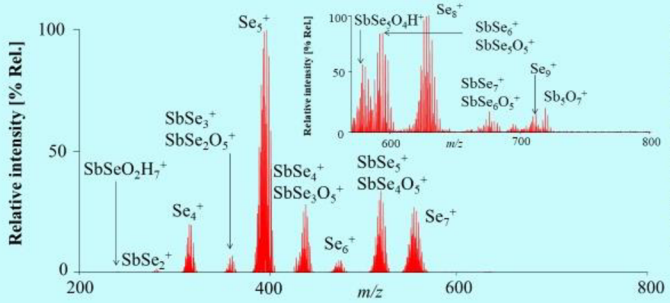

Fig. 3. Part of mass spectra concerning LDI of Sb:Se =10:1 in positive ion mode with laser energy 130 a.u. Inset is showing magnification of spectra in m/z range 550 – 800.

References

[1] Martin, T.M., Wood, P.T., Kolis, J.W.: Synthesis and Structure of an $[Sb_{12}Se_{20}]^{4-}$ Salt: The Largest Molecular Zintl Ion. Inorg. Chem. 33, 1587-1588 (1994)

[2] Hô, N., Laniel, J.M., Vallee, R., Villeneuve, A.: Photosensitivity of As_2S_3 chalcogenide thin films at 1.5 µm. Opt. Lett. 28, 965=967 (2003)

[3] Adam, J.L., Zhang, X. (Eds.).: Chalcogenide glasses. Preparation, Properties and applications. Woodhead Publishing, Cambridge, (2014)

[4] Vadapoo, R., Krishnan, S., Yilmaz, H., Marin, C.: Electronic structure of antimony selenide (Sb_2Se_3) from GW calculations. Phys. Status Solidi B. 3, 700-705 (2011)

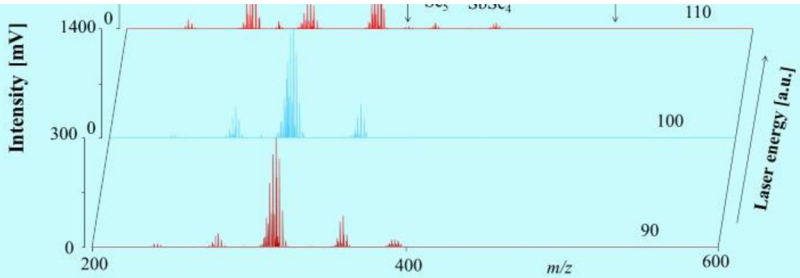

Fig. 5. Part of mass spectra concerning LDI of Sb:Se = 1:1 in the range 200 – 600 in negative ion mode with laser energy 90 – 110 a.u.

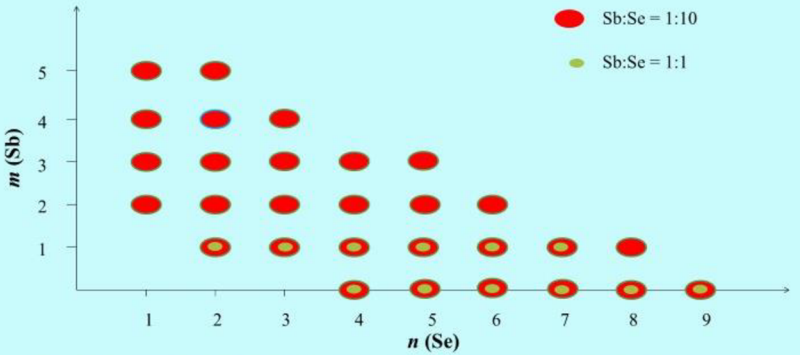

Fig. 6. Overview of Sb_mSe_n clusters stoichiometry-synthesized by laser ablation of antimony-selenium mixtures in the molar ratio Sb:Se =1:10 and Sb:Se =1:1.

Conclusions

Laser ablation synthesis (LAS) with quadrupole ion trap time-of-flight mass spectrometry (QIT-TOFMS) can be used as a kind of efficient synthesizer to generate Sb_mSe_n clusters. The clusters Sb_m, Se_n, and Sb_mSe_n as well as oxygenated or hydrogenated clusters were generated from the mixtures of the elements of antimony and selenium.

Acknowledgement

Support from the Grant Agency of Czech Republic (Project No. GA18-03823S) is greatly acknowledged. This research has been also supported by CEPLANT, the project R&D center for low-cost plasma and nanotechnology surface modifications CZ.1.05/2.1.00/03.0086 funding by European Regional Development Fund and Project CZ.1.07/2.3.00/30.0058 of the Ministry of Education, Youth and Sports of the Czech Republic.

Appendix 7

Fei HUANG, Lubomír PROKEŠ, and Josef HAVEL: Laser Ablation Synthesis (LAS) of Ge-Sb, Ge-Te, and Sb-Te clusters.

3rd Global Summit & Expo on Nanotechnology and Nanomedicine, Barcelona, Spain, September 18-20, 2019.

Laser Ablation Synthesis (LAS) of Ge-Sb, Ge-Te, and Sb-Te clusters

Fei Huang[1], Lubomír Prokeš[1,2,3], Josef Havel[1]

[1]Department of Chemistry, Faculty of Science, Masaryk University, Kamenice 5/A14, 625 00 Brno, Czech Republic, e-mail: 478620@mail.muni.cz
[2]CEPLANT, R&D Centre for Low-Cost Plasma and Nanotechnology Surface Modification, Masaryk University, , Kotlářská 2, 61137 Brno, Czech Republic
[3]Department of Physical Electronics, Faculty of Science, Masaryk University, Kotlářská 2, 61137 Brno, Czech Republic

INTRODUCTION

Germanium-Antimony-Tellurium (GST) is one of the most important phase-change-memory material. The $Ge_2Sb_2Te_5$ bulk material has been studied by using mass spectrometry in our laboratory [1] and recent detailed review of this phase change non-volatile memories is available [2].

The aim of this work is to use mass spectrometry following in details the formation of the binary clusters during LAS in order to cover wide concentration ranges and to contribute further to the knowledge of these materials.

chalcogenide glasses

rewritable optical discs

phase-change memories

Sample preparation for mass spectrometry

1) Germanium, antimony, selenium, and tellurium were separately powdered using an agate mortar. Then the powders were suspended in acetonitrile (1 mg/ml). From the suspensions, 10 µL was deposited on a target and dried.
2) A narrow piece of parafilm was used to fix the $Ge_aSb_bSe_cTe_d$ thin films on the target.

Instrumentation

Ge_mSb_n, Ge_mTe_o, and Sb_nTe_o clusters were generated (Fig. 1) and mass spectra were recorded in both positive and negative

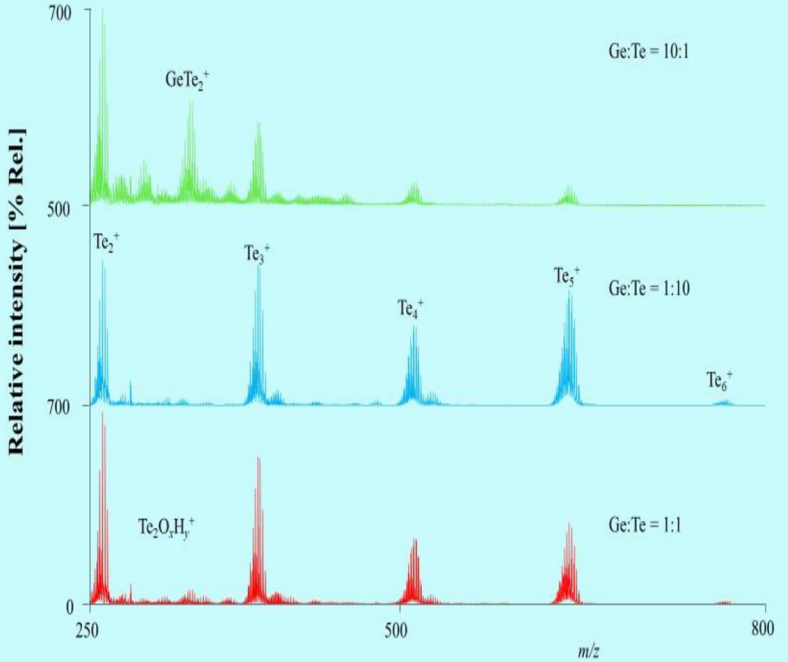

Fig. 4. Part of mass spectrum concerning LAS of Ge:Te =1:1, Ge:Te =1:10, and Ge:Te =10:1 in the m/z range 250-800 in positive ion mode with laser energy 120 a.u.

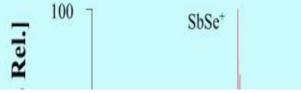

ion modes using mass spectrometer of AXIMA Resonance from Kratos Analytical Ltd (Manchester, UK) equipped with a nitrogen laser (337 nm) from Laser Science Inc. (Franklin, MA, USA). The laser power was scaled in arbitrary units from 0 to 180 a.u. External calibration was carried out using red phosphorus clusters.

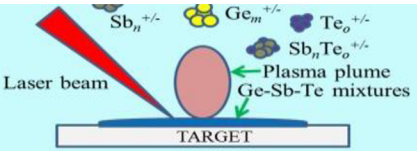

Fig. 1 Scheme of laser ablation.

Results

Examples of the spectra are given in Fig. 2-6.

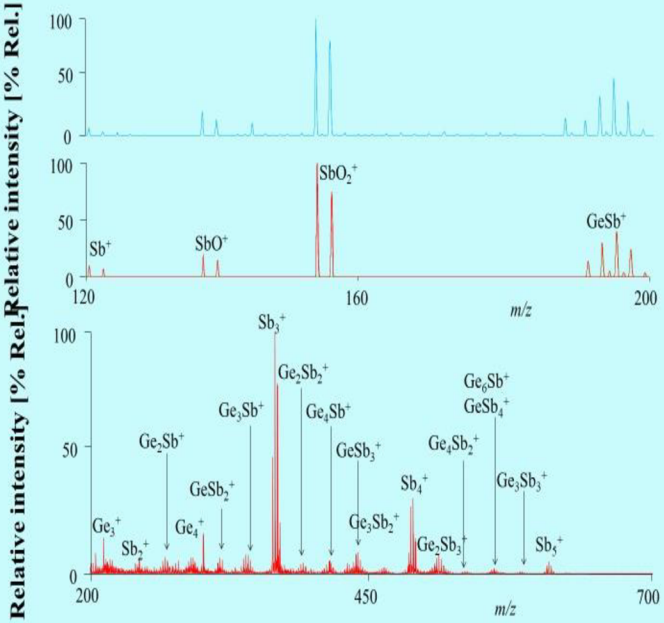

Fig. 2. Part of mass spectra concerning LAS of Ge:Sb =1:1 in the m/z range 120-200 in positive ion mode with laser energy 120 a.u.

Fig. 3. Part of mass spectra concerning LAS of Ge:Sb =10:1 in the m/z range 200–700 in positive ion mode with laser energy 120 a.u.

References

[1] R. Mawale, M. Ausekar, L. Prokeš, V. Nazabal, E. Baudet, T. Halenkovič, M. Bouška, M. Alberti, P. Němec, J. Havel, Laser Desorption Ionization of As_2Ch_3 (Ch = S, Se, and Te) Chalcogenides Using Quadrupole Ion Trap Time-of-Flight Mass Spectrometry: A Comparative Study. J. Am. Soc. Mass Spectrom. 28 (2017) 2569-2579.

[2] S. D. Pangavhane, P. Němec, V. Nazabal, A. Moreac, P. Jovári, J. Havel, Laser desorption ionization time-of-flight mass spectrometry of erbium-doped Ga-Ge-Sb-S glasses. Rapid Commun. Mass Spectrom. 28 (2014) 1221-1232.

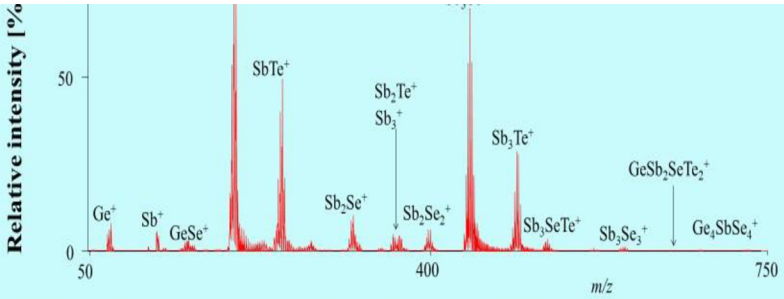

Fig. 5. Part of mass spectra concerning LDI of $Ge_{19.4}Sb_{11.7}Se_{53.9}Te_{10}$ thin film in the m/z range 50 – 750 in positive ion mode with laser energy 150 a.u.

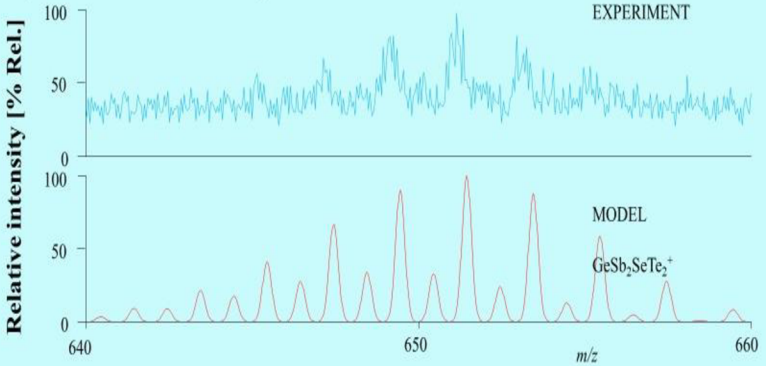

Fig. 6. comparison of experimental and theoretical isotopic patterns concerning $GeSb_2SeTe_2^+$.

Conclusions

Laser ablation synthesis (LAS) with quadrupole ion trap time-of-flight mass spectrometry (QIT-TOFMS) can be used as a kind of efficient synthesizer to generate Ge_mSb_n, Ge_mTe_o, and Sb_nTe_o clusters. Laser desorption ionization with quadrupole ion trap time-of-flight mass spectrometry was used as a type of efficient device to characterize $Ge_aSb_bSe_cTe_d$ thin films and mixtures of different elements.

Acknowledgement

Support from the Grant Agency of Czech Republic (Project No. GA18-03823S) is greatly acknowledged. This research has been also supported by CEPLANT, the project R&D center for low-cost plasma and nanotechnology surface modifications CZ.1.05/2.1.00/03.0086 funding by European Regional Development Fund.

10. List of oral presentations

1. **Fei HUANG**, Lubomír PROKEŠ, and Josef HAVEL: Mass Spectrometry of Chalcogenide Glasses. Conference of Ph.D. Students XD 107, Brno, Czech Republic, February 18, 2021.

11. Participation in projects

a) Project No. GA18-03823S of Czech Science Foundation, Advanced methods for the preparation of thin layers of chalcogenides and their modifications.

b) Project No. 19-24516S of Czech Science Foundation, Chalcogenide thin films doped with rare earth ions for the detection of gases in the mid-infrared region of the spectrum.

c) Project No. MUNI/A/1421/2019 and MUNI/A/1390/2020 for the Analytical and Physical and Chemical Methods for Geological, Biological, and Synthetic Materials.

12. Collaborations

a) Department of Graphics Art and Photophysics, Faculty of Chemical Technology, University of Pardubice, Studentská 573, 532 10 Pardubice, Czech Republic

b) Department of General and Inorganic Chemistry, Faculty of Chemical Technology, University of Pardubice, Studentská 95, 532 10 Pardubice, Czech Republic

c) Department of Chemistry, Faculty of Science, University of La Laguna, San Cristóbal de La Laguna, Santa Cruz de Tenerife, 38206 Tenerife, Spain

13. Curriculum vitae

PERSONAL DETAILS:

Name:	**Fei Huang**
Address:	Huang Zhuang 11, Huai'an, China
E-mail:	478620@mail.muni.cz
Date of Birth:	February 19, 1988
Mob-No:	+420-721667573

EDUCATION:

2018 - present: **Ph.D. in Analytical Chemistry**
Department of Chemistry, Faculty of Science, Masaryk University, Brno, Czech Republic
Ph.D. Thesis: Mass Spectrometry of Chalcogenide Materials
Supervisor: Prof. RNDr. Josef Havel, DrSc.

2014 - 2017: **Master of Science in Applied Chemistry**
Department of Chemistry and Chemical Engineering, Xi'an Shiyou (petroleum) University, Xi'an, China

2007 - 2011: **Bachelor of Science in Applied Chemistry**
Department of Chemistry and Chemical Engineering, Xi'an Shiyou (petroleum) University, Xi'an, China

WORK EXPERIENCES:

March-August 2020: Abroad Stay, Erasmus + Traineeships, University of La Laguna, Tenerife, Spain

2011-2014: Shaanxi Yanchang Coal Yulin Energy and Chemical Co.,Ltd., Yulin, China
Technician - Desalted Water Department

AWARDS:

1. Awarded scholarship of Centre for International Cooperation for students from countries out of OECD (2018, 2019, and 2020). Masaryk University, Brno, Czech Republic
2. Awarded the prize for excellent scientific results of Department of Chemistry (2018), Masaryk University, Brno, Czech Republic